Department of Electromagnetism and Condensed Matter Physics
University of Granada

Nonequilibrium Behavior of Hard Disks Systems

Autor: Jesús Javier del Pozo Mellado

Ph.D. Advisor: Pedro Luís Garrido Galera
Ph.D. co-Advisor: Pablo Ignacio Hurtado Fernández

– Date –

Editor: Editorial de la Universidad de Granada
Autor: Jesús Javier del Pozo Mellado
D.L.: GR 1930-2014
ISBN: 978-84-9083-101-4

Departamento de Electromagnetismo y Física de la Materia
Universidad de Granada

Fenómenos de No-equilibrio en un Sistema de Discos Rígidos

Autor:Jesús Javier del Pozo Mellado

Director: Pedro Luís Garrido Galera
coDirector: Pablo Ignacio Hurtado Fernández

– Fecha –

D. Pedro Luís Garrido Galera ,

CERTIFICA: que la presente memoria, *Nonequilibrium Behavior of Hard Disks Systems* (*Fenómenos de No-equilibrio en un Sistema de Discos Rígidos*), ha sido realizada por D. Jesús Javier del Pozo Mellado bajo su dirección en el Departamento de Electromagnetismo y Física de la Materia, así como que éste ha disfrutado de estancias en el extranjero, durante un periodo superior a tres meses, en el "Institute for Quantum Optics and Quantum Information" de la Universidad de Innsbruck, Austria .

Granada, Fecha

Fdo:

Agradecimientos

Contents

Introduction

One of the most strikingly features of Nature is that it can be described at different scales. Thought a continuous change of scale from the sub-atomic to the supra-galactic, the phenomenology and the relevant magnitudes needed to describe it, change in a rather surprising way. Once the spatio-temporal scale is chosen we can always define a set of representatives magnitudes that characterize the description of a given natural phenomenon. For example, if we are trying to describe sub-nuclear interactions, where spatial scale is about 10^{-15} m and the temporal is about 10^{-12} s, we need magnitudes like the the quarks' flavor, or their color. These magnitudes, although present, are not necessary to describe an atom in a scale of 10^{-10} m and 10^{-9} s, where the relevant magnitudes are, for example, the number of protons, neutrons and electrons. In both cases there are strong and electromagnetic interactions, but their relative significance changes with the scale. In the first case electromagnetic interactions are negligible compared with strong interactions, but, as we move to greater scales, strong interactions fade away and electromagnetic interactions take over. In this particular case, the cause of this shift in the description is easily identified, because the strong interaction is a short range force. But there are other situations where the cause of the shift is more subtle. One example of such cases can be found when we go to even greater scales. In a scale of 10^{10} m and 10^{6} s, the one associated with the Solar System, the relevant magnitudes are the mass of the planets and the Sun, and the Electromagnetic interactions become negligible. This is so even when Electromagnetic interactions are 14 order of magnitude greater than Gravitational interactions in every scale. However Electromagnetic interactions, in contrast with Gravitational ones, have positive and negative contributions that cancels out due to the general neutral character of stable matter, composed mainly by atoms of equal number of electrons and protons. To the trained eye these examples may seam trivial, however we must notice, not only the change in the description theory, but also that the magnitudes in each layer of description can be related with the phenomenology occurring in a level below. For example the magnitudes on the atomic scale, the protons and neutrons, are effective phenomena of the underlying sub-nuclear theory. In this way **how** new useful concepts emerge from the underlying theory is highly relevant to get a coherent description at all scales.

The particular process in each situation can be very complicated, like on our first example, or very easy, like the the second one, but it always tries to

compactify some degrees of freedom into effective phenomena through some sort of summation process. Typically, as we increase the number of elements and degrees of freedom, an analytical relation is increasingly difficult to obtain. However, when the number of degrees of freedom is sufficiently large, new, statistical rules can be used to relate the microscopic phenomenology to the macroscopic one. This approach is the core of one of the most successful theories of the past century, Statistical Mechanics.

Since the pioneering works of Boltzmann, Maxwell and Gibbs, Statistical Mechanics has obtained a mayor success in deriving the macroscopic laws of equilibrium Thermodynamics from the microscopic dynamics of the particles that constitute a given system. It's approach is based on the emergent phenomena that arise when a sufficiently large set of particles are constrain by the same macroscopic variables. For example, in the micro-canonical case, the constrains correspond to those of an isolated system, where the number of particles N, the volume V and the total energy E are fixed. If we leave the system under this conditions for sufficient amount of time, it reaches a stationary state characterized by a maximum entropy. And this entropy can be calculated within the framework of Statistical Mechanics from the dynamical properties of the individual particles, e.g. it's Hamiltonian. This microscopic understanding of Thermodynamics opened the path to further generalizations. In this way Statistical Mechanics became the principal tool to explain phenomena like the brownian motion, phase transitions or ferromagnetism. The power of the theory resides in the general character of the statistical derivations, which focus on how the different scales relate to each other, leaving the particular microscopical detail in a second plane. This general approach allowed Statistical Mechanics to enter in other disciplines, and its tools are now being used in fields like Biology, Economics or Sociology.

However, there is still a shadow in the horizon. The major limitation of Thermodynamics is that it is applicable only to equilibrium settings. However, Equilibrium situations in nature are the exception rather than the rule. Typically the systems are subject to environments that change in space, time or both. This can lead to very complex behaviors and emergence of patterns that would be forbidden under equilibrium conditions. Such important phenomena, for practical and philosophical reasons, like the behavior of the brain, transport phenomena, the whether or even life itself are non-equilibrium processes, making a fundamental understanding of non-equilibrium of paramount importance. The general hope was that Statistical Mechanics would allow us to get rid of this limitation, making possible to give a fundamental explanation to non-equilibrium phenomena. But, despite all the efforts, and the myriad of advances in this subject during the last century, a general theory, valid arbitrary far from equilibrium, is still lacking. The different strategies to tackle the problem have varied along time from macroscopic approaches to modern fluctuations theories. In each step new information is unraveled, closing the circle towards a profound understanding of this complex subject. In order to put into context the purpose of this thesis, let us briefly summarize the history of this process.

The first attempts to characterize the basic phenomenology of non-equilibrium

Physics follow the path of Thermodynamics, giving a macroscopic description in terms of macroscopic variables. Among the many examples two stand out for its great generality and scope. The Navier-Stokes equations of hydrodynamics and Transport equations.

Navier-Stokes equations describe in a general form how a continuous fluid moves. Despite not having found a general solution for this equations [1], they are used to computationally model the weather, the air flow in a wing, or ocean currents just to mention a few. Furthermore, the tremendous generality of this equations has allowed, when coupled with Maxwell's equations of Electromagnetism, to even study the plasma currents present in the Sun [1].

On the other hand, we have Transport equations which include different laws that share the same formal expression. This expression relates the fluxes present in a system with the imposed gradient (or force) on a related magnitude. In this category lies Fourier Law for energy transport, Fick's Law for mass transport, or Ohm's Law for electric transport. The first one to appear in the literature, and the one directly related with this thesis, is Fourier's Law [2, 3]. In his work Fourier related the flux of energy between to bodies maintained at different temperatures with the difference between these temperatures, by means of a coefficient which is a property of the body connecting the two reservoirs. Although he considered only a linear term in the gradient, the range of gradients for which this law is valid is surprisingly wide, as confirmed from simulations carried for a system of particles with a Lenard-Jones potential [4]. It is also remarkable that when there are several transport conditions acting at once, the coefficients for the different transport phenomena are related. In particular, for example, it is possible to induce an energy transport at constant temperature by imposing a pressure gradient, and also to induce a momentum transfer at constant pressure by imposing a temperature gradient. Turns out that the coefficients that characterize these cross effects are equal. Onsager?s Reciprocal Relations, proven under very general conditions [5, 6], assert that this equality must follow, obtaining for this work the Nobel Prize in Chemistry in 1968.

This two examples of macroscopic theories are related and compose the core of the named constitutive (or phenomenological) equations which are used in macroscopic theories of non-equilibrium [7]. The broad generality of these equations suggest, as in the thermodynamical case, that their properties have a statistical nature. In particular we should be able to calculate the diverse transport coefficients from the microscopic properties of a given system, as we can do, for example, with the specific heat of a substance in the equilibrium case. Key in this calculation is the role played by fluctuations.

The first evidence of this is in the series of papers of Einstein about brownian motion (an English recompilation can be found in [8]), where, for the first time, a relation is established between the response of a fluid to an external force and the equilibrium fluctuations of the fluid. This was further generalized in 1928 by Nyquist by establishing a relation between the fluctuations of the electrical potential and the resistance in a conductor [9]. His

[1] The problem of existence and smoothness of the Navier-Stokes equations is among the *Millennium Problems* of the Clay Mathematical Institute.

result was proven and generalized by Callen and Welton for linear dissipative systems, formulating the Fluctuation-Dissipation theorem [10]. Afterward Green and Kubo provided exact expressions for transport coefficients close to equilibrium in terms of time auto-correlation functions [11, 12]. These results highlighted the role of fluctuations but they are limited to systems close to equilibrium. When the systems are far from equilibrium general results are still very scarce. One of such rare general results is the Fluctuation Theorem first discussed in the context of simulations of sheared fluids [13], and formulated rigorously by Gallavotti and Cohen under very general assumptions [14].

It has not been until recently that non-equilibrium physics has undergone a true revolution. At the core of this revolution is the clarification of the role played by macroscopic fluctuations, with their statistics and associated structures, to understand non-equilibrium behavior [15, 16, 17, 18, 19, 20, 21]. The language of this revolution is the theory of large deviations, with large-deviation functions (LDFs), measuring the probability of fluctuations and optimal paths sustaining these rare events, as central objects in the theory. In fact, LDFs play in non-equilibrium systems a role akin to the equilibrium free energy [15, 16, 17, 18, 19, 20]. In this way, the long-sought general theory of non-equilibrium phenomena is currently envisaged as a theory of macroscopic fluctuations, and the calculation, measurement and understanding of LDFs and their associated optimal paths has become a fundamental issue in theoretical physics. This paradigm has led to a number of groundbreaking results valid arbitrarily far from equilibrium, many of them in the form of fluctuation theorems [15, 16, 17, 18, 19, 20, 21].

However there is still a lot of work to do, but at the light of what Statistical Mechanics meant to Thermodynamic, one can only wonder what doors will open a deep understanding of non-equilibrium phenomena.

In this thesis we want to push forward our understanding of non-equilibrium behavior by analyzing in detail the physics of a paradigmatic model, the Hard Body (HB) fluid. In particular we are going to focus on the two dimensional version of this model, the Hard Disks model, using for its study extensive molecular dynamics simulations and a complementary theoretical analysis. The Hard Body model and its relatives are among the most successful, inspiring and prolific models of physics. Modeling the particles as impenetrable bodies is one of the simpler ways to introduce an interaction among them, yet it contains the essential ingredients to understand a large class of complex phenomena, from phase transitions or heat transport to glassy dynamics, jamming, or the physics of liquid crystals and granular materials, just to mention a few [22, 23, 24, 25]. In addition, the study of HB-like models has motivated deep insights and new concepts, as fluctuation theorems [13, 14, 26] or the long-time tails in fluids [27], as well as important tools like molecular dynamics [28] or importance sampling in Monte Carlo simulations [29], which are nowadays cornerstones in physics. Such breadth of applications makes HB models a paradigm in condensed matter and statistical physics, specially in non-equilibrium settings [26, 30, 31, 32, 33, 34, 35, 36]. There remain however many important open problems in HB physics, from

the unknown equation of state in dimensions greater than one [22], to the nature of the melting transition and the weakly diverging heat conductivity of hard disks [30, 37, 38], making general results for HB models even more appealing. Our quest will bring us from a deeper understanding of the subtle Local Thermodynamic Equilibrium hypothesis, a cornerstone in modern theories of non-equilibrium physics, to the discovery of universal scaling laws in non-equilibrium fluids and finally to the introduction of a novel isometric fluctuation relation for current fluctuations valid arbitrarily far from equilibrium.

In particular in chapter 1 we give a description of the Hard Disks model and the algorithm needed to efficiently simulate it. We also present the results obtained for equilibrium simulations, which we used as a validity check for our program. We find, as expected, that temperature and density profiles under this situation are flat and consistent with the values imposed at the boundaries. We notice that in other equilibrium studies of this system, boundary effects are minimized by the use of periodic boundary conditions. However, due to the use of hard walls in order to simulate the thermal reservoirs, we find important boundary effects in our system. We performed a finite size scaling analysis to characterize these boundary effects, confirming that they disappear in the thermodynamic limit. We also study the pressure measured by two different methods. We found that the two approaches are consistent and they agree with other studies available in the literature [22, 38, 39, 40]. We conclude from these results that our simulation is correct and suitable to study non-equilibrium behavior.

In chapter 2 we give an empirical description of the non-equilibrium physics of our system. We mainly focus on the description of temperature and density profiles arising once the stationary state is reached. We find non-linear profiles and give experimental fits which are in very good agreement with our data. We pay a special attention to boundary effects, which turn out to be more complicated that in the equilibrium case. We show how boundary and size effects are tangled, being necessary one to obtain the other, and vice versa. This fact makes a traditional finite size scaling analysis rather complicated hindering a clear description of the thermodynamic limit behavior of our system. In chapter 4 we derive a scaling method which allows us to circumvent this problem. To close this chapter we studied a main observable of systems out of equilibrium, the energy current across the system. We show how this current depends on the external gradient and the number of particles.

In chapter 3 we study in detail the role of Local Thermal Equilibrium (LTE) and whether or not it is satisfied in our simulations. There is not a general theoretical proof of this hypothesis [30], and confirming its presence in a simulation is very hard. In order to do this we distinguish between macroscopic and microscopic LTE. To see whether macroscopic LTE holds we study if the equilibrium Equation of State (EoS) is valid locally in our system. Surprisingly, despite being out of equilibrium and the strong size dependence found for the density and the temperature profiles in chapter 2, the system follows locally the equilibrium EoS with high precision without any appreciable size effect. Furthermore the data obtained is in

very good agreement with equilibrium simulations available in the literature [41, 42, 39, 40, 43, 44]. This absence of finite size effects will help us in chapter 4 to construct a strategy to avoid spurious size dependence. To see whether microscopic LTE holds we check if the measured global distributions, of the velocity and the energy, match the theoretical equilibrium distributions derived from the assumption that Local Thermal Equilibrium holds. Although we don't find deviations for the global velocity distributions, up to finite size effects, the second moment of the energy distribution deviates systematically from the local equilibrium prediction. We find that the difference between these magnitudes depends linearly on the external gradient squared, with a slope of 1/40. Finally we notice that for high gradients and high mean packing fractions a liquid-solid coexistence occurs. We studied this non-equilibrium coexistence finding that LTE hypothesis breaks down in the portion of the system occupied by the solid. We show that the phenomenology of this solid is not equivalent to that of the equilibrium case. We can conclude in this chapter that LTE holds at the macroscopic level (at the liquid phase), and that deviations occur on the fluctuating level.

In chapter 4 we study the validity of Fourier's Law. In order to do this, we have to design a strategy to overcome the finite size effect studied in chapter 2, which distort a direct approach. We know from chapter 3 that Local Thermal Equilibrium holds in such a way that the Equation of State doesn't present finite size effects. Using this and supposing that Fourier's Law also holds, we theoretically derive a scaling property for the profiles of an infinite system of Hard Disks. This scaling Law is characterized by two universal master curves from which we can derive every possible profile. We find that the predictions of this theory are in very good agreement with our data. In particular it is quite remarkable that all the profiles for different system setups, for a given number of particles, collapse into a universal curve, indicating that Fourier's Law holds for our system. This implies, as a consequence of the scaling, what we called *Bulk-Boundary Decoupling*. It is generally believed that, once discarded the part of a system affected by boundary effects, the remaining bulk part should present finite size effects. Our combined results, of this chapter and the previous one, strongly suggest that this is not the case. In fact the system behaves as it were an infinite system were LTE and Fourier's Law holds, leaving, as a reminiscence of its finite character only two effects: an effective thermal reservoir, composed by the baths and region of the system affected by boundary effects, in whose values are concentrated all spurious size effects, and a size dependent thermal conductivity physically relevant, reminiscent of the known long time tails present on Hard Disks systems [27]. We believe that this analysis could have many applications in the description of the non-equilibrium stationary state of more complex fluids. In fact in appendix B we derive a scaling for soft potentials which are, in certain situations, the limiting case of the more realistic Lenard-Jones potentials [45, 46].

In chapter 5 we focus in the fluctuations of the energy current. We derive in detail the recently introduced Isometric Fluctuation Relation which is a consequence of the deep implications that temporal reversibility introduce at the fluctuating level. Our measurements are in good agreement with the

theory although our system does not satisfy, a priory, all the conditions of the theoretical derivation. This suggest that the Isometric Fluctuation Relation could be further generalized.

Introducción

Una de las características más sorprendentes de la Naturaleza es que se puede describir a diferentes escalas. A través de un cambio continuo de escala desde lo subatómico hasta lo supragaláctico, la fenomenología así como las magnitudes relevantes necesarias para describirla, cambian de una forma sorprendente. Una vez establecida la escala espacio-temporal siempre podemos definir las magnitudes representativas necesarias para describir un fenómeno determinado. Por ejemplo, si nuestra intención es describir las interacciones sub-nucleares, donde la escala espacial es del orden de los 10^{-15} m y la temporal de los 10^{-12} s, necesitamos magnitudes como el sabor y el color de los quarks. Estas magnitudes, aunque presentes, no son necesarias para describir un átomo en el orden de los 10^{-10} m y 10^{-9} s, donde las magnitudes relevantes pasan a ser el número de protones, neutrones y electrones, por ejemplo. En ambos casos están presentes las interacciones Electromagnética y Fuerte, pero su importancia relativa cambia con la escala. En el primer caso las interacciones Electromagnéticas son irrelevantes en comparación con las de carácter Fuerte, pero según nos vamos moviendo hacia escalas más grandes, las interacciones fuertes tienen cada vez menos importancia y las electromagnéticas toman el mando. En esta caso particular, la causa del cambio de descripción puede identificarse con claridad debido a que las interacciones fuertes son de corto alcance. Pero hay otras situaciones en la que el cambio en la descripción tiene causas más sutiles. Un ejemplo de este caso podemos encontramos cuando nos vamos a escalas más grandes. En el orden de los 10^{10} m y 10^{6} s, la escala del Sistema Solar, las magnitudes relevantes son las masas de los planetas y la del Sol, pasando a ser despreciables las interacciones Electromagnéticas. Y esto pasa incluso cuando las interacciones electromagnéticas son 14 ordenes de magnitud mayores que las gravitatorias en cualquier escala. Sin embargo la interacciones electromagnéticas, al contrario que las gravitatorias, tienen contribuciones positivas y negativas que se cancelan debido al carácter neutral de la materia estable, compuesta principalmente por el mismo número de protones y electrones. Para un experto estos ejemplos pueden parecer triviales, pero debemos darnos cuenta, no solo del cambio en la teoría descriptiva, sino también del hecho de que las magnitudes relevantes en cada nivel de descripción están relacionadas con la fenomenología del nivel inferior. Por ejemplo las magnitudes de la escala atómica, los protones y los neutrones, son fenómenos efectivos de la teoría subnuclear subyacente. De esta forma **como** emergen estos conceptos de la teoría subyacente es altamente relevante para obtener una descripción

coherente en todas las escalas.

El proceso concreto podrá ser muy complicado, como en nuestro primer ejemplo, o muy fácil como en el segundo, pero el objetivo siempre será compactificar determinados grados de libertad en ciertos fenómenos efectivos a través del uso de algún tipo de proceso de sumado. Típicamente según vamos aumentando el numero de elementos y de grados de libertad cada vez resulta más difícil encontrar una expresión analítica para este proceso. Sin embargo, cuando el número de grados de libertad es suficientemente alto, se pueden usar nuevas reglas estadísticas para relacionar el comportamiento microscópico con el macroscópico. Este enfoque es el núcleo de una de las teorías más exitosas del siglo pasado, la Mecánica Estadística.

Desde los trabajos pioneros de Boltzmann, Maxwell y Gibbs, la Mecánica Estadística ha obtenido un gran éxito a la hora de derivar las leyes de la Termodinámica del equilibrio a partir de la dinámica microscópica de las partículas que componen un determinado sistema. Su planteamiento se basa en los fenómenos emergentes que aparecen cuando un número suficientemente alto de partículas se ven restringidas por las mismas condiciones macroscópicas. Por ejemplo, en el caso microcanónico, las ligaduras se corresponden con las de un sistema aislado, donde el numero de partículas N, el volumen V y la energía total E se mantienen fijas. Si dejamos al sistema relajar el suficiente tiempo éste alcanza un estado estacionario caracterizado por una entropía máxima. Y esta entropía se puede calcular en el ámbito de la Mecánica Estadística a partir de las propiedades dinámicas de las partículas, esto es, a partir de su Hamiltoniano. Esta comprensión microscópica de la Termodinámica abrió el camino para su consiguiente generalización. De este modo la Mecánica Estadística se convirtió en la herramienta principal para explicar fenómenos como el movimiento Browniano, las transiciones de fase o el ferromagnetismo, sólo por mencionar algunos. La potencia de esta teoría reside en el carácter general de las derivaciones estadísticas, que se centran en como se relacionan las escalas entre si dejando los detalles microscópicos en un segundo plano. Este enfoque general permitió a la Mecánica Estadística entrar en otras disciplinas, y sus herramientas están siendo usadas actualmente en campos como la Biología, la Economía o la Sociología.

Sin embargo todavía hay nubes en el horizonte. La principal limitación de la Termodinámica es que sólo es aplicable a situaciones de equilibrio. Pero hay que recordar que el equilibrio en la Naturaleza es más la excepción que la regla. Típicamente los sistemas de interés están sometidos a entornos que cambian en el espacio, el tiempo o ambos. Esto se traduce en comportamientos complejos y la emergencia de patrones que estarían prohibidos bajos condiciones de equilibrio. Fenómenos tan importantes, desde un punto de vista práctico y filosófico, como el comportamiento del cerebro, los fenómenos de transporte, el clima o incluso la vida en sí misma, son procesos de no-equilibrio, convirtiendo la compresión fundamental del no-equilibrio en un asunto de máxima importancia. La impresión general dentro de la comunidad científica era que la Mecánica Estadística conseguiría deshacerse de esta licitación, haciendo posible una explicación fundamental de los fenómenos de no-equilibrio. Sin embargo, a pesar de todos los esfuerzos y la cantidad de avances en esta materia durante el pasado siglo, todavía no tenemos una

teoría general válida arbitrariamente lejos del equilibrio. Las diferentes estrategias para abordar este problema han cambiado a lo largo de los años pasando de las descripciones macroscópicas hasta las modernas teorías sobre fluctuaciones. En cada paso se ha ido desentrañando nueva información, cerrando el circulo hacia un entendimiento profundo de este complicado problema. Con el fin de poner en contexto el propósito de esta tesis, permitidnos resumir brevemente la historia de este proceso.

Los primeros intentos para caracterizar la fenomenología básica de la Física del no-equilibrio siguieron los pasos de la termodinámica, dando una descripción macroscópica en términos de variables macroscópicas. Entre los muchos ejemplos dos resaltan por su generalidad y alcance. Las ecuaciones de Navier-Stokes de la hidrodinámica y las ecuaciones de Transporte.

Las ecuaciones de Navier-Stokes describen de forma general como se mueve un fluido continuo. A pesar de que no se conoce una solución general para estas ecuaciones [2], se usan como modelo computacional para describir el clima, el flujo de aire en un ala, o los flujos oceánicos sólo por mencionar algunos ejemplos. Además la tremenda generalidad de estas ecuaciones incluso a permitido, cuando se las acopla con las ecuaciones de Maxwell del Electromagnetismo, estudiar los flujos de plasma presentes en el Sol [1].

Por otra parte tenemos las ecuaciones de Transporte que incluyen leyes diferentes que comparten la misma expresión formal. Esta expresión relaciona los flujos presentes en un sistema con el gradiente (o fuerza) impuesto en una magnitud relacionada. En esta categoría encontramos la ley de Fourier para el transporte de energía, la ley de Fick para la difusión de partículas, o la ley de Ohm para el transporte eléctrico. La primera en aparecer en la literatura, y la que está relacionada directamente con esta tesis, es la ley de Fourier [2, 3]. En su trabajo Fourier relacionó el flujo de energía entre dos cuerpos mantenidos a distintas temperaturas con la diferencia entre estas temperaturas, por medio de un coeficiente característico del material que une las dos fuentes térmicas. Aunque sólo consideró una relación lineal con el gradiente, el abanico de gradientes en los que esta ley es valida es sorprendentemente amplio, como confirman las simulaciones hechas para un sistema de partículas interaccionando con un potencial de Lenard-Jones [4]. También hay que destacar que cuando hay varias condiciones de transporte actuando a la vez, los coeficientes para los distintos fenómenos de transporte están relacionados. En particular, por ejemplo, es posible inducir un transporte de energía a temperatura constante imponiendo un gradiente de presión, y a su vez, es posible inducir un transporte de momento a presión constante imponiendo un gradiente de temperatura. Resulta que los coeficientes que caracterizan estos efectos cruzados son iguales entre sí. Las relaciones de reciprocidad de Onsager, probadas bajos condiciones muy generales [5, 6], afirman que esta igualdad debe cumplirse, obteniendo por este trabajo el premio Nobel de Química en el año 1968.

Estos dos ejemplos de teorías macroscópicas están relacionados y componen el núcleo de las llamadas ecuaciones constitutivas (o fenomenológicas) que se usan en las teorías macroscópicas de no-equilibrio [7]. La amplia ge-

[2] El problema de la existencia y diferenciabilidad de las soluciones a las ecuaciones de Navier-Stokes esta entre los *Problemas del Milenio* de Instituto Clay de Matemáticas.

neralidad de estas ecuaciones sugiere, como pasa en el caso termodinámico, que sus propiedades tienen un origen estadístico. En particular deberíamos ser capaces de calcular los diversos coeficientes de transporte a partir de las propiedades microscópicas de un determinado sistema, como podemos hacer, por ejemplo, con el calor especifico de una sustancia en el caso de equilibrio. La clave de este cálculo resulta ser el papel que juegan las fluctuaciones.

La primera evidencia de esto está en la serie de artículos de Einstein sobre el movimiento Browniano (una recopilación en inglés puede encontrarse en [8]), donde, por primera vez, se establece una relación entre la fuerza externa aplicada a un fluido y sus fluctuaciones de equilibrio. Esto fue generalizado en 1928 por Nyquist estableciendo una relación entre las fluctuaciones del potencial eléctrico y la resistencia en un conductor [9]. Su resultado fue probado y ampliado por Callen y Welton a sistemas disipativos lineales, formulando el teorema de Fluctuación-Disipación [10]. Más tarde Green y Kubo derivaron expresiones exactas para los coeficientes de transporte cerca del equilibrio en términos de funciones temporales de auto-correlación [11, 12]. Estos resultados resaltaron el papel de las fluctuaciones pero estaban limitados a sistemas cerca del equilibrio. Cuando los sistemas están alejados del equilibrio los resultados generales son todavía escasos. Una de estas raras excepciones es el teorema de Fluctuación discutido en un principio en el contexto de fluidos bajos efectos de cizalladura [13], y formulado rigurosamente por Gallavotti y Cohen bajos suposiciones muy generales [14].

No ha sido hasta hace poco que la Física del no-equilibrio a experimentado una autentica revolución. En el núcleo de esta revolución se encuentra la clarificación del papel jugado por las fluctuaciones macroscópicas, con su estadística y estructuras asociadas, a la hora de entender comportamientos de no-equilibrio [15, 16, 17, 18, 19, 20, 21]. El lenguaje de esta revolución es la teoría de largas desviaciones, donde las funciones de largas desviaciones (*Large-Deviation Functions (LDFs)*), que miden la probabilidad de las fluctuaciones y los caminos óptimos que sostienen estas desviaciones, se perfilan como los elementos centrales de la teoría. De hecho las LDFs juegan un papel similar a la energía libre en los sistemas de no-equilibrio [15, 16, 17, 18, 19, 20]. De este modo, la tan ansiada teoría general de los fenómenos de no-equilibrio se divisa actualmente como una teoría de fluctuaciones macroscópicas, y el cálculo, medición y entendimiento de las LDFs y sus caminos óptimos asociados se ha convertido en una cuestión fundamental de la Física teórica. Este paradigma ha liderado el camino hacia numerosos resultados innovadores válidos arbitrariamente lejos del equilibrio, muchos de ellos en forma de teoremas de fluctuación [15, 16, 17, 18, 19, 20, 21].

Sin embargo todavía hay mucho trabajo por hacer, pero a la luz de lo que la Mecánica Estadística significó para la Termodinámica, uno no puede sino maravillarse ante las puertas que abriría una comprensión profunda de los fenómenos de no-equilibrio.

En esta tesis queremos avanzar en el entendimiento de los comportamientos de no-equilibrio mediante un análisis detallado de un modelo paradigmático, el fluido de Cuerpos Sólidos (*Hard Body (HB)*). En particular nos centraremos en la versión de dimensión dos de este modelo, el modelo de

Discos Rígidos ((*Hard Disks (HD)*), usando para su estudio extensas simulaciones de dinámica molecular y análisis teóricos complementarios. El modelo de Cuerpos Rígidos y sus modelos relacionados está entre los modelos más exitosos, inspiradores y prolíficos de la Física. Modelar las partículas como cuerpos impenetrables es una de las maneras más simples de introducir una interacción entre ellas, sin embargo contiene los ingredientes esenciales para entender una gran clase de comportamientos complejos, desde las transiciones de fase o el transporte de calor a las dinámicas de vidrios, el "jamming", los cristales líquidos o los materiales granulares sólo por mencionar algunos [22, 23, 24, 25]. Además, el estudio de sistemas relacionados con los cuerpos rígidos ha motivado profundas revelaciones y nuevos conceptos, como los teoremas de fluctuación [13, 14, 26] o las colas de tiempos largos en fluidos [27], así como importantes herramientas como la dinámica molecular [28] o el muestreo Monte Carlo en simulaciones [29], que son en la actualidad piedras angulares en la Física. Esta amplitud de aplicaciones hacen de los modelos de Cuerpos Rígidos un paradigma en Física de la materia condensada y en la Física Estadística, especialmente en situaciones de no-equilibrio [26, 30, 31, 32, 33, 34, 35, 36].

Sin embargo todavía quedan muchos problemas importantes abiertos en la Física de los Cuerpos Rígidos, desde la desconocida ecuación de estado para dimensiones mayores que uno [22], a la naturaleza de la transición de fase en dos dimensiones o la divergencia débil de la conductividad térmica para Discos Rígidos [30, 37, 38], haciendo los resultados generales para Cuerpos Rígidos todavía más interesantes. Nuestra búsqueda nos llevará desde una comprensión de la sutil hipótesis de Equilibrio Local Térmico (*Local Thermal Equilibrium (LTE)*), una piedra angular en las teorías modernas de la Física de no-equilibrio, al descubrimiento de leyes de escala universales en fluidos de no equilibrio, hasta llegar finalmente a una novedosa relación isométrica fluctuante (*Isometric Fluctuation Relation (IFR)*)) para las fluctuaciones de la corriente válida arbitrariamente lejos del equilibrio.

En particular en el capítulo 1 damos una descripción detallada del modelo de discos rígidos así como del algoritmo necesario para simularlo eficientemente. Damos, además, los resultados obtenidos en simulaciones de equilibrio, las cuales hemos usado como comprobación de la bondad de nuestro programa. Encontramos que los perfiles de densidad y temperatura son planos y consistentes con los valores impuestos en la frontera. Notamos, que en otros trabajos donde estudian este sistema en equilibrio, se usan condiciones de contorno periódicas para reducir los efectos de borde. Sin embargo, debido al uso de muros rígidos para simular las fuentes térmicas, encontramos importantes efectos de borde en nuestro sistema. Realizamos un análisis de escalas finitas para caracterizar estos efectos de tamaño, confirmando que desaparecen en el límite termodinámico. También estudiamos la presión medida con dos métodos diferentes. Encontramos que las dos aproximaciones son consistentes y que coinciden con los resultados de otras simulaciones presentes en la literatura [22, 38, 39, 40]. Concluimos de estos resultados que nuestra simulación es correcta y adecuada para estudiar fenómenos de no-equilibrio.

En el capítulo 2 damos una descripción experimental dela Física de no-

equilibrio de nuestro sistema. Nos concentramos principalmente en la descripción de los perfiles de densidad y temperatura que emergen una vez alcanzado el estado estacionario. Encontramos perfiles no-lineales y damos ajustes experimentales que presentan un acuerdo muy bueno con nuestros datos. Le prestamos especial atención a los efectos de borde, que resultan ser más complicados que en el caso de equilibrio. Mostramos como los efectos de borde y de tamaño están enredados, siendo necesario uno para explicar el otro y viceversa. Esto hace que un análisis tradicional de escala sea muy complicado ocultando una descripción clara de nuestro sistema en el limite termodinámico. En el capitulo 4 derivamos un método de escala que nos permite salvar este problema. Para cerrar el capítulo estudiamos un observable principal de los sistemas fuera del equilibrio, la corriente de energía que atraviesa el sistema. Mostramos como esta corriente depende del gradiente externo y del número de partículas.

En el capitulo 3 estudiamos en detalle el papel del Equilibrio Local Térmico (LTE) y si se cumple o no en nuestro sistema. No hay una prueba teórica general de esta hipótesis [30], y confirmar su presencia en simulaciones es muy difícil. Para hacer ésto distinguimos entre LTE macroscópico y microscópico. Para comprobar si el LTE es valido a nivel macroscópico estudiamos si el sistema sigue la Ecuación de Estado de equilibrio localmente. Sorprendentemente, a pesar de estar fuera del equilibrio y del los fuertes efectos de tamaño encontrados en el capítulo 2 para los perfiles de densidad y de temperatura, el sistema sigue localmente la Ecuación de Estado con gran precisión y sin efectos apreciables de tamaño. Es más, los datos obtenidos concuerdan muy bien con los datos presentes en la literatura para simulaciones de equilibrio [41, 42, 39, 40, 43, 44]. Esta ausencia de efectos de tamaño nos ayudará en el capítulo 4 a construir una estrategia que nos permita evitar efectos de tamaño espurios. Para comprobar si el LTE es válido a nivel microscópico estudiamos si las distribuciones globales, de la velocidad y la energía, medidas para nuestro sistema se corresponden con las distribuciones derivadas de la suposición de que el LTE es válido. Aunque no encontramos desviaciones para la distribución global de la velocidad, salvo efectos de tamaño, los segundos momentos de la distribución de energía se desvían sistemáticamente de la predicción de equilibrio local. Encontramos que la diferencia entre estas dos magnitudes depende linealmente del gradiente externo al cuadrado con una pendiente de 1/40. Finalmente encontramos que para gradientes altos y densidades medias altas aparece una coexistencia de fases líquido-sólido. Estudiamos esta coexistencia de no-equilibrio encontrando que la hipótesis de LTE se viola en la parte del sistema ocupada por la fase sólida. Mostramos como la fenomenología de este solido no es equivalente a la del caso de equilibrio. Concluimos de este capítulo que el LTE se cumple a nivel macroscópico (en la fase líquida) y que se encuentran desviaciones a nivel fluctuante.

En el capítulo 4 estudiamos la validez de la ley de Fourier. Para ello, tenemos que diseñar una estrategia para separar los efectos de tamaño estudiados en el capítulo 2, que distorsionan un enfoque directo. Sabemos del capítulo 3 que el Equilibrio Local Térmico se cumple de forma que no presenta efectos de tamaño finito. Usando esto y suponiendo que la ley de Fourier se cumple para nuestro sistema derivamos teóricamente una ley de escala para

los perfiles de un sistema infinito de Discos Rígidos. Esta ley de escala se caracteriza por dos curvas universales de las que podemos derivar cualquier perfil posible. Encontramos que las predicciones de esta teoría concuerdan muy bien con nuestros datos. En particular es extraordinario que todos los perfiles obtenidos para las distintas condiciones externas, y para un numero de partículas dado, colapsen en una curva universal, indicando que la ley de Fourier se cumple en nuestro sistema. Esto implica, como consecuencia de la escala, lo que hemos llamado *"Bulk-Boundary Decoupling"*. Generalmente se cree que, una vez descartado la parte del sistema afectada por efectos de borde, el resto del sistema debe presentar efectos de tamaño finito. Nuestros resultados combinados, de este capítulo y del anterior, sugieren fuertemente que esto no es así. De hecho el sistema se comporta como si fuera infinito cumpliéndose además el LTE y la ley de Fourier, y dejando, como única reminiscencia de su carácter finito sólo dos efectos: una fuente térmica efectiva , compuesta por los baños y la región del sistema afectada por efectos de borde, en donde se concentran todos los efectos de tamaño finito espurios, y una conductividad térmica dependiente del tamaño físicamente relevante, reminiscencia de las conocidas colas para tiempos largos presentes en sistemas de Discos Rígidos [27]. Creemos que este análisis puede tener muchas aplicaciones en la descripción del estado estacionario de fluidos más complejos. De hecho en el apéndice B derivamos una escala para potenciales de núcleo suave que son, en ciertos casos, el comportamiento límite del más realista potencial de Lenard-Jones [45, 46].

En el capítulo 5 nos centramos en las fluctuaciones de la corriente de energía. Derivamos en detalle la recientemente introducida Relación Isométrica Fluctuante (*Isometric Fluctuation Relation (IFR)*) que es una consecuencia de las profundas implicaciones que introduce la reversibilidad temporal a nivel fluctuante. Nuestras medidas concuerdan con la teoría aunque nuestro sistema no cumple, a priori, todas las condiciones de la derivación teórica. Esto sugiere que la Relación Isométrica Fluctuante podría admitir futuras generalizaciones.

Chapter 1

Model

Our way of describing nature is based on the construction of models that approximate reality to a certain precision. However, in practical situations, we have to reach an agreement between a given acceptable precision and the complexity of the model. This is achieved by identifying the most important features of the system at hand, and equipping our model with such characteristics. In our particular case, as we mention in the Introduction, we are interested in general properties of non-equilibrium physics and, more precisely, in heat transport in a fluid. As our intention was to approach this problem form a computational point of view, we needed a model that could describe a fluid in a general form. So, what are the most basic characteristics of a fluid?

We know from Statistical Mechanics that the macroscopic behavior of a set of particles is determined by the microscopic Hamiltonian of the system. This Hamiltonian has two parts. A kinetic term, which accounts for the total kinetic energy of the particles in the system, and a potential term, which accounts for the interactions among particles. Typically the most interesting part, and also the most difficult to treat mathematically, is the potential term. The details of the interaction between the particles that compose the system usually sets the differences between distinct macroscopic behaviors. However for certain macroscopic situations this behavior can be quite similar, as in the case of low density for example.

This fact lead to the engineering of effective potentials that could account for the most relevant parts of the original electrostatic potential. This effective potentials took a mesoscopic look at the problem, using emerging effects due to the fact that there are many particles interacting at once. One of such simplifications is the well contrasted hypothesis of electrostatic screening, which leads to effective potentials which attracting part decays faster than $\frac{1}{r_{ij}^2}$ (where r_{ij} is the distance between particles), and make them tractable from a mathematical point of view. Another key element is the presence of a hard-core repulsion, which describes the Pauli repulsion at short ranges due to the overlapping of the electron's orbitals, and that is necessary in order to prevent a collapse of the system under conditions of high pressure. This basic characteristics can be implemented in different an-

alytical forms. The optimal specific form will depend of the physical system intended to describe.

In our particular case we where interested in far from equilibrium properties, therefore our particular set up is one with high gradients. This leads to situations where the temperature and pressure tends to be very high. In this kind of situations the attractive part of the potential can be neglected because, typically, the kinetic energy of our particles will be much higher than the bound energy necessary to stick two particles together, effectively forbidding this type of configurations. So the only relevant term left, in order to describe the general behavior of the fluid, is the hard core repulsion.

This kind of reasoning lead at the end of the 50's decade to a minimalistic model that was very well suited for the first computational simulations, the Hard Body model [47]. This kind of models are characterize by a potential of the form:

$$V(r_{ij}) = \begin{cases} 0 & if \quad \mid r_{ij} \mid > 2\sigma \\ \infty & if \quad \mid r_{ij} \mid \leq 2\sigma \end{cases} \tag{1.1}$$

Where r_{ij} and σ are the distance between the centers of the particles and it's radius respectively. This potential is equivalent to see the particles as impenetrable bodies and is one of the simpler ways to introduce interactions. Depending on the dimension these particles can be seen as rods (1d) , disks (2d), spheres (3d) or hyper-spheres(d≥4). Despite it's simplicity finding analytical results for this system has been a very hard problem of the past century. The reason for this is the discontinuity that it presents at $r_{ij} = 2\sigma$. However, from a computational point of view, this discontinuity has very useful advantages.

First the system is athermal, i.e. Temperature plays a trivial roll in order to describe it, reducing the problem to the calculation of the number of configurations available for a given packing fraction (entropic configurational term). Another important advantage is that the dynamic of the particles between collisions is that of a free particle. This allow to define relevant events and suppose that the particles follow a strait line between them, eliminating the necessity to solve $2dN$ differential equations, where N is the number of particles in the simulation and d the spatial dimension. These two observations compose the core of the two principal algorithmic ways to simulate Hard Body systems in equilibrium.

On one side we have Montecarlo methods which focus on the probability of going from one configuration to another where we stochastically move one particle, accounting a success if the movement doesn't make two particles overlap and a failure otherwise. On the other, we have Event Driven Molecular Dynamics where the problem is reduced to the calculation of the minimum time between all the possible events that can occur in a given particular configuration, evolve the system to that time, apply the collision rules to the particles involved and repeat the process. Depending on the specific situation both methods will have strong and weak points, nevertheless the algorithmic efficiency of the two has been enhance over the last 60 years to a high degree [48, 38, 49, 50, 51]. However in order to study the stationary state of a set of particles under a temperature gradient we believe that Event Driven Molecular Dynamics is a better fit.

First the modifications we need to introduce in the algorithm is just one special event of collision with a thermal wall. And second, Montecarlo algorithms neglect entirely dynamic effects, which can be important in a non-equilibrium situation. Also is not clear to us how to introduce a non-equilibrium condition in this kind of algorithm without making any assumption on the form of the spatial profiles.

Despite the initial simplicity of this model it's remarkable the number of interesting properties that it possess. Already in the first simulations carried out by Alder et al [28, 52] a transition to a solid state was observed in tree dimensions (hard spheres) and evidence of quasi-long range order was found for the two dimensional case (Hard disks). This was a quite surprising result for a system whose Hamiltonian lacks any attractive term. Moreover, it has a series of properties that makes it very appealing also from a theoretical point of view. First is a deterministic Hamiltonian system, this is interesting due to the fact that a great majority of non-equilibrium studies are based in stochastic models, i.e. they use a description in terms of a Langevin equation [53, 54, 55]. These models have succeeded in proving a lot of non-equilibrium hypothesis. But they are essentially mesoscopic, in the sense that the are based in coarse-grained dynamics, therefore there is not yet a prove form the Hamiltonian dynamics. The most important of these hypothesis being that of Local Thermal Equilibrium [30].

However Hard Disks systems have a property which could complicate the phenomenology, the Long-time Tails for the velocity auto-correlation function. This property was discovered also by Alder and Wainwright in their series of Hard Body simulations [27]. It is characterize by a exponential decay of the velocity auto-correlation function until one value of time (t_{exp}) from which the velocity auto-correlation decay starts to behave like a power law with time $t^{-d/2}$, where d is the dimension of the system. This has serious consequences when trying to calculate the transport coefficients in the framework of linear response theory. In particular the thermal conductivity in two dimensions diverges in the thermodynamic limit. However in a finite system is very difficult to observe this behavior, being necessary to simulate a large number of particles to get ride of boundary effects. On top of that in a system driven out of equilibrium like in our case, the velocity auto-correlation function is additionally modified by the collisions of the particles with the thermal walls, introducing a characteristic time t_{w} related with the mean time elapsed between successive collisions of a particle with one of the thermal walls, when, due to the characteristics of the collision, all the information of the previous values of the velocities is erased. Typically this t_{w} will be less than the necessary time to observe a power law behavior of the velocity auto-correlation function, mitigating, in this way, the effects due to Long-Time Tails.

1.1 Algorithm

The fundamental computational problem we have to solve in order to simulate a hard disk system is finding the minimal collision time between all the possible collision events and the particles involved. In principle it is necessary to calculate the time associated with every event to be sure that

we pick the minimum. However, it's known, since the first simulations carried by Alder , that this strategy is impracticable because, for every step, we would have to do $O(N^2)$ operations, which will impede us to simulate systems sufficiently large. In the paper by Alder [47] this is addressed by a virtual division of the system into boxes. In this way, in order to calculate the possible events associated with a particle, it is only necessary to check the future collisions with particles in the adjacent virtual boxes and keep a track of what virtual box a particle is in.

However this can be further improved. We have to notice that, typically, a collision occurring in one point of the system doesn't have to affect to future events of particles far away of the colliding particle. So, in principle, it will be a good strategy not to recalculate these events. To take advantage of this fact, a new kind of algorithms appeared based in the use of a future event list. In this kind of algorithms an ordered list of future events is generated at the beginning. After picking the first event, the one with minimum time, and evolving the system, new events associated with the colliding particles are introduced in the list and invalidated future events are removed from it. This requires from our algorithm a way in which it can handle efficiently the list and discriminate between valid and invalid future events. There are numerous ways to address this problem, although an optimum strategy usually depends on the density of the system. This is a problem for us because, in a typical configuration of the system in the stationary state, there is a density profile associated to the temperature profile. So we needed an algorithm that have a good efficiency in a wide range of density values. For this reason we chose, between all the possibilities available in the literature[48, 49, 51], the *local minima algorithm (LMA)* developed in the paper of *M. Marín,et al* [48], which has a good consistent efficiency in the complete range of possible density values.

The basic idea of this algorithm is that of 'divide and conquer'. Rather than having a monumental list with all the future events, this algorithm divides it in two parts. The first part consists in a list of future events associated with every particle. Every event in the list have associated the global time when the event is going to occur, the number of collisions the particle (and his partner particle) has suffered until the event was recorded, and the partner element in the collision, which could be a particle, a wall or a virtual wall. Events recorded in the list of the particle i are not recorded in the list of the partner particle. Each of this N lists, where N is the number of particles, has a *local minimum event* , that is, the event with the lowest associated time within the list.

The second part consist in a *Complete Binary Tree (CBT).* In computer sciences a CBT is a data structure that associates to a starting node, called root, two other children nodes (hence binary), and to each of this nodes another two, repeating this process until we have a total of $2N - 1$ nodes. Constructed in this way we will have N *leaves*, or nodes without children, in the last layer to which we will associate our N particles. This structure presents the useful property that any node i, if it has children, they will be located at the indexes $2i$ and $2i + 1$. The use of this CBT is analogous to a

sports tournament. Two sisters leaves compare the time associated with his local minimum event and the index of that with lowest time is copied in the parent node. This process is repeated until one index reach the root. This will be the particle with the lowest global time. After evolving the system and recalculating the new local minima lists for the particles involved, the process is repeated. However only will be necessary to modify the encounters in which the particles get involved, i.e. from the leaves i and j to the root (see figure [1.1]). In this way the accesses to the CBT are minimized increasing effectiveness.

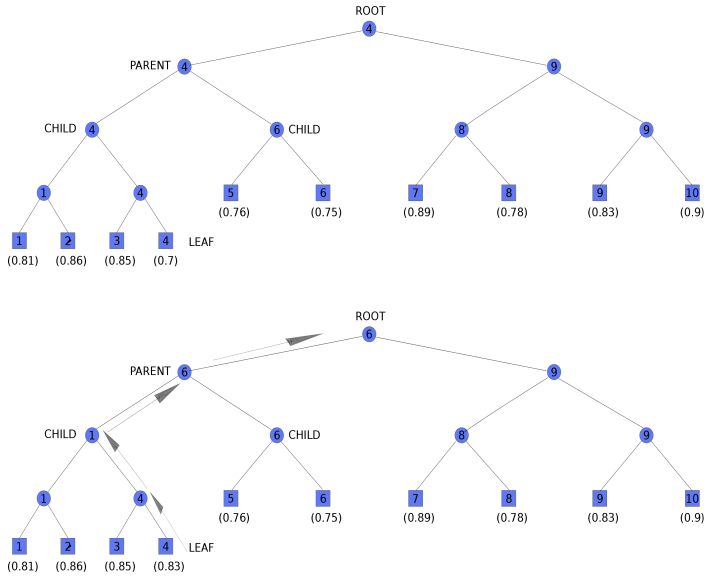

Figure 1.1: CBT structure for $N = 10$. Internal nodes are represented by circles and leaves by squares. Each leaf have a particle assigned. The minimum local time is in parenthesis. On top we can see the result of one 'tournament', notice that particle number 4 was the one with minimum global time. Below we can see that the local time for particle 4 has changed. The actualization is carried out only in the affected nodes, following the arrows. Notice that now is particle 6 the one with minimum global time.

The last element of the algorithm is the strategy to handle the invalidated events. In the original paper, Marin et al, argued that given the nature of the algorithm this kind of events rarely reach the root of the CBT, therefore they decided that, rather than locate and remove the invalidated events, it would be more efficient to check if the event that reach the root is a valid one. As an indicator we use the number of collisions. We compare, for the particles involved in the collision, the actual number of suffered collisions with the one stored in the local minima list. If this number coincides, meaning that the particles didn't collide since the collision was recorded, the event is valid. If the event turn out to be an invalid one, the next event on the local list is

picked and the CBT is updated as in the case of an actual valid collision. In Appendix A we give a copy of the code used with some brief comments.

1.2 Dynamic of the Model

As we saw in the Introduction the evolution of a hard disks system will be determined by the Hamiltonian:

$$H = \sum_{i=1}^{N} \left(\frac{p_i}{2m} + \frac{1}{2} \sum_{j \neq i} V(|\vec{r}_i - \vec{r}_j|) \right) \tag{1.2}$$

With the potential determined by:

$$V(r_{ij}) = \begin{cases} 0 & if \quad \mid r_i - r_j \mid > 2\sigma \\ \infty & if \quad \mid r_i - r_j \mid \leq 2\sigma \end{cases} \tag{1.3}$$

where σ is the radius of the particles. Therefore the equations of movement for the particles between collisions will be that of a free particle, that is:

$$\vec{r}_i(t_{min}) = \vec{r}_i + \vec{v}_i t_{min}$$

Where t_{min} is the minimum global time between all possible future events. To calculate the time we introduce in the local lists we are going to distinguish between three cases:

- *Particle-Particle Event (PPE)*: Given two particles with positions $\vec{r}_1$ and $\vec{r}_2$, and velocities $\vec{v}_1$ and $\vec{v}_2$, after a time t the particles will be at:

$$\vec{r}_i(t) = \vec{r}_i + \vec{v}_i \cdot t \qquad i = 1, 2. \tag{1.4}$$

  The particles will collide only if they are approaching each other, so:

$$(\vec{r}_1 - \vec{r}_2) \cdot (\vec{v}_1 - \vec{v}_2) < 0 \tag{1.5}$$

  Even if this condition is satisfied could be the case that the particles cross each other without colliding. To check if they are going to collide we must see if there is a time t in which the distance between the two particles is equal to it's diameter:

$$(\vec{r}_1(t) - \vec{r}_2(t)) \cdot (\vec{r}_1(t) - \vec{r}_2(t)) = 4\sigma^2 \tag{1.6}$$

  This previous checks reduce considerably the number of times calculations. From the last equation we can obtain the collision time:

$$t_{\pm} = \frac{1}{v^2} \left[-x \cdot v_x - y \cdot v_y \pm \left[4\sigma^2 \cdot v^2 - (x \cdot v_y - y \cdot v_x)^2 \right]^{1/2} \right] \tag{1.7}$$

  where $\vec{r}_1 - \vec{r}_2 = (x, y)$, $\vec{v}_1 - \vec{v}_2 = (v_x, v_y)$ and $v^2 = v_x^2 + v_y^2$. We can do one more further check by looking to the discriminant of this quadratic equation. The particles will collided if $4\sigma^2 v^2 > (x v_y - y v_x)^2$, or equivalently if:

$$2\sigma v > |xv_y - yv_x|$$

Therefore the time of collision between two particles is:

$$t_{col} = \frac{1}{v^2}\left[-x \cdot v_x - y \cdot v_y - \left[4\sigma^2 \cdot v^2 - (x \cdot v_y - y \cdot v_x)^2\right]^{1/2}\right] \quad (1.8)$$

- *Particle-Wall Event (PWE)*: As we will see our particular configuration has periodic boundary conditions in the y direction, so it only will be necessary to calculate the time of collision with the thermal walls. This walls are located at $x_h = 0$ and $x_c = 1$ and the particles will hit them with it's surface, so the time of collision will be:

$$t_{col} = \sigma - x/v_x$$
$$t_{col} = (1 - \sigma - x)/v_x$$

- *Particle-(Virtual Wall) Event (PVE)*: As part of the algorithm we divided the system into virtual boxes with the objective of reducing the number of calculations. However this requires to keep a record of the particles in a given virtual box. When a particle hit a virtual wall we have to actualize the content of that virtual box and the one to which the particle goes. If the particle is in the box (i, j) the walls will be located at $x_l = \frac{i}{N_{VB}}$, $x_r = \frac{i+1}{N_{VB}}$, $y_b = \frac{j}{N_{VB}}$, $y_a = \frac{j+1}{N_{VB}}$, where x_l is the coordinate of the left wall, x_r of the right wall,y_b of the bottom wall, y_a of the above wall and N_{VB} is the number of boxes in one dimension (that is we have a total of $N_{VB} \times N_{VB}$ boxes). We consider that a particle is in a given virtual box if it's center is, therefore only the minimum (positive) time between this four will be recorded in the local lists. The collision times will be:

$$\begin{array}{ll} t_{col} = \frac{x_l - x}{v_x} & t_{col} = \frac{x_r - x}{v_x} \\ t_{col} = \frac{y_b - y}{v_y} & t_{col} = \frac{y_a - y}{v_y} \end{array} \quad (1.9)$$

Now that we have the collision times associated to every event we are going to define the collision rules in each case:

- *Particle-Particle Event (PPE)*: We are going to simulate elastic particles so the momentum and the energy will be strictly conserved. Given two particles with positions $\vec{r}_1$, $\vec{r}_2$ and velocities $\vec{v}_1$, $\vec{v}_2$ the vector that connects the centers of the particles will be $\vec{r}_\parallel = \vec{r}_2 - \vec{r}_1 = (x, y)$ (with $x^2 + y^2 = 4\sigma^2$). Lets define $\vec{r}_\perp = (-y, x)$ as a vector perpendicular to $\vec{r}_\parallel$. The collision rules will be:

$$v'_{1\perp} = v_{1\perp} \quad v'_{2\perp} = v_{2\perp} \quad v'_{1\parallel} = v_{2\parallel} \quad v'_{2\parallel} = v_{1\parallel}$$

Where $v_\perp$ is the projection of the vector $\vec{v}$ over the direction given by $\vec{r}_\perp$, namely $v_\perp = \vec{v} \cdot \vec{r}_\perp / 4\sigma^2$ and $v_\parallel$ is it's projection over the vector in the direction of $\vec{r}_\parallel$, that is $v_\parallel = \vec{v} \cdot \vec{r}_\parallel / 4\sigma^2$. Primed arguments

correspond to the values after the collision. This rules can be expressed in Cartesian coordinates as:

$$v_1'^x = v_1^x + \frac{x}{4\sigma^2} \cdot [x \cdot (v_2^x - v_1^x) + y \cdot (v_2^y - v_1^y)] \tag{1.10}$$

$$v_1'^y = v_1^y + \frac{y}{4\sigma^2} \cdot [x \cdot (v_2^x - v_1^x) + y \cdot (v_2^y - v_1^y)] \tag{1.11}$$

$$v_2'^x = v_2^x - \frac{x}{4\sigma^2} \cdot [x \cdot (v_2^x - v_1^x) + y \cdot (v_2^y - v_1^y)] \tag{1.12}$$

$$v_2'^y = v_2^y - \frac{y}{4\sigma^2} \cdot [x \cdot (v_2^x - v_1^x) + y \cdot (v_2^y - v_1^y)] \tag{1.13}$$

- *Particle-Wall Event (PWE)*: In our simulations we used Stochastic reservoirs. In this kind of reservoirs every time a particle hit the wall it gets a new velocity sorted from a Maxwellian distribution at the temperature of the wall with the condition that the component on the x direction changes it's sign. The distributions are:

$$\begin{aligned} P(v_x) &= \frac{|v_x|}{\sqrt{2\pi T_w}} e^{\frac{-v_x^2}{2T_w}} \\ P(v_y) &= \frac{1}{\sqrt{2\pi T_w}} e^{\frac{-v_y^2}{2T_w}} \end{aligned} \tag{1.14}$$

- *Particle-(Virtual Wall) Event (PVE)*: Due to that a virtual event is not relevant to the dynamic of the system, and in order to minimize the actualization of the position of the particles, the only action performed in this kind of event is an addition of new future events to the lists.

1.3 Arrangement of the Model

All the previous descriptions are valid for a general simulation of Hard Disks. In this section we will concentrate in the specific configuration that we chose in order to study the non-equilibrium stationary state. In figure 1.2 we can see an actual typical configuration of the model stationary state.

The system consist in a squared box of length 1 with periodic boundary conditions in the y direction. The system is driven out of equilibrium by two thermal baths along the x-direction operating at different temperatures. The left wall will always be the hot thermal wall at a temperature T_h, and the right wall will be the cold one at a temperature $T_c = 1$. Due to the athermal property of the Hard Disk system we can always set the temperature of the cold wall to 1 with a trivial rescaling of the measured magnitudes. This point will be investigated in more detail in chapter 2. Therefore the free parameters that we can tune are: the maximum number of particles N_{Max}, the Bulk area density (or packing fraction) $\bar{\eta} = \frac{\pi\sigma^2 N_{\text{Bulk}}}{S}$ and the hot temperature T_h. We are going to work in units where the masses of the particles and the Boltzmann constant are equal to 1.

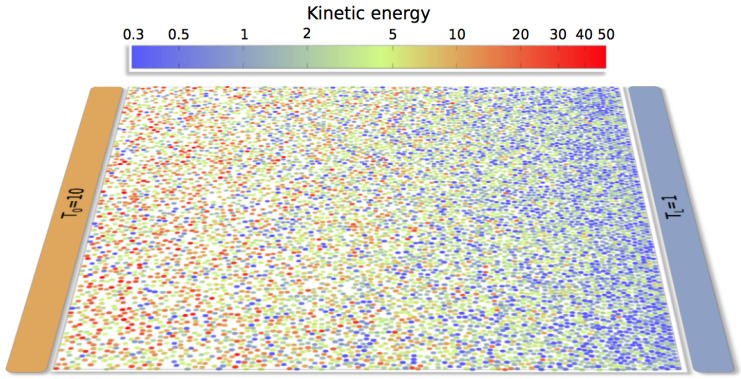

Figure 1.2: Snapshot of a typical configuration with $N = 7838$ hard disks at $\bar{\eta} = 0.5$, subject to a temperature gradient ($T_0 = 10$, $T_L = 1$). Colors represent kinetic energy.

We defined the maximum number of particles (N_{Max}) as the particles that the system would have in a close-packed configuration. However, due to the square geometry of the box, is not possible to fit that number of particles in our system, so our number of simulated particles (N_{Bulk}) will be slightly lower. With this parameters we can calculate the radius of the particles (σ) and the number of Bulk particles (N_{Bulk}). The method used is the following: First we set the radius of the particles to the value that N_{Max} particles will have in a box of surface S in a close-packing configuration.

$$\sigma = \sqrt{\frac{\eta_{\text{cp}} S}{N_{\text{Max}} \pi}} \qquad \text{with} \qquad \eta_{\text{cp}} = \frac{\pi}{2\sqrt{3}} \text{ (close-packing fraction)}$$

Then we place the particles in a hexagonal lattice one by one until we can't add more particles without overlapping them. This will be our initial configuration in positions and the number of particles that we could fit in this way will be the value of N_{Bulk}. Once this is done, we reduce the radius of the particles so that packing fraction of our system match the one introduced as a parameter:

$$\sigma = \sqrt{\frac{\eta S}{N_{\text{Bulk}} \pi}}$$

The initial velocities are drawn from a Maxwellian distribution with temperature $T_v = \frac{T_h + T_c}{2}$. We check that the velocity of the center of mass of the particles is strictly zero. By giving a different set of velocities we can generate the different initial conditions. As the dynamics is event driven, time will be determined by the number of collisions. However in order to make the measurements more intuitive we instead fixed a time. The procedure to chose this time is the following: First we evolved the system for $10^4 N_{\text{Bulk}}$ collisions which we check is sufficient to reach the stationary state. Once the stationary state is reached we measure the mean time in performing $10 N_{\text{Bulk}}$ collisions. From this moment ahead the measurements will be separated by

this interval. In this way the number of collisions between measurements will fluctuate.

In order to make our local measurements we divided the system into 15 virtual boxes along the x direction. We measure the temperature, the packing fraction, the number of particles and the virial pressure associated to those boxes. In the case of the packing fraction and the temperature, if a particle happens to be crossing the virtual wall at that instant, we assign to each box values proportional to the area of the particle overlapping with the box. This is done in order to minimize errors in the calculation of the profiles that, although are negligible in the case of the mean profiles, will be significant when we study the fluctuating profiles in chapter 5.

1.4 Equilibrium Results

In order to check the correctness of the program we performed a set of simulations under equilibrium conditions. For this purpose we set the temperature to equal values and varied the system mean packing fraction and number of particles. The temperature value will be 5 in our particular units, although, due to the athermality of the system, the actual value of the temperature is not relevant and the general behavior of the system can be derived with a simple rescaling of the velocities. In particular the local value of the packing fraction will be the same because it is an adimensional variable. The pressure will have a slightly more complicated rescaling. In order to see this we can look to the general form of the equation of state:

$$P = k_b T \rho Z(\eta) \quad with \quad \rho = \frac{N}{V} = \frac{\eta}{\pi\sigma^2} \tag{1.15}$$

Where ρ is the number density and $Z(\eta)$ is the compressibility factor which is a function of the packing fraction. In the limit of $\eta \to 0$, $Z(\eta)$ should tend to 1 in order to recover the ideal gas behavior. Notice that the Boltzmann constant does not change with a rescaling of the velocities due to the fact that all energy of the system is in the form of kinetic energy. Using the relation between the packing fraction and the number density we can see that our pressure has units of $k_b T/\sigma^2$. The dependence on the square of the radius is problematic because, due to the way in which we defined our system, different system sizes will have different particle radius, therefore the pressure between different system sizes will not be directly comparable. So in order to get a more clear cut view of the phenomenology of the system we can define a new variable $Q = P\pi\sigma^2$ which allow us to get ride of this problem. If we use Q is easy to see that it will depend linearly on the temperature of the system allowing us to relate any result for a particular temperature with the one that we simulated.

Another important technical point is the thermal and density jumps at the boundaries. This effect is observed in many different systems at no-equilibrium [4, 54, 56, 57]. As we will see our results agree in general with the discussions carried out on those papers. Typically the effect is localized in a very narrow portion of the system near the walls and the principal manifestation is a distortion of the measured values at the first and last

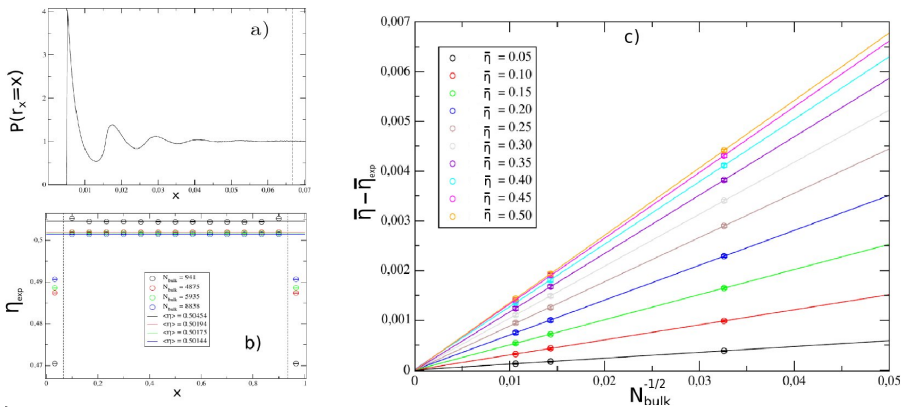

Figure 1.3: a) Discrete probability density for the position of the center of the particles for $N_{\text{Bulk}} = 2900$ and $\bar{\eta} = 0.5$, the doted line represent the limit of the first box. b) Mean experimental packing fractions calculated excluding the first and last observation boxes. c) Finite Size Scaling of the difference between the imposed packing fraction and the measured one.

observation boxes. This jump is much more evident in the density profiles and in this case it appears even for equilibrium conditions. The reason for this behavior are the spatial correlations induced by the hard wall. To illustrate this point in figure 1.3a we represented the discrete probability of finding the center of a particle at distance x from the hot wall. It can be seen that the probability is zero until it reach $x = \sigma$, where we have our first peak. Thenceforth the probability form resembles that of a damped oscillatory motion, although only qualitatively. The actual theoretical expression is more complicated and can be calculated given the radius and the mean packing fraction. In [22] a calculation is provided in the framework of Density Functional Theory which go beyond the scope of this Thesis. For us the important fact will be that the effect is restricted to the observational boxes near the thermal walls and that the perturbation introduced will go to zero in the thermodynamic limit. In figure 1.3b the constant profiles can be seen for $\bar{\eta} = 0.5$ and the different system sizes.

In figure 1.3c we represented the dependence of the difference between the experimentally measured mean packing fraction, taking off the boxes near the walls, and the impose packing fraction versus the number of particles. Although we have simulated only 4 system sizes, we can see that the expected $N_{\text{Bulk}}^{-\frac{1}{2}}$ dependence is in very good agreement with our data and yields a value of zero difference in the limit $N_{\text{Bulk}} \to \infty$. For completeness in Table 1.1 we give the parameters of the linear fit.

The temperature is not affected by finite size effects on these equilibrium configurations. In figure 1.4 we represented the temperature profiles for different system sizes and different packing fractions. We can see that there is no jump in the values of the temperature neither is an appreciable dependence with the number of particles or the packing fraction. Furthermore the

η	Slope	Intercept(10^{-6})	R
0.05	$0.0119\pm0.5\cdot10^{-4}$	-4±1	0.9999814
0.10	$0.0307\pm3\cdot10^{-4}$	-9±5	0.9999297
0.15	$0.0509\pm4\cdot10^{-4}$	-8±9	0.9999245
0.20	$0.0699\pm3\cdot10^{-4}$	4±7	0.9999777
0.25	$0.0889\pm9\cdot10^{-4}$	-3±12	0.9998949
0.30	$0.1050\pm1\cdot10^{-4}$	-1±3	0.9999984
0.35	$0.1172\pm3\cdot10^{-4}$	-10±7	0.9999924
0.40	$0.1253\pm4\cdot10^{-4}$	2±7	0.999991
0.45	$0.1317\pm13\cdot10^{-4}$	4±25	0.9999039
0.50	$0.1355\pm1\cdot10^{-4}$	-8±1	0.9999998

Table 1.1: Parameters of the fit shown in figure 1.3c

value throughout the system is equal to the imposed value.

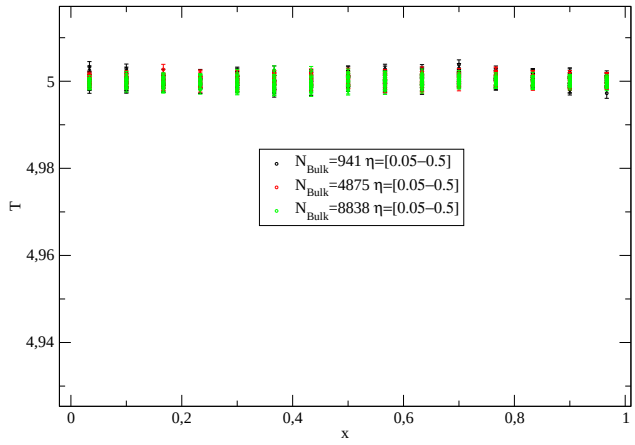

Figure 1.4: Temperature profiles for different N_{Bulk}. Finite size effects are negligible.

The pressure is a well defined concept in a closed system where particles interact with the wall of its container:

$$P_w = \frac{1}{L_y \tau_{\text{col}}} \sum_{n=1}^{N_{\text{col}}} \Delta p_{x,n} \tag{1.16}$$

where the sum extends to all N_{col} collisions with the wall (assumed to be vertical) occurring on the time interval τ_{col}. Such collisions take place at instants t_n, and $\Delta p_{x,n} = \lim_{\epsilon\to 0}[p_x(t_n+\epsilon) - p_x(t_n-\epsilon)]$ is the linear momen-

tum variation on the perpendicular direction to the wall after the collision with it.

On the other hand at equilibrium one can use the virial theorem to compute the pressure. In the hard disk case one gets [58]:

$$P_v = \frac{NT}{L_x L_y} + \frac{1}{2L_x L_y \tau_{\rm col}} \sum_{n=1}^{N_{\rm col}} \vec{r}_n \cdot \vec{v}_n \tag{1.17}$$

This sum is similar to the wall case but now it extends to *any* particle-particle collision and $\vec{r}_n = \vec{r}_i(t_n) - \vec{r}_j(t_n)$, $\vec{v}_n = \vec{v}_i(t_n) - \vec{v}_j(t_n)$ with (i, j) the pair of particles colliding at instant t_n.

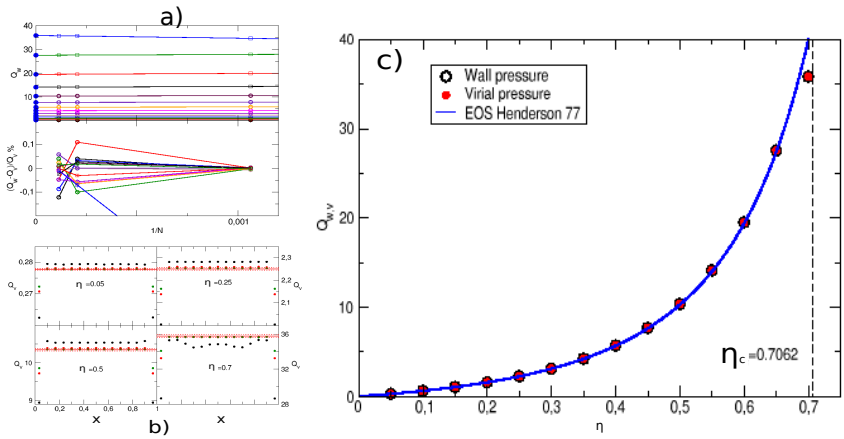

Figure 1.5: a) Wall pressure and virial pressure (see text) computed for a set of systems at equilibrium with temperature $T = 5$, several mean areal packing fractions $\bar{\eta}$ and three different sizes. Solid blue symbols are a linear extrapolation of the data for a given areal density. Below we show the relative error (in %) obtained between the wall pressure and the virial pressure. b) Virial pressure profiles. Red lines are the linear extrapolation fit of the values of the virial pressure, obtained by averaging boxes from 2 to 14 (both included), for the three different sizes. Dotted lines are the error of such extrapolation. c) Extrapolations to infinite size obtained for the wall pressure and virial pressure as a function of the mean packing fraction. Solid line is the value of the pressure obtained by the Henderson equation of state [22]. Dashed line is the expected value for the critical density where a phase transition occurs for a hard disk system at equilibrium.

Our intention is to compare these magnitudes under our non-equilibrium configurations with the aim to check is there is any kind of mechanical equilibrium in those cases. However under equilibrium conditions these two magnitudes should yield the same value. We used this fact to check the validity of our program by performing 42 simulations at equilibrium with the stochastic boundaries at $T = 5$, three system sizes $N_{\rm Bulk} = 941, 4875, 8838$ and 14 different mean packing fractions: $\bar{\eta} = 0.05, \ldots, 0.7$.

Wall pressures are measured at the boundaries $x = 0$ and $x = 1$. The averaged values are shown in Figure 1.5a where we compare it with the mean virial pressure. In figure 1.5b we measured it at each of the 15 boxes of the system. We can see that there is a well defined spatial structure at the boundaries (boxes 1 and 15) but it is almost constant on the bulk. We defined as the virial pressure the average over the 13 cells where the local virial pressure values are constant. We see that the relative error between the wall pressure and the local virial pressures are, at most, of the 0.1% for each size and it is smaller than the respective error bars. It is curious to realize that the wall pressure, which is measured with particles that are part of boxes 1 or 15 colliding with the wall, is equal to the virial pressure of central boxes, but different from the virial pressure calculated on those boxes. We think that such boundary deviations are due to the already mentioned spatial correlations of the density near the wall.

We linearly extrapolated the three sizes to obtain an *infinite size* wall and virial pressure values for each packing fraction. In Figure 1.5c we represented their values and compare the data with the Henderson'77 [22] equation of state for hard disks

$$Q_{H77} = \eta T \left[\frac{1 + \eta^2/8}{(1-\eta)^2} - 0.043 \frac{\eta^4}{(1-\eta)^3} \right] \tag{1.18}$$

where in our case $T = 5$. The coincidence is very good except when we approach the density for the transition gas-liquid at $\eta_c = 0.7062$. It is known that the equation of state (1.18) it is one of the best for densities less than $\eta \simeq 0.65$ but it doesnt reproduce at all the phase transition.

After performing this analysis of a equilibrium configuration we are confident that our program works correctly. It also allows us to get a first impression on the boundary effects present for this kind of simulation. This effects are remarkable in the case of the packing fractions where the spatial correlations, occurring due to the use of hard walls, became significant for a finite number of particles. This behavior is transferred to the measurement of the virial pressure. However we saw that in both cases these effects disappear in the thermodynamic limit.

Chapter 2

Non-equilibrium Stationary State

In this chapter we are going to deal with one of the simplest cases of non-equilibrium phenomena. When a system is put in contact with at least two thermal reservoirs at different temperatures, it evolves towards a stationary state. In the case of a fluid this stationary state is characterized not only by a temperature profile, but also, as the particles are free to move around in the system, by a nontrivial density profile. The goal of a macroscopic description of this system will be to give a theoretical expression, in the limit of large number of particles, for the profiles in term of the parameters of the system. In our case these are the mean density and the temperature of the hot bath. Following de Groot and Mazur [7], this profiles will be determined by continuity equations relating the fluxes across the system with the gradient imposed. However, this approach use as a given fact that certain constitutive phenomenological relations, diffusion like type of equations, hold for the system at hand. In this way, in order to apply this theory, it will be necessary to give a microscopic foundation to the phenomenological law and, in case it is correct in all regimes, calculate the constants that relates the fluxes with the gradients. In the case of thermal transport the constitutive equation is the well known Fourier's law. It states that the flux of energy (J) it's related to the gradient of temperature by means of a constant, the thermal conductivity (κ) :

$$J = -\kappa \nabla T_{\text{ext}} \tag{2.1}$$

It's important to notice that this is a purely phenomenological law derived from experiments of heat transport in which, although a reading is recorded with a thermometer, we can't, in general, relate that measurement with an actual thermodynamic temperature of the system. In order to do this, we have to add to our theoretical description the strong hypothesis of Local Thermal Equilibrium (LTE). This hypothesis is based on the assumption that the time necessary to achieve a local thermalization of the system is very small, when compared with the characteristic time of the non-equilibrium process. This allows to define locally a temperature, density and pressure as well as to use locally any equilibrium thermodynamic relation. If we assume

that LTE holds, the expression for κ will depend on the local values of the density and temperature. In this way we can define a local Fourier law as:

$$J = -\kappa(\eta, T)\frac{dT}{dx} \tag{2.2}$$

To test if this relation is valid locally we are going to calculate the conductivity using expression 2.2 for a wide number of configurations that are far from equilibrium. If the calculated value is independent of the external gradient applied we can conclude that Fourier's Law holds. This will require an analysis of the profiles and their size and boundary effects. Such a direct approach is rarely seen in the literature.

Despite of the many papers using the Hard Disks system at equilibrium, is remarkable that there are only a few studying this system under actual non equilibrium conditions, some notable exceptions are the papers by Risso and Cordero [57, 59] and Mareschal et al [60, 56, 61]. We believe this is due to the great difficulties arising in this kind of studies. Since the first simulations of equilibrium systems, boundary effects have been a mayor concern. The general strategy to mitigate these effects is the use of periodic boundary conditions. However this type of boundaries are incompatible with a direct use of a thermal reservoir. This led to a number of simulation methods where the reservoirs are substituted by a modification of the dynamics of the particles, which allow to conserve the periodic boundary conditions [62, 63]. Without detracting those approaches, we believe that a direct treatment is potentially more clear. Furthermore, the exponential growth in computational power allows us now to simulate larger systems, with the hope of survey these boundary effects.

To try to shed some light into these questions in this chapter we are going to characterize the general morphology of the non-equilibrium stationary state. First we are going to focus on the temperature and density profiles, how they depend on the gradient applied, the mean density of the system and the number of particles. We will give experimental fits to these profiles and will try to analyze the size and boundary effects. Next we are going to focus on the energy flux across the system and its dependence on the various parameters used. The question of the validity of LTE hypothesis will be treated in the next chapter.

Before we proceed to analyze the results of the profiles we want to mention an important technical issue. As explained in section 1.3 we divide our system into measurement boxes. The number of boxes is fixed for every system size so, even in the thermodynamic limit, this boxes will have a macroscopic character, and due to the nonlinear dependence of the profiles with the x coordinate is expected that the measured values differ from the actual values at the center of the box. In order to correct this effect we are going to use a Taylor series expansion around the center of the box.

Let's T_C and η_C be the local temperature and areal density measured in a box centered at x_c of size Δ. Assuming that there exist temperature and density profiles $T(x)$ and $\eta(x)$ we can relate both by:

$$T_C = \frac{1}{\Delta\eta_C}\int_{x_c-\Delta/2}^{x_c+\Delta/2} dx\,\eta(x)T(x) \quad , \quad \eta_C = \frac{1}{\Delta}\int_{x_c-\Delta/2}^{x_c+\Delta/2} dx\,\eta(x) \tag{2.3}$$

We can expand the profiles around x_c inside a box and make the integrals. We keep results up to Δ^2 order:

$$\begin{aligned} T_C &= \frac{1}{\eta_C}\left[\eta(x_c)T(x_c) + \frac{\Delta^2}{24}\frac{d^2}{dx^2}\left[\eta(x)T(x)\right]_{x=x_c} + O(\Delta^3)\right] \\ \eta_C &= \eta(x_c) + \frac{\Delta^2}{24}\frac{d^2\eta(x)}{dx^2}|_{x=x_c} + O(\Delta^3) \end{aligned} \tag{2.4}$$

We get the desired result inverting the above expressions and discretizing the derivatives using the values of the neighbor boxes:

$$\begin{aligned} T(x_c) &= T_C - \frac{1}{24}\left[\frac{2}{\eta_C}(\eta_{C+1} - \eta_C)(T_{C+1} - T_C) + T_{C+1} - 2T_C + T_{C-1}\right] \\ \eta(x_c) &= \eta_C - \frac{1}{24}\left[\eta_{C+1} - 2\eta_C + \eta_{C-1}\right] \end{aligned} \tag{2.5}$$

Typically the corrections are small (0.1%) but, as we will see, relevant to study deviations from the local equilibrium predictions.

We performed simulations with a large set of different parameters. In table 2.1 we give a summary of them.

N_{Bulk}	∇T_{ext}	$\bar{\eta}$
1456	[1,2,...,18,19]	0.5
2244	[1,2,...,18,19]	0.5
2900	[1,2,...,18,19]	0.5
	9	[0.05,0.1,...,0.65,0.7]
	19	[0.05,0.1,...,0.65,0.7]
	[1,2,...,18,19]	0.7
3729	[1,2,...,18,19]	0.5
4367	[1,2,...,18,19]	0.5
5226	[1,2,...,18,19]	0.5
5935	[1,2,...,18,19]	0.5
	2	[0.650,0.655,...,0.750,0.755]
6853	[1,2,...,18,19]	0.5
7838	[1,2,...,18,19]	0.5
	[1,2,...,18,19]	0.7
8838	[1,2,...,18,19]	0.5

Table 2.1: Summary of all the external parameters used in the simulations.

2.1 Temperature profiles

In figure 2.1a we can see the typical shape of the temperature profile for our system. The profile is smooth and non linear for all temperature gradients, although they become more linear as we decrease the gradient. It is also observed a small difference between the extrapolated temperature at $x = 0$ and the impose temperature of the wall. We did a phenomenological analysis

to the temperature profiles. We tried several analytical forms and the one with which we obtained better results was: $T(x)^{\alpha} = a + bx$. This form was deduced for some two-dimensional Hamiltonian and stochastic models [64]. In table 2.2 we see the coefficients obtained.

∇T_{ext}	a_0	a_1	α	χ^2	R
1	1.612	-0.603	0.699	2.051e-06	0.999999
2	2.158	-1.144	0.709	7.42298e-07	1.000000
3	2.643	-1.626	0.709	3.03581e-06	1.000000
4	3.093	-2.075	0.709	1.26663e-05	0.999999
5	3.538	-2.521	0.712	3.95863e-05	0.999999
6	3.931	-2.914	0.710	0.000106999	0.999998
7	4.324	-3.309	0.710	0.000180338	0.999998
8	4.722	-3.710	0.712	0.000379898	0.999996
9	5.103	-4.095	0.713	0.000564661	0.999996
9.5	5.306	-4.301	0.715	0.000791723	0.999995
10	5.498	-4.495	0.716	0.000945252	0.999994
11	5.833	-4.833	0.715	0.00123657	0.999994
12	6.222	-5.230	0.718	0.00172625	0.999993
13	6.574	-5.589	0.719	0.00233933	0.999991
14	6.923	-5.945	0.719	0.00275901	0.999991
15	7.276	-6.306	0.721	0.00426485	0.999988
16	7.591	-6.628	0.720	0.00465778	0.999989
17	7.987	-7.039	0.724	0.00638423	0.999986
18	8.319	-7.379	0.724	0.00681082	0.999987
19	8.558	-7.628	0.721	0.00744746	0.999987

Table 2.2: Fit coefficients for $N_{\text{Bulk}} = 8838$ and $\bar{\eta} = 0.5$. Notice that when the gradient applied is low, we get a correlation coefficient of 1 or nearly 1, indicating that, maybe, our assumed analytical form has too many parameters for these data. For these gradients the profiles are almost linear.

One remarkable thing about these fits is the weak, but systematic, dependence of the α coefficient with the gradient applied. This coefficient has also very little dependence on the number of simulated particles. To illustrate this in figure 2.1b we give α as a function of ∇T for the different simulated system sizes.

Despite the apparent very good agreement between our fits and the measured values, we detected a number of inconsistencies that hamper the physical meaning of the $T(x)^{\alpha} = a + bx$ law. First we must mention the practical difficulties of the fitting algorithm. Due to the great variability of the values of the temperatures any maximum likelihood method will try to adjust better the higher values of our curve. In return the lower values, namely those near the cold bath, will be poorly adjusted. The consequence of this miss mach is dramatic for high gradients, in the sense that our phenomenological fits give an extrapolated value of the temperature at $x = 0$ below that of the thermal wall, which is totally nonphysical.

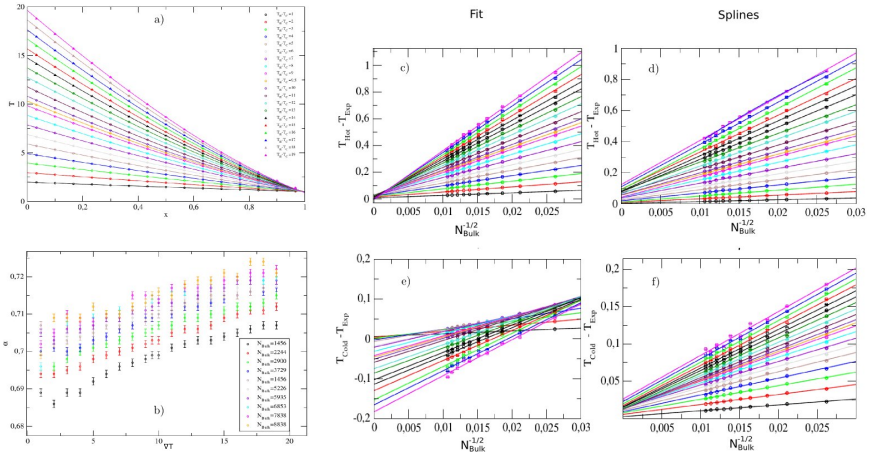

Figure 2.1: a) Temperature profiles for $N_{\text{Bulk}} = 8838$ and $\bar{\eta} = 0.5$. b) α parameter as a function of the gradient for the different simulated system sizes. c) Difference between the extrapolated value and the imposed value at the two walls. Beside the results for our fit, we represent the results using an interpolation by cubic splines extrapolated to the position of the walls.

This fact is more evident when we try to analyze the behavior of the boundary effects. These effects are usually constrain to the measurement boxes near the walls [57, 4] and, as the number of particles of the system goes to infinity, the difference between the extrapolated value and the imposed value should tend to zero. We study the extrapolations to the wall by two methods. The first is the already mentioned extrapolation from the non-linear fits, the second is a cubic splines interpolation extended to the points $x = 0$ and $x = 1$. In figure 2.1c we represented the imposed temperature minus the extrapolated temperature as a function of $N_{\text{Bulk}}^{-1/2}$ for the two methods.

As we can see, for small gradients the two methods give the same result of zero difference in the large number of particles limit. For large gradients it is not longer clear that this zero difference should be the limiting value, although we strongly believe that simulations with more particles will probably settle that there is no gap. It is also clear that the given extrapolation for the temperature at $x = 1$ give a erroneous behavior in this limit.

The second inconsistency that we observe, has to do with the behavior of the exponent with the mean packing fraction $\bar{\eta}$. In figure 2.2a we can see the temperature profiles for $T_H = 20$, $T_C = 1$ and $\bar{\eta}$ in the range $[0.05 - 0.80]$ and in table 2.3 a summary of the fit parameters.

We can see in Figure 2.2b that the α parameter has a non trivial dependence with mean packing fraction. However in our system we have a density profile associated with the temperature profile, therefore this strong dependence of the exponent on the areal density, is another clear sign of the phenomenological character of this law.

Finally we want to make some comments on the general aspect of the size effects associated with the temperature profiles. In Figure 2.3 we plot the

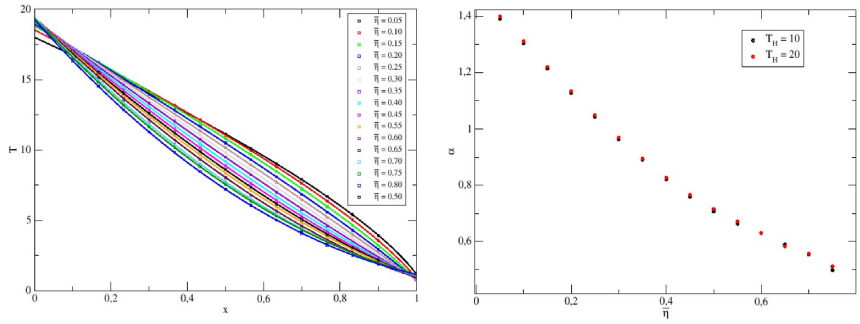

Figure 2.2: a) Temperature profiles for $\nabla T = 19$. We can see how the profiles changes from convex to concave as we increase the mean packing fraction. b) Dependence of the α parameter with the mean packing fraction.

$\bar{\eta}$	a_0	a_1	α	χ^2	R
0.05	57.00	-55.76	1.399	0.00633408	0.999984
0.10	45.90	-45.12	1.311	0.00097683	0.999998
0.15	35.85	-35.20	1.220	0.000874132	0.999998
0.20	28.01	-27.36	1.133	0.00329832	0.999994
0.25	22.02	-21.31	1.049	0.00694016	0.999987
0.30	17.49	-16.71	0.969	0.0099943	0.999982
0.35	14.08	-13.22	0.894	0.011538	0.999979
0.40	11.54	-10.62	0.826	0.0114494	0.999980
0.45	9.650	-8.685	0.765	0.00988003	0.999983
0.50	8.315	-7.323	0.715	0.00677496	0.999988
0.55	7.313	-6.313	0.671	0.00325825	0.999994
0.60	6.477	-5.518	0.630	0.0043217	0.999992
0.65	5.636	-4.690	0.583	0.0154027	0.999973
0.70	5.214	-4.187	0.557	0.00376188	0.999993
0.75	4.557	-3.485	0.512	0.00122979	0.999998
0.80	3.921	-2.864	0.462	0.00525047	0.999990

Table 2.3: Fit coefficients for $N_{\text{Bulk}} = 2900$ and $\nabla T_{\text{ext}} = 19$.

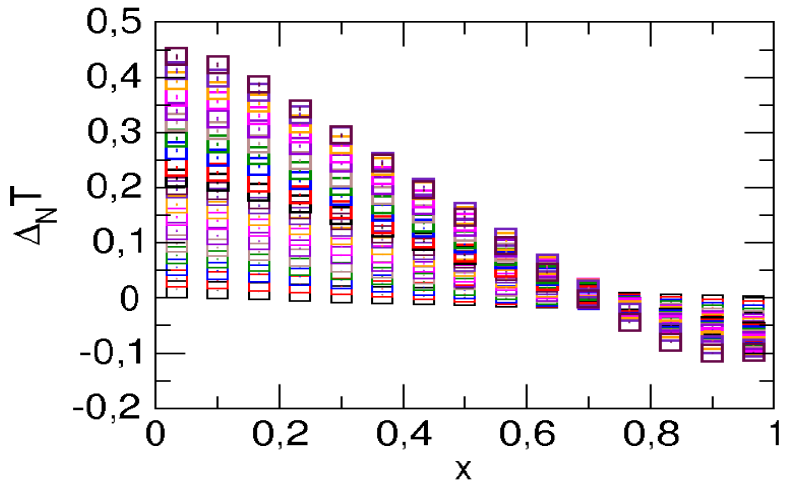

Figure 2.3: Difference between the temperature profiles for the largest and smallest system simulated ($N_{\text{Bulk}} = 8838$ and $N_{\text{Bulk}} = 1456$) and $\bar{\eta} = 0.5$. As the gradient applied grows also grows the difference between the profiles

differences between the profiles for $N_{\text{Bulk}} = 8838$ and $N_{\text{Bulk}} = 1456$ ($\Delta_N T$). Notice that if we exclude the boxes near the walls the differences are almost linear. We can think about this effect as a tilt of the profiles. This tilt is more pronounced for smaller number of particles but the general form of the profiles is quite similar. We can conclude from the morphological analysis performed that, despite the smoothness of the temperature and the good behavior of the gap with the number of particles, the global form of the bulk profiles has a strong dependence on the size of the system caused by boundary effects which are difficult to get ride off.

2.2 Density profiles

When the system reach the stationary state we will have an areal density profile associated to every temperature profile. The zones of the system with high temperature will correspond with zones of low areal density, making the pressure across the system constant, i.e. we will have a sort of mechanical equilibrium. In chapter 3 we will inspect with more detail the validity of this assertion, which depend on the validity of the LTE hypothesis for our system. Nevertheless we are going to describe the general morphology of our system at the stationary state as we did in the case of the temperature. This will give us some intuition on the general forms of the profiles as well as the typical boundary effects and size dependence appearing in our system.

In figure 2.4a we can see the typical shape of our density profiles. As now we don't have a theoretical expression to check, we tried different forms for the fits. The one that worked better in all the range of temperature gradients has this form $\eta(x) = \frac{a_0}{(x-a_1)}$. This fits are the solid lines in the

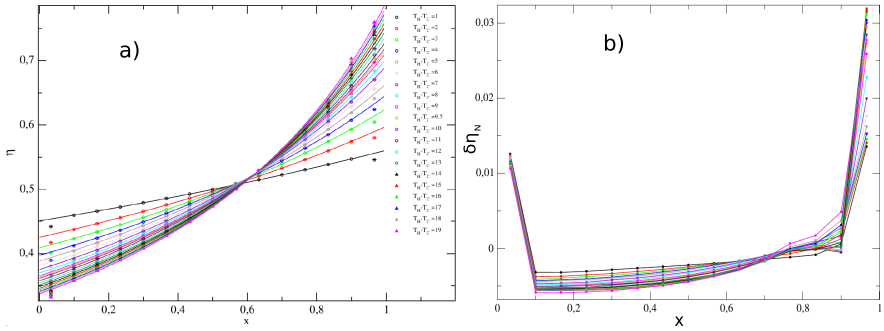

Figure 2.4: a) Density profiles for $N_{\text{Bulk}} = 8838$, $\bar{\eta} = 0.5$ and all simulated temperature gradients. b) Difference between the areal density profiles for the largest and smallest system simulated ($N_{\text{Bulk}} = 8838$ and $N_{\text{Bulk}} = 1456$) and $\bar{\eta} = 0.5$.

figure, and, as we did with the temperatures, the first and last measurement boxes where excluded to perform the fits. In table 2.4 we give the values of the parameters obtained for $N_{\text{Bulk}} = 8838$ and $\bar{\eta} = 0.5$.

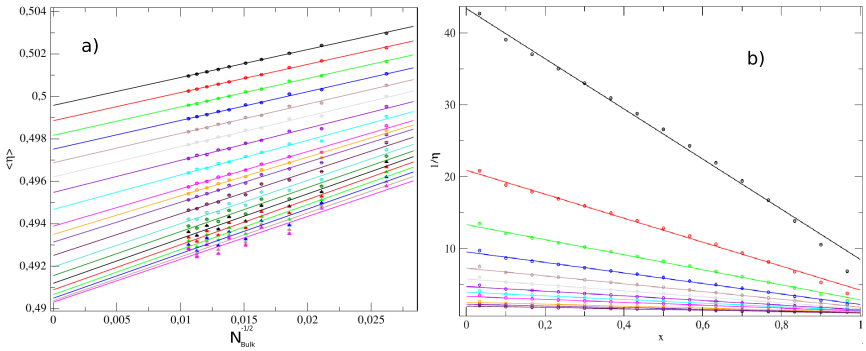

Figure 2.5: a) Average areal density among boxes from 2 to 14, both included, as a function of $N_{\text{Bulk}}^{-1/2}$. Gradients represented from top to bottom $\nabla T = 1, 2, ..., 19$, and $\bar{\eta} = 0.5$. b) Profiles of $1/\eta$ and linear fits excluding the first and last measurement boxes for $N_{\text{Bulk}} = 2900$, $T_h = 20$ and, from top to bottom, $\bar{\eta} \in [0.05, 0.1, ..., 0.65]$

We can see a few interesting things in this plot. First the variation of the areal density profiles with the temperature gradient slows down for high gradients. Notice that for high gradients the areal density values near the cold wall get over 0.7, which is approximately the solidification value of this system. When this happens the compressibility of the fluid gets substantially reduce conditioning the values of the rest of the profile. In chapter 3 we will study this non-equilibrium phase coexistence in detail. We must also notice that significant areal density jumps appear near the walls. The origin of this jumps is the same as in the equilibrium case, namely the spatial correlations

∇T_{ext}	a_0	a_1	χ^2	R
1	-2.30337	5.1114	0.000242038	0.993018
2	-1.47259	3.46478	0.000248798	0.997050
3	-1.18269	2.89353	0.000254347	0.998055
4	-1.03022	2.59477	0.000249135	0.998556
5	-0.935133	2.40951	0.000230397	0.998904
6	-0.869076	2.28153	0.000210437	0.999148
7	-0.819863	2.18686	0.000190456	0.999345
8	-0.781439	2.11347	0.000194851	0.999448
9	-0.749991	2.0537	0.000239563	0.999442
9.5	-0.736242	2.02764	0.000268645	0.999422
10	-0.723447	2.00338	0.000299379	0.999396
11	-0.700595	1.95995	0.000352542	0.999351
12	-0.680255	1.92128	0.000379049	0.999345
13	-0.66224	1.88688	0.000370906	0.999383
14	-0.6466	1.85706	0.000361199	0.999411
15	-0.63258	1.83034	0.00034679	0.999441
16	-0.619727	1.80572	0.000313606	0.999484
17	-0.607979	1.78326	0.000284289	0.999516
18	-0.598009	1.76424	0.000271581	0.999526
19	-0.587645	1.74421	0.000252256	0.999533

Table 2.4: Fit parameters for $N_{\text{Bulk}} = 8838$ and $\bar{\eta} = 0.5$

induce on the particles by the hard wall. However now it is not possible to apply the same theoretical formalism that we suggested in the equilibrium case. The reason for this is that, in order to apply it, we have to know the areal density near the wall. However, now this areal density will depend on the particular form of the profiles which in return will depend in the boundary effects. Furthermore, if we try to do an analysis of the mean areal density, as we did in the equilibrium case, now we don't get a clear result due to the no linearity of the profiles. In figure 2.5a we plot the size dependence of the mean packing fractions, measured in the central boxes, for the different gradients. We can see that the limit mean areal density changes with the gradient. This limiting value will depend on the global analytical form of the limit density profile, therefore, without some information on how this profile might be, we can't compare our results. Nevertheless the analytical form used to describe the areal density profiles works very well across the whole range of temperature gradients.

As we did with the temperature, we checked is this simple fit will work for other mean packing fractions. To better appreciate a possible deviation from our analytical form we represented, in Figure 2.5b, $1/\eta$ as a function of x. If our analytical form is correct we should see a linear dependence. However we see that for areal densities in the range of $\bar{\eta} \in [0.05, 0.20]$ a strait line is not sufficient to fit the data. This indicate that our simple law breaks down for low mean packing fractions.

Finally we want to give some comments on the size dependence of the

specific shape of the areal density profiles. In Figure 2.4b we represented the difference between the profiles for the largest system simulated $N_{\text{Bulk}} = 8838$ and the smallest one $N_{\text{Bulk}} = 1456$. We see that the size dependence is of the order of 2% as in the case of the temperature profiles, however now the form of the differences is more complicated. First we can see that the areal density differences at the boxes 1 and 15 differs from the difference at the bulk and they are not equal between them. In the the box near the hot boundary, $x = 0$, the difference is almost independent of the gradient applied, in contrast with the box near the cold wall, $x = 1$, where there is a significant dependence with the gradient. And second now the difference is not quasilinear for moderately high gradients, $\nabla T_{\text{ext}} \geq 6$, i.e. this difference is not a small tilt of the profiles but an intrinsic change of behavior. We believe that this is caused, apart from the mentioned spatial correlations induced by the hard wall, by a liquid-solid coexistence near the cold wall, which we will study in detail in chapter 3.

2.3 Heat Current

We define the heat current as the average energy transmitted in any of the thermal walls per unit time. That is,

$$j_w = \frac{1}{L\tau} \sum_{\text{col}} (\Delta E_c)_{\text{col}} \tag{2.6}$$

In our case, we sum over particle collisions the increments of kinetic energy each time that a particle hits a given thermal wall and divide over the time between measurements τ. As we mentioned in section 1.3 τ is the average time in which the system performs $10N$ collisions.

In Figure 2.6 we can see that τ scales with $N^{-1/2}$. That can be understood by using a kinetic theory argument. We know that the collision frequency is given by

$$\Gamma = \frac{Nv}{2l} \tag{2.7}$$

where $v = (\pi k_B T/2m)^{1/2}$ is the mean velocity and $l = \pi r/4\sqrt{2}\theta\eta$ being θ the pair correlation function at contact which is a function of the areal density. In our case $\Gamma = 10N/\tau$ and $\eta = N\pi r^2/L^2$ and therefore $\tau \simeq r \simeq N^{-1/2}$ because when we change N, we change r in order to maintain η constant. For each gradient we fit a second order polynomial in $1/N$ to the data and we extrapolate to the infinite size value. We see in figure 2.6 the smooth dependence of the data on $1/N$ (left figure) and the extrapolation points. In figure 2.6 (right) we plot the τ dependence on T_0 for each size and we included the extrapolated data to the infinity size (red solid circles). We see that size effects are not important for $N^{1/2}\tau$. We have found an effective fit to the infinite size extrapolated data:

$$\tau N^{1/2} = 2.9865 \left(\Delta T_{\text{ext}} + 1.8365\right)^{-0.457} \tag{2.8}$$

In order to do the fit we have included the equilibrium Enskog value for $\tau N^{1/2} = 2.2627$ that is obtained by using $\theta = (1 - 7\eta/16)/(1 - \eta)^2$ in the

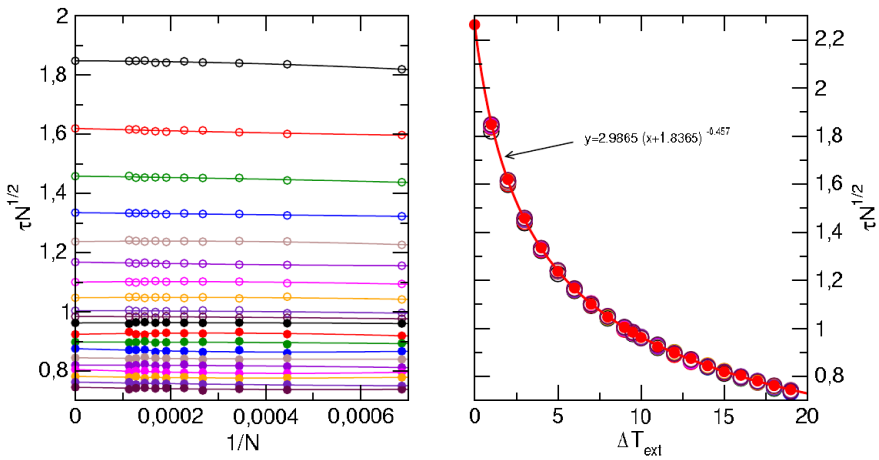

Figure 2.6: Left: Averaged time between $10N$ collisions for $T_0 = 2, 3, \ldots, 20$ (from bottom to top) and $T_1 = 1$ as a function of $1/N$ for $\bar{\eta} = 0.5$. The points on the $x = 0$ axis correspond to the extrapolation of a parabolic least square fit to the data (solid lines) for each T_0. Right: Behavior of the scaled measurement time τ as a function of the gradient.

above formulas. We see that $\tau N^{1/2} \simeq \Delta T_{\text{ext}}^{-0.457}$ for large gradients. Of course this is an effective fit but we tried many more regular ones and we only succeed with such singular one.

We have measured the energy current through the hot and cold thermal walls and both give the same results in average. We first find that the natural scale for j_w is $r \simeq N^{-1/2}$. Moreover, the moments of the current also scale with τ as $m_k(j_w) \simeq \tau^{k-1}$. In this way we can fit smooth second order polynomials in $1/N$ for each gradient data set and we get good extrapolations to the infinite value limit.

We see that the energy current increases following a nonlinear law:

$$j_w = 1.9232\Delta T_{\text{ext}} + 1.3639\Delta T_{\text{ext}}^{3/2} \tag{2.9}$$

We use this behavior because we taken into account that for small ΔT_{ext} values we expect a linear regime as Fourier's Law predicts. On the other hand, for large values of the gradient the interaction between particles is not dominant compared with their kinetic energy and thus, the thermal conductivity should behave as $T^{1/2}$. That is, the Fourier's law in this case is $j_w = -T^{1/2}dT/dx$ and solving the equation we get that $j_w \simeq \Delta T_{\text{ext}}^{3/2}$. The rescaled second momentum of j_w seems to follow a less singular behavior as a function of ΔT_{ext}. In fact we fit a third order polynomial (see Figure 2.7). The rescaled third momentum seems to have a similar behavior as the second one but it tends to zero with N large. We cannot exclude the zero value of m_3 for all ΔT_{ext} when $N \to \infty$. Finally, the kurtosis deviates from the pure Gaussian value 3 for small systems but it moves consistently towards it as the size of the system increases, also we find no systematic

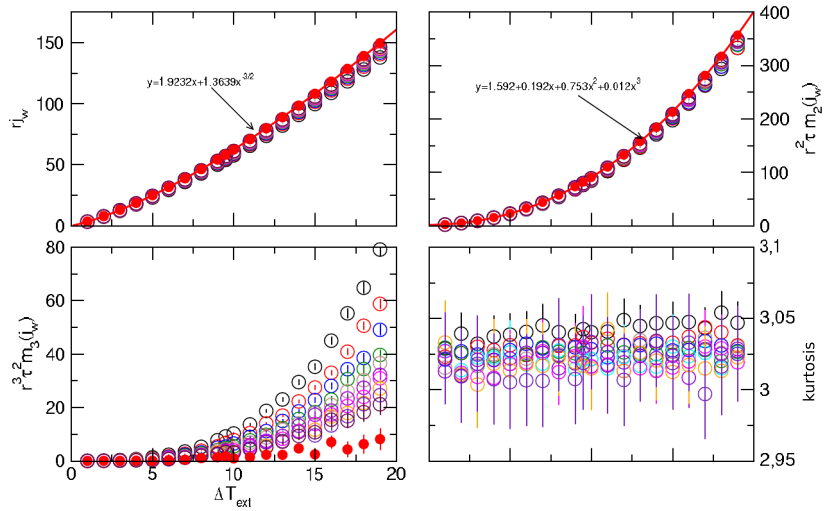

Figure 2.7: The moments of the current of energy j_w for $\bar{\eta} = 0.5$ as a function of ΔT_{ext} for different sizes N. from bottom to top in all figures. Solid red points are the extrapolation to the infinite size limit obtained with a second order polynomial in $1/N$. Solid red line is a phenomenological fit of the infinite size limit.

dependence with ΔT_{ext}. We also studied the behavior of j_w as a function of the mean density of the system for a fixed temperature gradient that we have chosen to be $T_0 = 3$. We have chosen a density interval where we know a solid-like phase appears on the system. We want to observe if there is any kind of singular behavior in the current. The unique anomaly we find is in the second momenta in which we detect a change of behavior at $\eta = 0.691$ where there is a local minimum on the fluctuations and on the value of the expected equilibrium phase transition at $\eta = 0.706$ where it seems that $m_2(j_w)$ have a turning point (see Figure 2.8). We don't have any theoretical description for this behavior, which could be an interesting point to perform further analysis.

There are other possible definitions of the energy current. For instance, for hard disks, the most natural could be:

$$j_B = \frac{1}{N} \sum_{i=1}^{N} \frac{1}{2} m \vec{v}_i^2 v_{i,x} \tag{2.10}$$

The main problem with this expression is that, as we will see in chapter 3, local equilibrium holds for our system and the non-equilibrium behavior seems to live on the fluctuating level. That is, when we average the data, the system seems to behave as it is in mainly at equilibrium and the extrapolation to infinite sizes should (apparently) go to zero because the local equilibrium measure is even in the velocities. We show in Figure 2.9 the behavior of j_B as a function of $1/N^{1/2}$ for different gradients. We see that the second moment of j_B behaves normally and it scales with N. $m_3(j_B)$

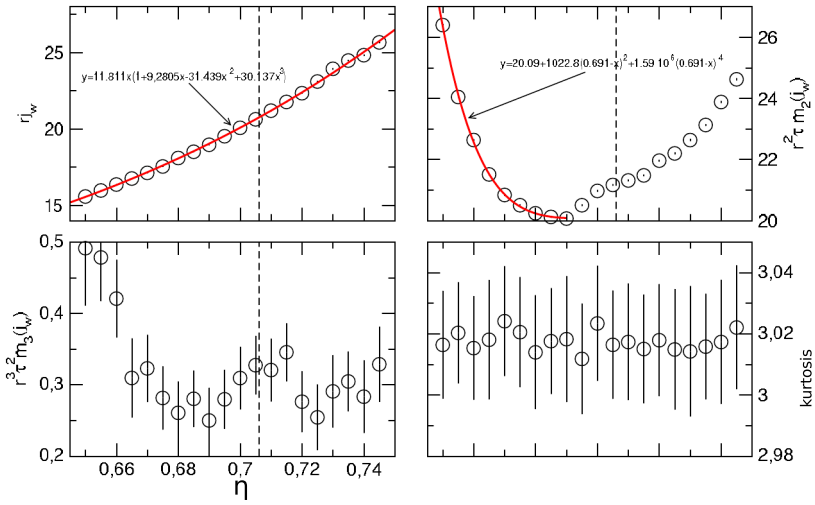

Figure 2.8: The moments of the current of energy j_w for a fixed temperature gradient $T_0 = 3$ and $T_1 = 1$ as a function of $\bar{\eta} \in [0.65, 0.745]$ for $N = 5226$ particles. Solid red line are in each case the best fit shown.

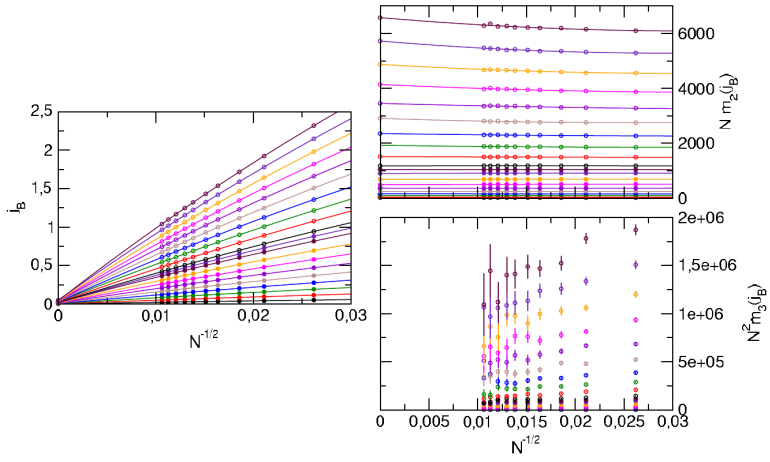

Figure 2.9: The moments of the current of energy j_B as a function of $1/N$ for $\eta = 0.5$, $T_1 = 1$ and $T_0 = 2, \ldots, 20$ from bottom to top in all figures. The points on the $x = 0$ axis correspond to the extrapolation of a parabolic least square fit to the data (solid lines) for each T_0.

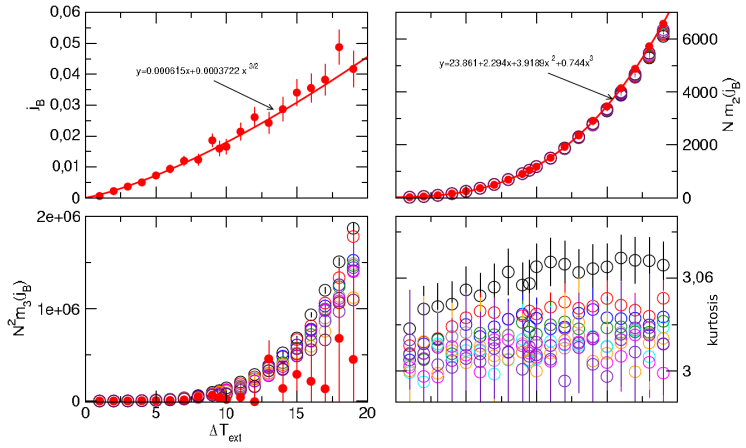

Figure 2.10: The moments of the current of energy j_B for $\bar{\eta} = 0.5$ as a function of ΔT_{ext} for different sizes N. from bottom to top in all figures. Solid red points are the extrapolation to the infinite size limit obtained in Fig.2.9. Solid red line is a phenomenological fit of the infinite size limit.

has the same problem as j_B and we cannot even try to fit a smooth curve. The fact that j_B has that strong dependence on N makes its analysis to the infinite size behavior very problematic and depending on the function that we use to fit the data. The effect is clear in Figure 2.10. The data for j_B is very noisy but it has a similar behavior to that of j_w. The most important fact is that the infinite size limit for j_B is non zero and it confirms that local equilibrium is not the stationary measure of the system. However we should be cautious with this conclusion because in this case the limiting j_B is very dependent on the function that we use to fit the data.

The last question we should answer is if j_w is proportional to j_B. We plot in Figure 2.11 the measured j_B/r vs. rj_w (the scale in each case is to get similar values on both magnitudes). The data present a small dependence on N. In fact we see that the best fit is a parabolic like function with only one parameter $C(N)$ that we plot in the inset as a function of $N^{-1/2}$. The numerical extrapolated behavior of j_B/r as a function of rj_w is then given by:

$$r^{-1}j_B = 1.625 rj_w \left(1 + 0.000386 rj_w\right) \tag{2.11}$$

that is, for small gradients, say $T_0 \in [0, 5]$ both currents are almost proportional. However, for large gradients one sees a systematic deviation from linear behavior. Therefore we conclude that is not equivalent to use any energy-like current observable.

2.4 Concluding Remarks

In this chapter we analyzed the temperature and density profiles as well as the heat current across the system. We find that temperature and density

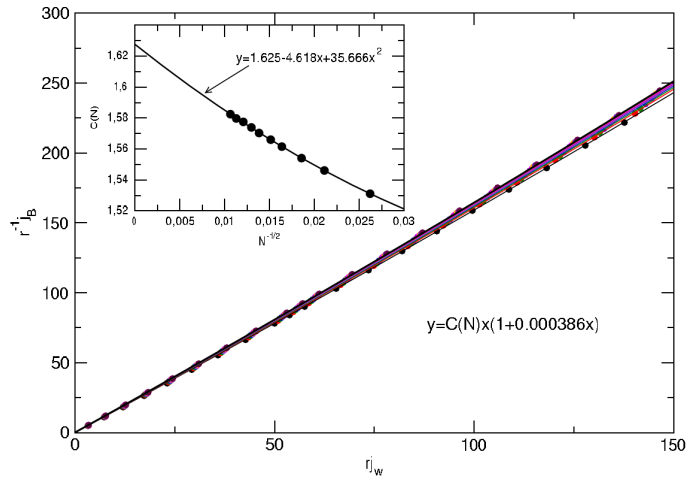

Figure 2.11: The bulk current j_B vs j_w. Each point is the measured values of both currents for a given ΔT_{ext} and N. Equal color points correspond to a given N. Lines are the fits of the data to the function written in the figure. The inset shows the behavior of the coefficient $C(N)$ obtained by the fit.

profiles are nonlinear which indicate that the conductivity across the system is not constant. This will prevent us to perform an analysis equivalent to the performed in [57], i.e. in terms of the external gradient. If we want to check if Fourier's Law holds we need to do it locally. This represent a challenge because the temperature and density profiles have a highly non-trivial dependence with the system size. Without a clear clarification of this effects it will be impossible to discern between a behavior related to the heat conductivity or one related with the behavior of the profiles. In chapter 4 we give an argument to solve this problem.

Chapter 3

On Local Thermodynamic Equilibrium in Non-equilibrium Fluids

In chapter 2 we have implicitly assumed that the system temperature and density profiles are relevant observables in the macroscopic characterization of our system. Here, local temperature means the average local kinetic energy. That is, we have in mind that *Local Thermal Equilibrium* holds in our system. From a theoretical point of view, the existence of LTE is a very hard unresolved problem (see for instance [65]). If LTE holds we expect that several things occur (at least at the thermodynamic limit):

- Local observables measured at each macroscopic point, $\vec{x}$, would follow the corresponding equilibrium values with respect the local temperature $T(x)$, local areal density $\eta(x)$, etc, and, locally, the thermodynamic relations should hold. For instance, the local pressure (defined by its virial form), the local temperature and the local areal density are related by the equation of state of the system that in our case is of the form:
$$Q = P\pi r^2 = T\eta Z(\eta) \tag{3.1}$$

- Measured global observables should be the average with respect a configurational measure that is approximately the product of local equilibrium Gibbs measures depending on local temperatures and areal densities.

In practice, is very hard to prove local equilibrium from a computer simulation. However, we may have some indications suggesting that both properties hold in our system, by studying a small set of observables. In any case deviations are typically so small that we should make a special emphasis on finite size effects that may distort the analysis.

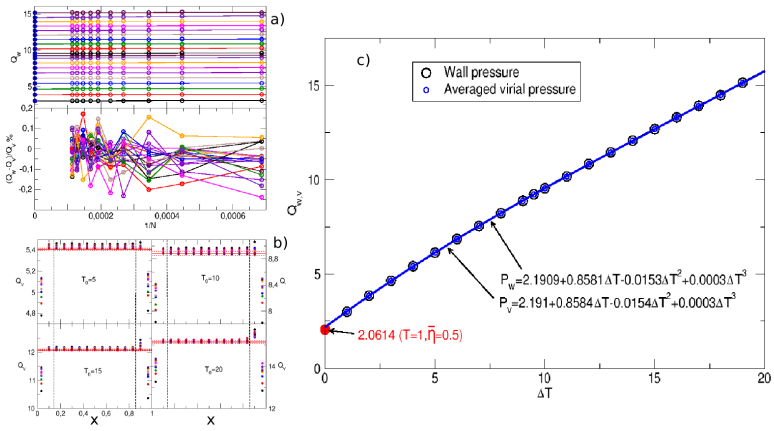

Figure 3.1: a)Wall pressure and virial pressure (see text) computed for a set of systems under the action of several thermal gradients and system sizes for a mean packing fraction of $\bar{\eta} = 0.5$. In top figure each symbol are for wall pressure obtained from gradients (from bottom to top): 1, 2, ..., 19 and ten different sizes. Solid blue symbols are a linear extrapolation of the data to obtain their infinite size value. Below we show the relative error (in %) between the wall pressure and the virial pressure. b) Virial pressure measured at each of the 15 boxes of a system. Red lines are the linear extrapolation fit of the three average values of the virial pressure obtained by averaging boxes from 2 to 14 (both included). Dotted lines are the error of such extrapolation. c) Wall pressure and virial pressure of a system under the action of thermal gradients for $\bar{\eta} = 0.5$. Solid line is a phenomenological fit. Solid symbol is the pressure equilibrium value line for $T = 1$ obtained from Henderson equation of estate 1.18.

3.1 Mechanical Equilibrium and Equation of State

When the system reach the stationary non-equilibrium state we measured the wall pressure and the virial pressure at each box. The overall behavior about pressures is quite similar to the already explained for the equilibrium case. For instance, in figure 3.1a we can see that the wall pressure and the virial pressure, measured on the central boxes, coincide for each size (up to a 0.2%) and for their respective infinite size extrapolation. Therefore the system at a non-equilibrium steady state have a kind of *mechanical* equilibrium in which the virial pressure is constant along the system (as in equilibrium) and it coincides with the wall pressure. Moreover, it seems that there is a local equilibrium property in which the virial pressure still has locally some physical meaning. We plot in Figure 3.1c the extrapolation to infinite size of the virial and wall pressures as a function of the external thermal gradient. The phenomenological cubic fit is very good and it is coherent with the expected equilibrium value for zero gradient.

We can assume with some confidence that local equilibrium holds and, therefore, the local equation of state should hold:

$$Q = T(x)\eta(x)Z(\eta(x)). \tag{3.2}$$

This relation only depends on the local values of the temperature, packing fraction and pressure on each measurement box, therefore in Figure 3.2 we represented $\bar{Q} \equiv Q/\eta(x)T(x)$ versus $\eta(x)$ for all our available data, with the only exception of the boxes next to the thermal walls. As a reference we included Henderson 77 Equation of State (EoS) given by eq. 1.18 and a set of data coming from other equilibrium computer simulations. Let us remark, for instance, the first data available by Metropolis et al. (1953) by doing Monte Carlo simulations on hard disks [41], or the very good data obtained by Alder et al. (1968) for the solid-like phase [42]. Also we include the data obtained by two of the best computer simulations on hard disks in equilibrium: Erpenbeck and Luban (1985) [39] and Kolafa and Rottner (2006) [40]. In these studies they simulated as much as 50000 particles in equilibrium, founding small deviations to the Henderson expression in the range of $\eta \in [0.4, 0.65]$. Finally we also represent more recent data focused on the phase transition (fluid-solid) that occurs between $\eta = 0.7062$ and $\eta = 0.7201$ [66], Mak (2006) [43] and Engel (2013) [44], which where perform in order to specify the kind phase transition present in this system.

We can see that, although our purpose in this study was not to calculate this magnitude, our data is in excellent agreement with other equilibrium computer simulation (less than a 1% of relative error) despite the fact of being in a non-equilibrium situation. This is quite shocking by itself, but also for other several reasons. First, we saw in chapter 2 the strong finite size effects present in the profiles of temperature and areal density which add up to the moderate ones we saw in figure 3.1 for the pressure. However, these effects totally compensate each other, leaving any possible systematic behavior with N within the error bars. Furthermore, we should remark that the mean number of particle in each box is quite low, going from about 70 particles for the system with $N_{\text{Bulk}} = 1456$ to about 750 for the system with $N_{\text{Bulk}} = 8838$, in contrast with the cited equilibrium simulations. On top of that we can see in the bottom inset of Figure 3.2 that a simple running average over the points, i.e. supposing that they are independent, reproduce the same deviations from Henderson EoS, in the range of $\eta \in [0.4, 0.65]$, already seen in the cited works. All this suggest that Local Thermal Equilibrium is such a strong property of the system that allows us to treat, at least at the macroscopic level, the values obtained for the temperature, packing fraction and pressure, in each measurement box, as if they were the equilibrium values of an *infinite system*. This means that all size effects previously analyzed for the Bulk part of our system disappear, leaving as a reminiscence an effective thermal reservoir, composed by the baths and the first and last boxes, in whose values are concentrated all size and boundary effects. This property, that we called Bulk-Boundary decoupling, will be better understood in the context of chapter 4.

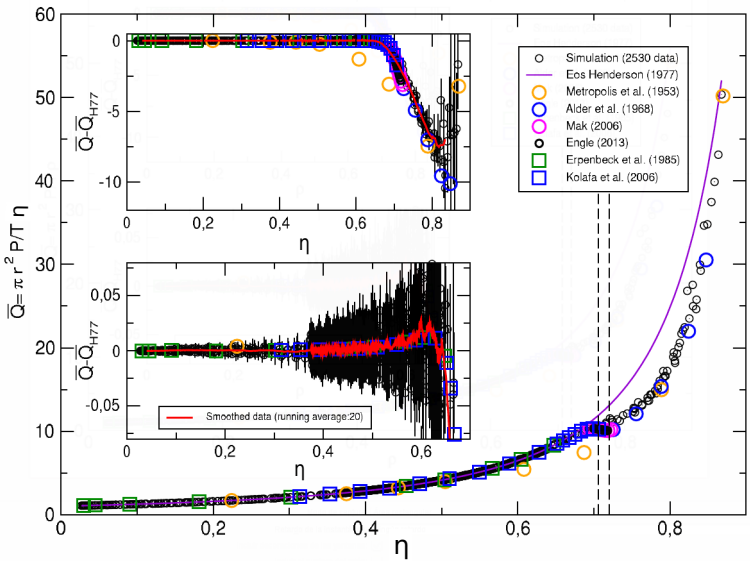

Figure 3.2: Experimental equation of state for hard disks. We plot for each box $\bar{Q} = Q/\eta(x)T(x)$ against the box density $\eta(x)$ for all simulated systems mentioned on Table 2.1. Color data are different results obtained by other authors. Solid line is the Henderson 77 EoS (1.18). Vertical dashed lines are the expected transition points. Top inset is the difference $\bar{Q} - \bar{Q}_{H77}$ and in the bottom inset we focus on densities $\eta < 0.65$. Red data is just a running average over 20 data points.

3.2 Liquid-Solid Coexistence

Finally, our data seems to reproduce the solid phase and it follows that data from Metropolis [41] and Alder [42]. This case is interesting by itself because typically, for a large enough average density, *not all boxes* of the system are in the solid phase. In fact there is a kind of *non-equilibrium* coexistence of local equilibrium phases already seen in a recent paper by Wooszczuk and Lipowski (2010) [67]. Let us study the solid phase more carefully.

In figure 3.3c we show a typical configuration in which there is coexistence between liquid and solid phases. In Figure 3.3a we have measured the number of disk centers on a little box of width 1/10000. In the plot we show that disk centers are, in average, aligned in well defined layers parallel to the cold thermostat. The disk centers are aligned to the right part of the system and they fluctuate more as we move to hotter parts. There are not structure at all when we reach the liquid phase. We also see the effect of the hot boundary into the liquid. There is an averaged ordered structure related to the presence of the hard wall. We also see in the inset an amplification of the distribution near the cold wall. Red lines are the virtual boxes in which we measure local equilibrium observables. There is a systematic, *box depending*, effect when we measure the box disk density (see figure 3.3b).

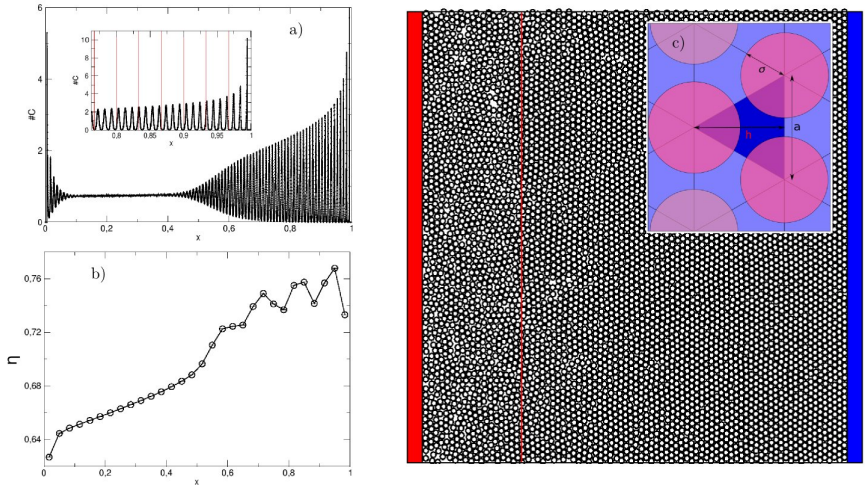

Figure 3.3: Typical hard disk configuration at the stationary state in which there is liquid-solid phase coexistence. $N_{max} = 6000$, $\eta = 0.745$, $T_0 = 3$ and $T_1 = 1$. Vertical line shows the box in which liquid exists to the left of it and solid appears to the right.

Boxes contains a small number of disk lines and there are interface effects when a line of disk is in the boundary of a box. That finite size effect only appears in the solid phase and we should correct it to obtain a well defined average value for the density at each box.

From the structure showed in figure 3.3a we are able to measure the parameters that define the underlying average hexagonal local structure in the solid: the distance between centers in a vertical line of disks (a) and the distance between center lines (h) (see figure 3.3c). The results are shown in figure 3.4.

We observe that the hexagonal structure of the solid phase is not regular and it depends on x. In fact it seems that there are two well defined regions: Region I near the cold wall where a is practically constant and its value depends on the average areal density $\bar{\eta}$, larger in any case than 2σ, i.e. there are not overlapping. h depends linearly on x and it has values smaller than the one corresponding to a regular hexagonal lattice, that is, $h(x) < h_0(x) = \sqrt{3}a(x)/2$. Therefore we have a *compressed* hexagonal lattice. Region (II) where a grows with smaller x and reaches a maximum value around 2.35σ independently of the density. $h(x)$ grows smoothly when decreasing x but with some nonlinear behavior until it reaches the value $h(x) = 2\sigma$ where disks lose their natural geometric constraint and they can move freely (in average) along the vertical direction. That seems to define the transition from solid to the liquid phase. In Figure 3.4c we plotted h/h_0 versus x in order to see if the regular hexagonal structure is the limiting behavior at some x zone. That is not clear. For small densities h systematically deviates from h_0 maybe due to finite size effects. For large densities seems that most of the Region II have $h(x)$ that is almost $h_0(x)$ up to the liquid transition. That is, in those cases the lattice structure goes, from large x to smaller ones,

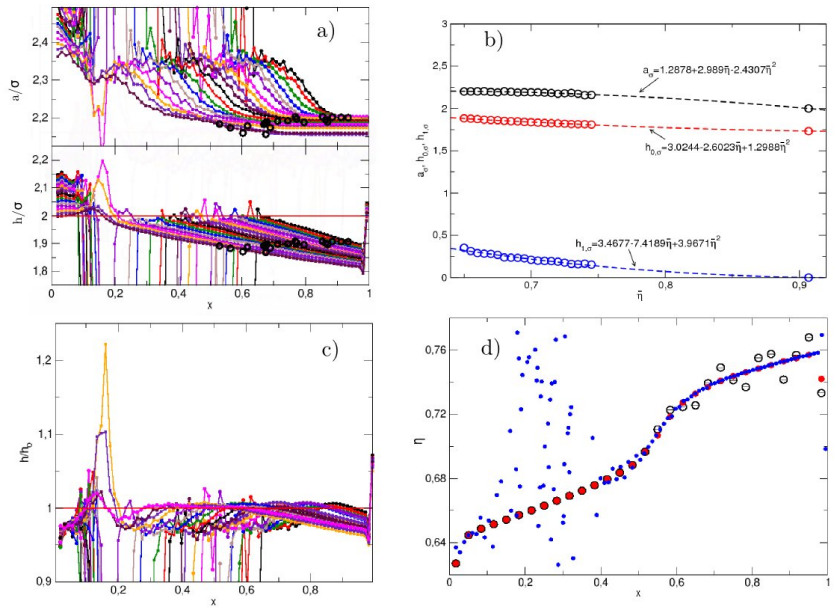

Figure 3.4: Hexagonal local lattice structure of the hard disk solid phase for $T_0 = 3$, $N_{\text{Bulk}} = 5935$ and 1.5×10^6 averaged configurations. Each curve is for a system areal density $\bar{\eta}$ ranging from 0.65 up to 0.745 in steps of 0.005. a)Measured $a(x)$ and $h(x)$ values in units of the radius of the disks. Black circles correspond to the x^* values where local h and a follow the regular hexagonal lattice relation: $h(x^*) = \sqrt{3}\, a(x^*)/2$. b)$a/\sigma$, $h_{0,\sigma}$ and $h_{1,\sigma}$ (see text) as a function of the mean packing fraction. c) h/h_0 vs x, where $h_0 = \sqrt{3}\, a(x)/2$. The curves with the peak near the right wall correspond to the smaller densities. d) Areal density profiles' correction procedure. Black points are measured data. Blue points are the packing fraction using eq. 3.3. Red points are the corrected data.

from a *compressed* hexagonal lattice (Region I) up to a regular hexagonal lattice (Region II). We can define a criteria to find the x^* that separate both regions: $h(x^*) = \sqrt{3}\, a(x^*)/2$. We show in figure 3.4a the x^* points and, at least qualitatively, they work quite well. Finally we studied with more care Region I. In figure 3.4b we have plotted the a/σ's constant values and we have fitted to the $h(x)/\sigma$ values the line $h(x)/\sigma = h_{0,\sigma} + h_{1,\sigma}(1 - x)$. We see its regular behavior with $\bar{\eta}$ and their tendency to the theoretical *closed packed limit*.

Once clarified the structure of the solid phase in our system we can design a way to define correctly the areal density as a function of position. First we compute the centers distribution on a $1/10^4$ x-mesh (see Figure 3.4a). Then we localize the maximum and the minimum of the distribution. We compute the total number of disks that are between two consecutive minimum, that will be the number of disks in one disk line. This number divided by L_y give us an estimation of the local value of $a = a(x)$. The local value of $h(x)$ is obtained as the average between the maximum at x and its nearest

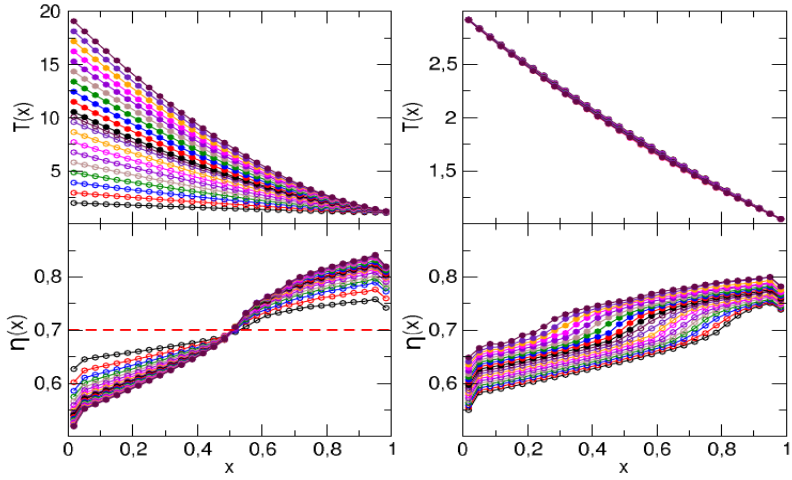

Figure 3.5: Temperature and density profiles for systems with coexisting non-equilibrium phases. Left figures are for $N_{\text{Bulk}} = 7838$, $\bar{\eta} = 0.7$, and $T_0 = 2, 3, \ldots, 20$ and $T_1 = 1$. Right figures are for $N_{\text{Bulk}} = 5935$, $T_0 = 3$, $T_1 = 1$ and $\bar{\eta} = 0.65, 0.655, 0.660, \ldots, 0.745$.

maximums. Finally the local density is the corresponding to an infinite triangular *compressed* lattice with parameters $a(x)$ and $h(x)$:

$$\eta(x) = \frac{\pi\sigma^2}{a(x)h(x)} \tag{3.3}$$

On Figure 3.4d is plotted the density measured in the virtual boxes (black circles), and using the information of the underlying lattice structure by following the above scheme (blue dots). We may recover a density in a virtual box by interpolating them (red dots). We see that this method is useful as long as we are on the solid phase and it breaks down when we are on the liquid phase. Nevertheless using the solid phase scheme, we recover the right values of η when we average enough local points for instance in a virtual box.

With this method we may draw the temperature and density profiles for several cases with coexisting non-equilibrium phases. In figure 3.5a we plot temperature profiles for a system with $N_{\text{Bulk}} = 7838$, mean areal density $\bar{\eta} = 0.7$ and temperature gradients ranging from 1 up to 19. Also, we fixed the temperature gradient $T_0 = 3$ and studied the profiles as a function of the system average density $\bar{\eta}$ for systems with $N_{\text{Bulk}} = 5935$. We observe:

- Temperature profiles are regular and behave similarly to the ones with an unique liquid phase (see figure 2.3). No singular behavior is found when crossing liquid to crystal phases.

- Density profiles are also regular but its convexity changes when going from the liquid to the crystal phase.

- The size of the crystal phase depend only on the mean packing fraction $\bar{\eta}$. The local densities depend also on the imposed gradient.
- Size effects are important in the solid phase: one particle more or less in a solid column with around 80 particles, changes appreciably the local density.
- There are some effects due to slow relaxation to the final stationary state that affect to the observed measured profiles.

There is a final question to be addressed: local equilibrium holds in the crystal phase? If the answer is positive then we can use the local data to reproduce the equilibrium equation of state for the crystal phase. First we have measured the wall pressure as a function of several η-values and temperature gradients. We find a monotone behavior. In fact the data may be well fitted with a second order polynomial. Size effects are small and there is no effect when the average areal density crosses the equilibrium density transition point (see Figure 3.6a). Second we studied the local pressure using its virial form. We saw that in the liquid phase both quantities were equal. Now things change.

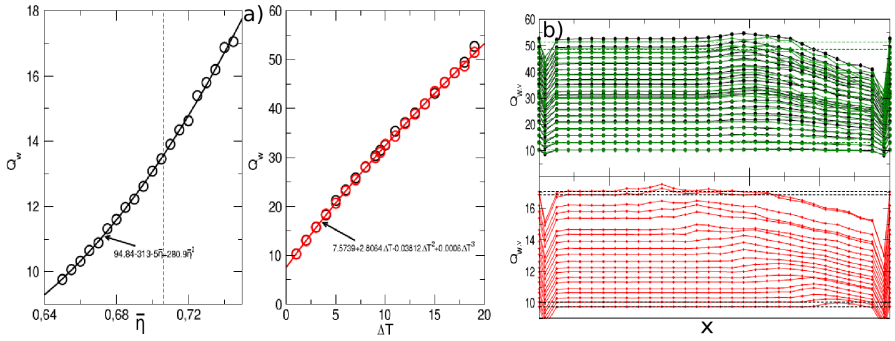

Figure 3.6: a) Left: Wall pressure as a function of mean packing fraction $\bar{\eta}$ for $N_{\text{Bulk}} = 5935$ and $T_0 = 3$. Right: Wall pressure as a function of the external gradient for a mean packing fraction of $\bar{\eta} = 0.7$. Red points are for $N_{\text{Bulk}} = 7838$ and black point for $N_{\text{Bulk}} = 2900$ b) Top: Virial pressure, Q_v, versus x for different temperature gradients (top) for $N_{\text{Bulk}} = 2900$ (black circles), $N_{\text{Bulk}} = 7838$ (green circles), $\bar{\eta} = 0.7$, and $T_0 = 2, 3, \ldots, 20$ and $T_1 = 1$. Bottom: Q_v versus areal density $\bar{\eta}$ for $N_{\text{Bulk}} = 5935$, $T_0 = 3$, $T_1 = 1$ and $\bar{\eta} = 0.65, 0.655, 0.660, \ldots, 0.745$. Dotted lines are the corresponding wall pressure for a given density or gradient. The first and last point of every curve is the value of the wall pressure Q_w

In figure 3.6b we show the local virial pressure in several system situations. We may remark:

- The local virial pressure has some local structure: in the liquid phase its value is the same of the wall pressure, Q_w, however in the solid phase the virial pressure increases for intermediate densities and decreases when the density increases.

- Temperature gradient stresses the x-dependence.
- The average density expands the x-structure.

The x-dependence of Q_v may imply that local equilibrium doesn't hold. In order to confirm this point we have plotted the local triangular structure h/h_0 as a function of Q_v/T. We want to see if the local magnitude depend only on the local triangular structure.

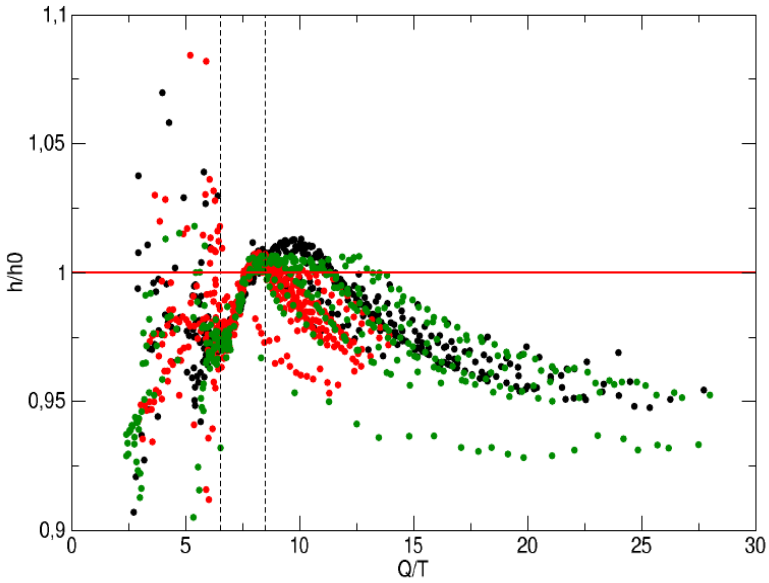

Figure 3.7: Rescaled local triangular structure $h(x)/h_0(x)$ versus the local virial pressure, $Q_v(x)/T(x)$, for $N_{\text{Bulk}} = 2900$ (black circles), $N_{\text{Bulk}} = 7838$ (green circles), $\bar{\eta} = 0.7$, $T_0 = 2, 3, \ldots, 20$ and $T_1 = 1$, and for $N_{\text{Bulk}} = 5935$, $T_0 = 3$, $T_1 = 1$ and $\bar{\eta} = 0.65, 0.655, 0.660, \ldots, 0.745$.

We see that the data do not scale. There is a small region between $Q_v/T = 6$ and 8 where there is an apparent scaling. However, when plotting such data versus the local density the scaling disappears. Therefore we can conclude that when the system mean packing fraction is large enough, it appears a crystal like phase that is a regular triangular lattice deformed. Such structure is macroscopically correlated. Moreover, local equilibrium does not hold in it and therefore its nature depends directly to the external conditions applied to the system. It is a non-equilibrium crystal phase.

3.3 Global Velocity Distribution

We wanted to check if local equilibrium holds in a global way. We though that we could see any deviation to local equilibrium if we measured global

properties of the system and compared them to the local equilibrium corresponding values. In particular we measured the average velocity moments at the stationary state:

$$v_n \equiv \frac{1}{N_d N} \sum_{l=1}^{N_d} \sum_{i=1}^{N} |\vec{v}_i|^n \qquad n = 1, 2, 3, 4 \tag{3.4}$$

where N_d is the number of data measured. To obtain errors bars we also measured v_5, ..., v_8. To get good enough data we reached values $N_d N \simeq 6 \times 10^9$. We compared the obtained values with the corresponding local equilibrium ones, $v_n^{(\mathrm{le})}$. Then we first should define what we mean as local equilibrium. Assuming that temperature varies only on the x-direction, the local equilibrium probability to get a particle configuration with moments $\vec{p}_i$ and positions $\vec{r}_i$ is given by [65]:

$$\mu^{(\mathrm{le})}(\vec{p}_1, \ldots, \vec{p}_N, \vec{r}_1, \ldots, \vec{r}_N) \simeq \exp\left\{ -\sum_{i=1}^{N} \beta(\epsilon x_i) \left[\frac{\vec{p}_i{}^2}{2m} + \sum_{j \neq i} \Phi(\vec{r}_i - \vec{r}_j) \right] \right\}. \tag{3.5}$$

Where ϵ is the parameter that connects the microscopic scale with the hydrodynamic one. Under this hypothesis one may argue that the probability density that any particle has a velocity with modulus equal to v is given by:

$$f(v) = v \int_0^1 dx \frac{\eta(x)}{\bar{\eta} T(x)} \exp\left[-\frac{v^2}{2T(x)} \right] \tag{3.6}$$

with

$$\bar{\eta} = \int_0^1 dx \eta(x). \tag{3.7}$$

Then

$$\tilde{v}_n^{(\mathrm{le})} \equiv \langle v^n \rangle = \frac{a_n}{\bar{\eta}} \int_0^1 dx \eta(x) T(x)^{n/2} \tag{3.8}$$

where $a_1 = (\pi/2)^{1/2}$, $a_2 = 2$, $a_3 = 3(\pi/2)^{1/2}$ and $a_4 = 8$. Before to compare $\tilde{v}_n^{(\mathrm{le})}$ with the direct measure v_n from eq. (3.4) we should slightly manipulate equation (3.8) to adapt it to our measurements. Three things should be done: (a) To express equation (3.8) as a function of box temperatures and densities T_C and η_C following eqs. (2.5). (b) To include the fact that T_C and η_C have error bars and thus should be considered as fluctuating values around their average. This influences, for instance, the average value of $T(x)^{n/2}$. In this respect we have also to account in the calculus of the fluctuations of $\eta(x)$ the role of a constant global $\bar{\eta}$. And finally (c) To compute the error bars of $v_n^{(\mathrm{le})}$.

(a) *Conversion to box variables.* We should convert expression (3.8) with respect to box variables. To do that we write

$$\tilde{v}_n^{(\mathrm{le})} = \frac{a_n}{\bar{\eta}} \sum_C \int_{x_c - \Delta/2}^{x_c + \Delta/2} dx \eta(x) T(x)^{n/2} \tag{3.9}$$

where x_c are the center of the boxes. We may expand the later expression up to order Δ^2 and we get

$$\tilde{v}_n^{(\mathrm{le})} = \tfrac{a_n}{\bar{\eta}}\Delta \sum_C \Bigg[\eta(x_c)T(x_c)^{n/2} + \tfrac{\Delta^2}{24}\Bigg[\left.\tfrac{d^2\eta(x)}{dx^2}\right|_{x=x_c} T(x_c)^{n/2} + n\left.\tfrac{d\eta(x)}{dx}\right|_{x=x_c} T(x_c)^{n/2-1}\left.\tfrac{dT(x)}{dx}\right|_{x=x_c} + \tfrac{n}{2}\left(\tfrac{n}{2}-1\right)\eta(x_c)T(x_c)^{n/2-2} + \left(\left.\tfrac{dT(x)}{dx}\right|_{x=x_c}\right)^2 + \tfrac{n}{2}\eta(x_c)T(x_c)^{n/2-1}\left.\tfrac{d^2T(x)}{dx^2}\right|_{x=x_c}\Bigg]\Bigg] \tag{3.10}$$

that can be written as

$$\tilde{v}_n^{(\mathrm{le})} = \frac{\Delta a_n}{\bar{\eta}}\sum_C \eta_C T_C^{n/2} + \frac{\Delta a_n}{96\bar{\eta}} n\,(n-2)\sum_C \eta_C T_C^{n/2-2}\,(T_{C+1}-T_C)^2 \tag{3.11}$$

(b) *The effects of the fluctuations of box temperature and density.* Due to the finite number of measurements done, any magnitude and, in particular, the box magnitudes fluctuate and that influences the observed averaged behavior. Let us assume that the fluctuations are gaussian like:

$$\eta_C = \bar{\eta}_C + \xi_C\psi_C \quad P(\psi_1,\ldots,\psi_M) = \sqrt{2\pi M}\prod_{i=1}^{M}\left[\frac{1}{\sqrt{2\pi}}e^{-\psi_i^2/2}\right]\delta\left(\sum_{i=1}^{M}\psi_i\right)$$
$$T_C = \bar{T}_C + \theta_C\phi_C \quad Q(\phi_1,\ldots,\phi_M) = \prod_{i=1}^{M}\left[\frac{1}{\sqrt{2\pi}}e^{-\phi_i^2/2}\right] \tag{3.12}$$

where $M = 15$ is the number of boxes and ξ_C and θ_C are the experimental errors of density and temperature at box C, and ψ_C and ϕ_C are the Gaussian random variables with zero mean and variance one. Notice that we included the fact that the total areal density is constant. In our case we can assume that the errors are of order Δ and we will expand the results up to order θ^2 or ξ^2. Now we have to substitute η_C and T_C in equation (3.11) by expressions in (3.12) and then average with respect P and Q distributions. That is,

$$v_n^{(\mathrm{le})} \equiv \langle\tilde{v}_n^{(\mathrm{le})}\rangle_{\psi,\phi} = \frac{\Delta a_n}{\bar{\eta}}\sum_C \bar{\eta}_C\langle T_C^{n/2}\rangle_\phi + \frac{\Delta a_n}{96\bar{\eta}} n\,(n-2)\sum_C \bar{\eta}_C\bar{T}_C^{n/2-2}\left(\bar{T}_{C+1}-\bar{T}_C\right)^2 + O(\Delta^3) \tag{3.13}$$

where

$$\langle T_C^{n/2}\rangle_\phi = \bar{T}_C^{n/2} + \frac{1}{8}n(n-2)\bar{T}_C^{n/2-2}\theta_C^2 + O(\theta_C^4) \tag{3.14}$$

Therefore the fluctuations in the box add a small correction to $v_n^{(\mathrm{le})}$

(c) *Computing the $v_n^{(\mathrm{le})}$ error bars.* Once we know how to compute $v_n^{(\mathrm{le})}$ from our set of data we want to obtain the error bars, χ_n:

$$\chi_n^2 = \langle (\tilde{v}_n^{(\mathrm{le})})^2 \rangle_{\psi,\phi} - \langle \tilde{v}_n^{(\mathrm{le})} \rangle_{\psi,\phi}^2 \tag{3.15}$$

and, in particular, one needs to know that

$$\langle (\psi_C)^2 \rangle_\psi = 1 - \frac{1}{M} \qquad \langle \psi_C \psi_{C'} \rangle_\psi = -\frac{1}{M} \quad \text{if} \quad C \neq C' \tag{3.16}$$

and we get

$$\chi_n^2 = \left(\frac{\Delta a_n}{\bar{\eta}} \right)^2 \left[\sum_C \left(b_n \theta_C^2 \bar{\eta}_C^2 \bar{T}_C^{n-2} + \xi_C^2 \bar{T}_C^n \right) - \frac{1}{M} \left[\sum_C \xi_C \bar{T}_C^{n/2} \right]^2 \right] \tag{3.17}$$

with $b_1 = 1/4$, $b_2 = 1$, $b_3 = 9/4$ and $b_4 = 4$.

In order to see the relevance of the above corrections let us define

$$(v_n^{(\mathrm{le})})_0 \equiv \frac{\Delta a_n}{\bar{\eta}} \sum_C \bar{\eta}_C T_C^{n/2} \qquad (v_n^{(\mathrm{le})})_{\mathrm{corr}} \equiv v_n^{(\mathrm{le})} - (v_n^{(\mathrm{le})})_0 \tag{3.18}$$

That is, $(v_n^{(\mathrm{le})})_{\mathrm{corr}}$ contains the Δ^2 effects due to the finite sizes of the boxes and the effects of the errors of the temperature and density profiles.

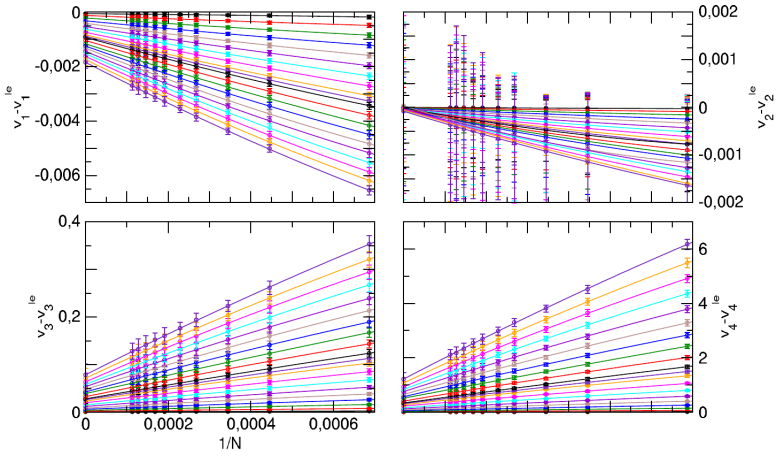

Figure 3.8: Difference between measured averaged velocity moments, v_i $i = 1, \ldots, 4$ and the predicted ones coming from local equilibrium without corrections,$(v_i^{(\mathrm{le})})_0$ at each box as a function of the inverse of particle number N. Error bars are included. Solid lines are a least square fit to the curve $y = a_0 + a_1/N + a_2/N^2$. The data for $1/N = 0$ are the values of the a_0 coefficients of the fits for each case.

We see in figure 3.8 the finite size analysis of both parts of $v_n^{(\mathrm{le})}$. In both cases we find a smooth behavior as a $1/N$ function that can be very well

fitted with a parabolic function: $a_0+a_1/N+a_2/N^2$. We take a_0's coefficients as the infinite size behavior for each gradient and we compute the inherited error bars of these coefficients from the errors of the measured data. In figure 3.9 we represent the values of the difference between the measured moments and the local equilibrium ones as a function of the temperature difference for different values of N. We see that, consistently, all differences tend to be small as the size increases. Red symbols are the extrapolation to infinite N of $v_n - (v_n^{(\mathrm{le})})_0$. Black symbols are $v_n - (v_n^{(\mathrm{le})})_{\mathrm{corr}}$ where we include all the corrections. We see that (i) the differences are very small but our data is good enough to resolve structure at such level of precision, (ii) the corrections always move the local equilibrium data in the boxes towards zero and (iii) the error bars of the extrapolations include in most cases the zero value. Notice that que are considered only Δ^2 corrections.

We may conclude in this section that local equilibrium ansatz is consistent with the measured global average powers of the velocity of particles *at the thermodynamic limit*. We think that the deviations to local equilibrium observed for finite systems are mainly due to boundary effects.

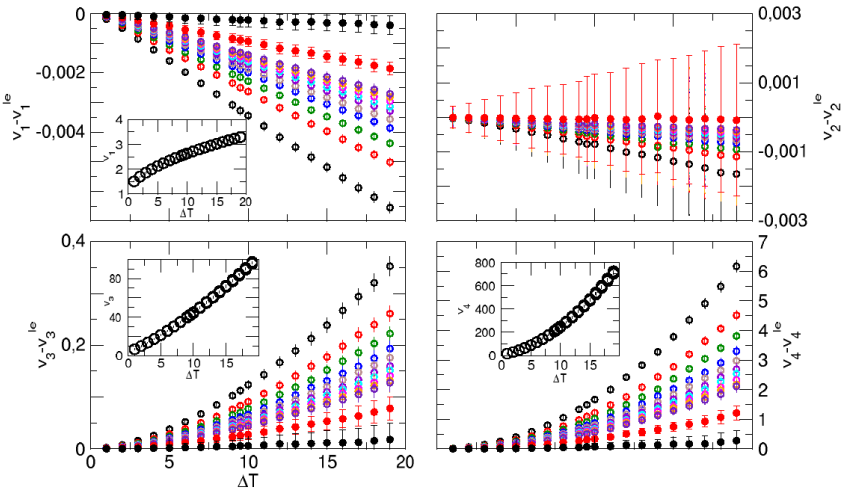

Figure 3.9: Values of the difference between velocity moments and local equilibrium ones as a function of the external increment of temperature for different sizes. The smallest size are the black dots. Red solid dots are the extrapolation to infinite size of data for a given temperature increment. Black dots are the red solid dots values plus the correction due to the finite size box density and temperature. Insets are the measured averaged velocity moments for different sizes and temperature increments.

3.4 Breakdown of Local Equilibrium

As we saw above, the system of hard disks seems to have the local equilibrium property in its liquid phase at least in the macroscopic level. We want to

check if there is any deviation of local equilibrium at the fluctuating level. For that we focus in measuring the fluctuations of the global energy density:

$$m_n(U) \equiv \langle (U - \langle U \rangle)^n \rangle \quad , \quad U = \sum_{i=1}^{N} \frac{1}{2} m \vec{v}_i^2, \tag{3.19}$$

and we compare it with its local equilibrium counterpart. Let us remind the equilibrium expressions of the energy fluctuations in the grand canonical ensemble:

$$m_n(U) = \frac{(-1)^{n+1}}{\partial \beta^n} \partial^n \ln \Xi, \tag{3.20}$$

where $U = \langle H_N \rangle$, and

$$\Xi = \sum_{N=0}^{\infty} z^N Z_N \quad , \quad Z_N = \frac{1}{N! h^{2N}} \int_S d\vec{x}_N \int d\vec{p}_N e^{-\beta H_N}. \tag{3.21}$$

For hard disks the canonical partition function Z_N can be written:

$$Z_N = \frac{(2\pi)^N}{N! h^{2N} \beta^N} Q(N, S, r), \tag{3.22}$$

where Q is the configurational part of the canonical partition function and it doesn't depend on the temperature. The energy fluctuations are:

$$\begin{aligned} m_2(U) &= T^2 \left[\langle N \rangle + m_2(N) \right] \\ m_3(U) &= T^3 \left[2\langle N \rangle + 3 m_2(N) + m_3(N) \right]. \end{aligned} \tag{3.23}$$

Assuming now that local equilibrium holds we get:

$$\begin{aligned} \langle U \rangle^{(\mathrm{le})} &= \int_0^1 dx \langle N \rangle_x T(x) \\ m_n(U)^{(\mathrm{le})} &= \int_0^1 dx m_n(U_x). \end{aligned} \tag{3.24}$$

Finally, if N is the system total number of particles we get

$$\begin{aligned} u^{(\mathrm{le})} &= \frac{\langle U \rangle}{N} = \int_0^1 dx \frac{\eta(x)}{\eta} T(x) \\ N m_2(u)^{(\mathrm{le})} &= \frac{m_2(U)}{N} = \int_0^1 dx \frac{\eta(x)}{\eta} T(x)^2 \left[1 + \frac{m_2(N_x)}{\langle N \rangle_x} \right] \\ N^2 m_3(u)^{(\mathrm{le})} &= \frac{m_3(U)}{N} = \int_0^1 dx \frac{\eta(x)}{\eta} T(x)^3 \left[1 + \frac{3}{2} \frac{m_2(N_x)}{\langle N \rangle_x} + \frac{1}{2} \frac{m_3(N_x)}{\langle N \rangle_x} \right]. \end{aligned} \tag{3.25}$$

In figure 3.10 we study the size effects when measuring the second momentum of the energy density on a direct approach or by using the local equilibrium approximation. In both cases there is a small but systematic

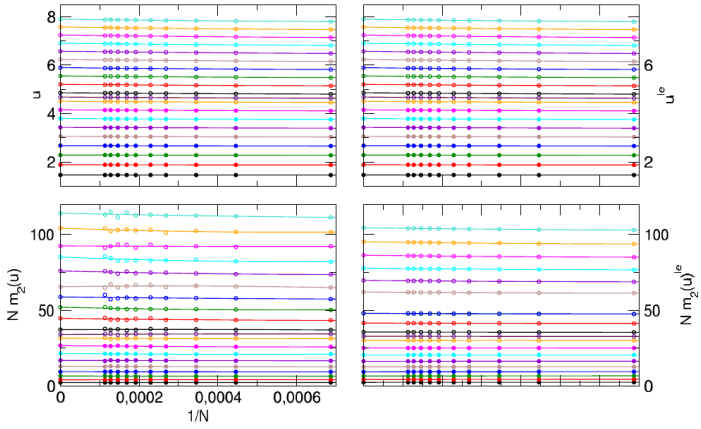

Figure 3.10: Left figure: energy density, u and the its second momentum, $m_2(u)$ as a function of the inverse of particle number N for different gradients (from bottom to top $T_0 = 2, 3, \ldots, 20$) and $\bar{\eta} = 0.5$. Error bars are included. Solid lines are the data least square fit $y = a_0 + a_1/N + a_2/N^2$. The data for $1/N = 0$ are the values of the a_0 coefficients of the fits for each case. Right figure: energy density $u^{(\mathrm{le})}$ and its second momentum, $m_2(u)^{(\mathrm{le})}$ using the local equilibrium approximation (see text).

size effect that should be taken into account. We find that the best fit to the data is a second order polynomial on $1/N$ in both cases. In this way we can extrapolate the infinite size behavior.

Figure 3.11 shows the behavior of the energy and energy momentum as a function of the external gradient for different sizes. We see that the effects of size are very small for u and $Nm_2(u)$. $N^2 m_3(u)$ is much more fluctuating and size dependent showing that we are reaching the sensitivity and precision of our computer simulation. Finally the kurtosis behaves in a gaussian manner with values near 3 for all sizes. Black solid circles are the infinite size behavior of u and $Nm_2(u)$ by fitting a second order polynomial in $1/N$ to our data. Red solid circles are also the infinite behavior of $u^{(\mathrm{le})}$ and $m_2(u)^{(\mathrm{le})}$. We see that $u \sim u^{(\mathrm{le})}$ for all the external gradient range. However the energy fluctuations shows a increasing deviation from its local equilibrium counterpart. In the inset we plot their difference versus ΔT^2 and we fit the data to a line, finding a phenomenological slope of 0.025 that is around 1/40. Let us remind that some one dimensional stochastic models (WASEP and KMP) have corrections of $Nm_2(u) - Nm_2(u)^{(\mathrm{le})}$ of order ΔT^2 and its coefficient is $\pm 1/12$.

In conclusion, we see that at the fluctuating level and for large external gradients we can see deviations from local equilibrium.

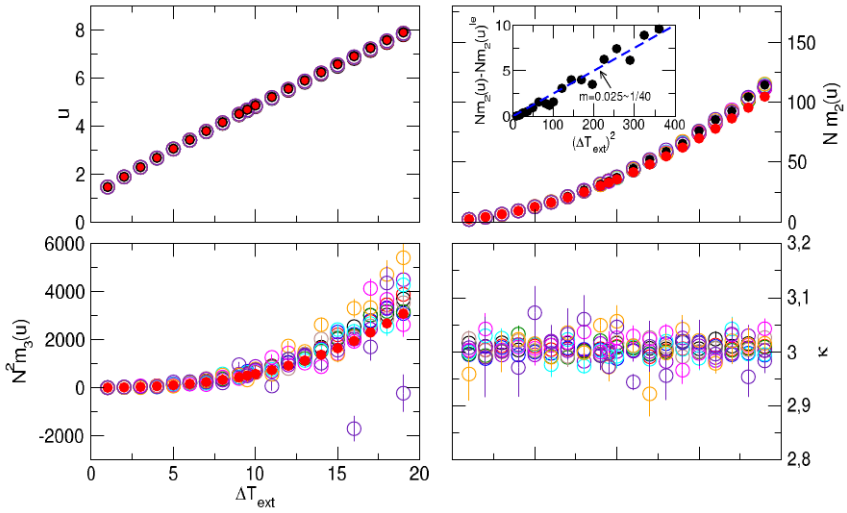

Figure 3.11: Energy density, u and the its second momentum, $m_2(u)$, third momentum, $m_3(u)$, and kurtosis, $\kappa = m_4(u)/m_2(u)^2$ as a function of the external gradient for different sizes and $\bar{\eta} = 0.5$. Error bars are included. Black solid points are the infinite size extrapolation via second order polynomials in $1/N$ to the data. Red solid points are the infinite size extrapolation of energy and its momentum in the local equilibrium approximation. The inset shows the difference between the direct measures and the local equilibrium ones versus the square of the external gradient. The blue dotted line is a linear fit with slope 0.025.

Chapter 4

Scaling Law and Bulk-Boundary Decoupling in Non-equilibrium Fluids

We saw in chapter 2 that the temperature and packing fraction profiles present a series of size effect which are very difficult to treat with a traditional finite size scaling. Our intention is to derive the heat conductivity as a function of these profiles and the heat current. Therefore, without a clear picture of the size effects associated to each of these magnitudes, is impossible to study the thermodynamic limit of the heat conductivity. In this chapter we give a strategy to circumvent this problem. First we are going to prove a scaling law for Hard Disks, which can be generalize to any athermal system (see appendix B), with the following starting hypothesis:

(a) The system obeys Local Thermal Equilibrium at the macroscopic level, therefore locally the temperature, density and pressure are related by an Equation of State.

(b) Fourier's law holds locally.

The actual formal expression for these equations will be irrelevant as long as the temperature and density dependence are separable, which is automatically satisfied by athermal systems. As we saw in chapter 3 we can be confident that hypothesis (a) holds and that the system follows the equilibrium Equation of Estate without finite size effects. Therefore if the scaling fails then it will mean that Fourier's Law breakdown for our system. This will allow us to find the limits associated with this hypothesis and study the thermal conductivity for this system.

4.1 The scaling property of Fourier's law for hard disks

Let us define our hard disk system in a box of side L where there are N disks of radius σ. We apply a temperature gradient in the x-direction, that is, we fix the temperature T_0 at $x = 0$ and T_1 at $x = L$.

The system stationary state follows the Fourier's law :

$$J = -\kappa(T(x), \eta(x)) \frac{dT(x)}{dx} \quad x \in [0, L] \tag{4.1}$$

where J is the heat current that it is assumed to be constant along the system, κ is the thermal conductivity that depends on the local temperature $T(x)$ and on the local areal density $\eta(x) = \pi\sigma^2 n(x)$ where $n(x) \equiv N(x)/L^2$ is the local particle density per unit area. In the hard disk case κ is of the form:

$$\kappa(T, \eta) = \sqrt{T} g(\eta) \tag{4.2}$$

In particular, the Enskog theory applied to the hard disk system [68] predicts:

$$g(\eta) = \frac{1}{\sigma\pi^{1/2}} a_1(s) \left[\frac{1}{\xi} + 3\eta + \left(\frac{9}{4} + \frac{4}{\pi a_1(s)} \right) \eta^2 \xi \right] \tag{4.3}$$

with $\xi = (1 - 7\eta/16)/(1 - \eta)^2$ and $a_1(s)$ are the Sonine polynomial approximation up to s order ($a_1(1) = 1$, $a_1(3) = 1.029$). However it is already known that this result deviates significantly from simulations results [57].

We assume that, at this macroscopic level, local equilibrium holds in the sense that the local density and the local temperature are related by its equilibrium equation of state that is of the form:

$$Q = TZ(\eta) \tag{4.4}$$

where $Q = P\pi\sigma^2$ and P is the pressure. We have assumed units where the Boltzmann constant equals to one. $Z(\eta)$ is unknown but there are many proposals that almost fit actual numerical simulations results [22].

Equations (4.1), (4.2) and (4.4) are the necessary equations to completely describe the system macroscopic behavior. That is, we can write down the Fourier's law (4.1) as a function of the density profile:

$$\frac{J}{Q^{3/2}} = F(\eta) \frac{d\eta(x)}{dx} \tag{4.5}$$

where

$$F(\eta) = g(\eta) \frac{dZ(\eta)}{d\eta} Z^{-5/2}(\eta) \tag{4.6}$$

We will assume that $F(\eta) > 0$ for all the studied $\bar{\eta}$ and then $\eta(x)$ is a monotone increasing function. Then the density profile $\eta(x)$ is given by:

$$\frac{x}{L} = \frac{\int_{\eta_0}^{\eta(x)} d\eta\, F(\eta)}{\int_{\eta_0}^{\eta_1} d\eta\, F(\eta)} \tag{4.7}$$

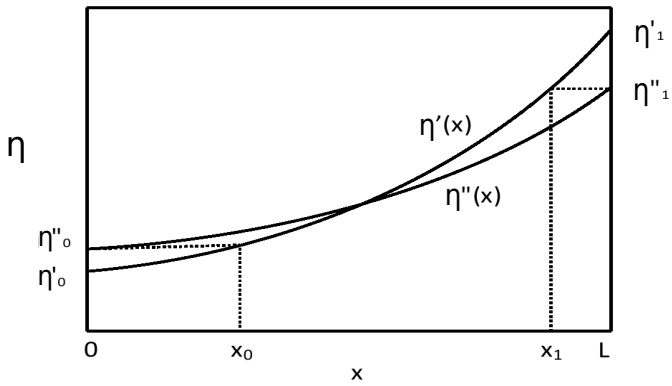

Figure 4.1: Schematic form of two arbitrary solutions of the density profile obtained by solving the Fourier's law for hard disks. The meaning of labels is explained in the text

where $\eta_{0,1}$ can be obtained from the initial given data T_0, T_1 and $\bar{\eta}$ by solving the coupled equations

$$\frac{T_0}{T_1} = \frac{Z(\eta_1)}{Z(\eta_0)} \tag{4.8}$$

$$\bar{\eta} = \frac{1}{L}\int_0^L dx\,\eta(x) = \frac{\int_{\eta_0}^{\eta_1} d\eta\,\eta F(\eta)}{\int_{\eta_0}^{\eta_1} d\eta\,F(\eta)} \tag{4.9}$$

As a byproduct we can find the heat current J and the reduced pressure Q:

$$Q = T_0 Z(\eta_0) \tag{4.10}$$

$$J = \frac{Q^{3/2}}{L}\int_{\eta_0}^{\eta_1} d\eta\,F(\eta) \tag{4.11}$$

Obviously we don't know the expressions for the thermal conductivity (4.2) and the equation of state (4.4) but we can derive several useful properties of the temperature and density profiles that we can use to analyze the data from computer simulations.

Let $\eta'(x)$ and $\eta"(x)$ two solutions of the Fourier's law each one for a different set of values T_0, T_1, $\bar{\eta}$ and the same system length L. Let $\eta'_0 = \eta'(0)$, $\eta"_0 = \eta"(0)$, $\eta'_1 = \eta'(L)$ and $\eta"_1 = \eta"(L)$ and we define x_0 and x_1 as the solutions of the equations $\eta'(x_0) = \eta"_0$ and $\eta'(x_1) = \eta"_1$ respectively (see figure 4.1). Then the following properties hold:

Property 1:

$$\frac{1}{L}\int_{\eta'_0}^{\eta'_1} d\eta\,F(\eta) = \frac{1}{x_1 - x_0}\int_{\eta"_0}^{\eta"_1} d\eta\,F(\eta) \tag{4.12}$$

Proof: We use (4.7) applied to the solution $\eta'(x)$ evaluate at the points x_0

and x_1. Then

$$\frac{x_0}{L} = \frac{\int_{\eta_0'}^{\eta'(x_0)} d\eta\, F(\eta)}{\int_{\eta_0'}^{\eta_1'} d\eta\, F(\eta)} \quad ; \frac{x_1}{L} = \frac{\int_{\eta_0'}^{\eta'(x_1)} d\eta\, F(\eta)}{\int_{\eta_0'}^{\eta_1'} d\eta\, F(\eta)} \tag{4.13}$$

Subtracting both expressions and using the fact that $\eta'(x_0) = \eta"_0$ and $\eta'(x_1) = \eta"_1$ we get (4.12).

Property 2: The profiles $\eta'(x)$ and $\eta"(x)$ are related by the following scaling:

$$\eta"(L\frac{x - x_0}{x_1 - x_0}) = \eta'(x) \qquad \forall\, x \in [x_0, x_1] \tag{4.14}$$

Proof: The profile $\eta"(x)$ is defined by

$$\frac{x}{L} = \frac{\int_{\eta"_0}^{\eta"(x)} d\eta\, F(\eta)}{\int_{\eta"_0}^{\eta"_1} d\eta\, F(\eta)} \tag{4.15}$$

we define the change of variables:

$$y = x_0 + x\frac{x_1 - x_0}{L} \tag{4.16}$$

then equation (4.15) reads:

$$y - x_0 = L\frac{\int_{\eta"_0}^{\eta"(L(y-x_0)/(x_1-x_0))} d\eta\, F(\eta)}{\int_{\eta_0'}^{\eta_1'} d\eta\, F(\eta)} \tag{4.17}$$

where we have applied Property 1. Finally substituting in the later equation the expression x_0/L from eq. (4.13) we get

$$\frac{y}{L} = \frac{\int_{\eta_0'}^{\eta"(L(y-x_0)/(x_1-x_0))} d\eta\, F(\eta)}{\int_{\eta_0'}^{\eta_1'} d\eta\, F(\eta)} \tag{4.18}$$

that is, by definition, the implicit equation for the profile $\eta'(y)$ and therefore the scaling relation (4.14) should hold.

Property 3: The scaling behavior of density profiles is transferred to the corresponding temperature profiles in the following way:

$$\frac{T'(x)}{Q'} = \frac{T"(L\frac{x-x_0}{x_1-x_0})}{Q"} \tag{4.19}$$

where Q' and $Q"$ are the reduced pressures corresponding to the system with density profiles $\eta'(x)$ and $\eta"(x)$ respectively.

Proof: We have assumed that the equation of state holds locally. That means:

$$T'(x) = Q'Z(\eta'(x))^{-1} \quad , \quad T"(x) = Q"Z(\eta"(x))^{-1} \tag{4.20}$$

By using the scaling property (4.14) we can relate both temperature profiles:

$$\frac{T"(L\frac{x-x_0}{x_1-x_0})}{Q"} = Z(\eta"(L\frac{x - x_0}{x_1 - x_0})) \tag{4.21}$$

$$= Z(\eta'(x)) = \frac{T'(x)}{Q'} \tag{4.22}$$

Property 4: The reduced pressures and currents of the corresponding profiles $\eta'(x)$ and $\eta"(x)$ are related by:

$$\frac{J'}{LQ'^{3/2}} = \frac{J"}{(x_1 - x_0)Q"^{3/2}} \tag{4.23}$$

Proof: We know from eq. (4.11):

$$\frac{J'L}{Q'^{3/2}} = \int_{\eta'_0}^{\eta'_1} d\eta\, F(\eta) \tag{4.24}$$

$$\frac{J''L}{Q"^{3/2}} = \int_{\eta"_0}^{\eta"_1} d\eta\, F(\eta) \tag{4.25}$$

Dividing both equation and using Property 1 (4.12) we get the desired result.

4.2 Experimental Test of the Scaling Law

We know that if local equilibrium and Fourier's law hold then for a given set of external parameters (say average density, and the wall temperatures at the extremes) there is a well defined solution of the equations whose solution are a density and temperature profiles $\eta(x)$ and $T(x)$ respectively. Moreover, these profiles and any other solution of a different set of external parameters, $\bar{\eta}(x)$ and $\bar{T}(x)$, are related in the following way:

$$\eta(x) = \bar{\eta}\left(\frac{J\bar{Q}^{3/2}}{\bar{J}Q^{3/2}}(x - x_0)\right) \quad T(x) = \frac{Q}{\bar{Q}}\bar{T}\left(\frac{J\bar{Q}^{3/2}}{\bar{J}Q^{3/2}}(x - x_0)\right) \tag{4.26}$$

where J and Q are the stationary heat current and the scaled pressure respectively for the system with density profile $\eta(x)$ and $\bar{J}$, $\bar{Q}$ the ones for the system with density profile $\bar{\eta}(x)$. x_0 is related with the set of the system parameters in both cases.

We saw in chapter 2 that it is not clear that Fourier's law holds for our system. We were not able to study the infinite size limit of the temperature profiles even though they behave in a very smooth way. Thermal resistance at the boundaries and finite size effects on the currents and pressure make very difficult to obtain a coherent finite size study of the system. Moreover, we also saw that density profiles have a lot of structure near the boundaries and they are very sensitive to the system size making their analysis much more difficult. However we have also shown in chapter 3 that the bulk of the system follows the EoS of Hard Disks to a high accuracy, suggesting that it was not necessary to perform a finite size analysis on the profiles. For this reason we try to circumvent these problems by discarding the data near the thermal wall and performing the scaling over the remaining points. We will see how the rest of the data scale as the theory predicts.

This **Bulk-Boundary Decoupling** (BBD), that we advance in chapter 3, is a property by which the system naturally reorganizes itself in two well defined regions:

- The stochastic boundary plus the boxes near them that we will call *effective thermal walls*.

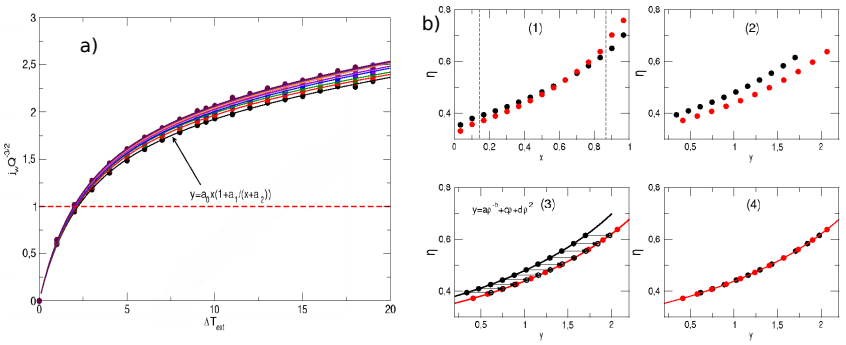

Figure 4.2: a) Measured $JQ^{3/2}$ for systems with $\eta = 0.5$, $T_1 = 1$, $T_0 = 2$, 3, ..., 20 for all the ten sizes (black points are the smaller size data). b) Strategy followed to scale all the data. We use as example the density profiles obtained for $\eta = 0.5$, $T_1 = 1$, $N = 8838$ and $T_0 = 10.5$ (black points) and $T_0 = 20$ (red points). The data interpolation is done with the formula in (3) with parameters: $a = -0.2634$, $b = 1.7576$, $c = 5.2094$ and $d = -2.3545$ for the black data points and $a = -0.2123$, $b = 1.8653$, $c = 5.6701$ and $d = -2.6221$ for the red data points.

- The rest of the system, which behave as an infinite fluid system in LTE.

The effective thermal walls create new boundary conditions to the bulk part that lacks of boundary effects like, for instance, the thermal resistance or density structure near it. Then, the bulk part follows the ideal Fourier's law with effective boundary temperatures and average density. Obviously, we have no predictive control of the effective boundary conditions. We will show in the rest of this section that they exist and that we can numerically study the thermal transport of an ideal hard disk system without worrying for boundary size effects. BBD maybe a common property of particle systems with well behaved interactions but we can only proof its existence via the scaling property of the profiles.

Let us show that the bulk part of our system have the scaling property. First, let us define a *reference profile* as the one with the property $\bar{J} = \bar{Q}^{3/2}$. There are infinite many of them and they are related by a shift on the x-coordinate. For instance in Figure 4.2a we show the behavior of $JQ^{3/2}$ for our simulations with $\eta = 0.5$, temperatures $T_1 = 1$, $T_0 = 2$, 3, ..., 20 and ten different sizes. We see that one can find $JQ^{3/2} = 1$ when $\Delta T_{ext} \simeq 2$.

With respect the *reference profile*, $\bar{\eta}(x)$, we should prove that the profiles from the numerical simulation have the properties:

$$\eta(x) = \bar{\eta}(y + y_0) \quad , \quad \frac{T(x)}{Q} = \frac{\bar{T}(y + y_0)}{\bar{Q}} \tag{4.27}$$

where $y = JQ^{-3/2}x$. That is, the bulk part of all the profiles obtained from different thermal gradients, averaged densities or sizes, should be part of a

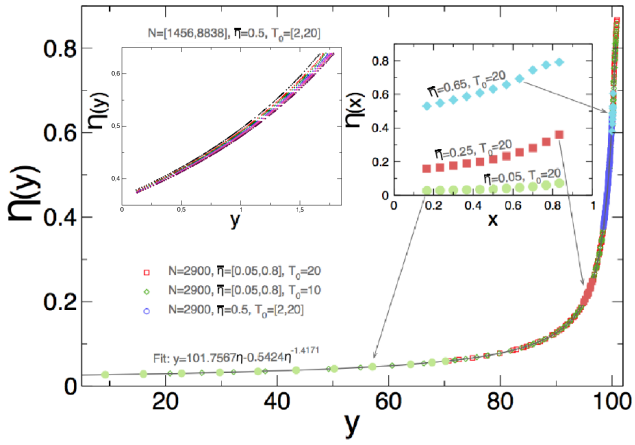

Figure 4.3: Collapse of scaled bulk density profiles measured for $N_{\text{Bulk}} = 2900$ and three different sets of conditions (see legend) for a total of 572 data points. Left inset: Collapse with 2200 data points obtained for $\bar{\eta} = 0.5$, $T_0 \in [2, 20]$ and different sizes $N \in [1456, 8838]$. Right inset: Widely different bulk density profiles measured for different conditions collapse onto different parts of the same universal master curve.

universal curve (the reference profile) except by a coordinate shift, related to the boundary effects. The strategy is simple and it is shown for the density profile in Figure 4.2b. We follow four steps: (1) we discard the two near the walls data points from our 15 points in all the measured profiles. (2) We rescale the coordinate x using the measured values of J and Q ($y = JQ^{-3/2}x$) for all the profiles. (3) We interpolate a function through the points for each profile and (4) Fixing one profile, we look for the best shift for the interpolated curves (say the one that minimizes the distance between the fixed profile and the data to be moved) and we apply it to the data set.

We have found that the best function to interpolate the density profiles data coming form any temperature gradient, size or average density is given by the implicit form:

$$x = \frac{a}{\eta^b} + c\eta + d\eta^2 \tag{4.28}$$

where a, b, c and d are fitted to interpolate a data set.

In Figure 4.3 we show the scaled data for $N = 2900$ and three set of simulations. One with fixed average areal density 0.5 and 20 different temperature gradients, and two sets with fixed temperature gradient and different average areal density ranging from 0.05 up to 0.8. The full data set is fitted to the curve:

$$y = 101.75674\bar{\eta} - 0.542411\bar{\eta}^{-1.41714} \tag{4.29}$$

with a correlation coefficient of 0.99999. The left inset shows the scaled packing fraction profiles for $\bar{\eta} = 0.5$, $T_1 = 1$ and $T_0 = 2, \ldots, 20$. Where we

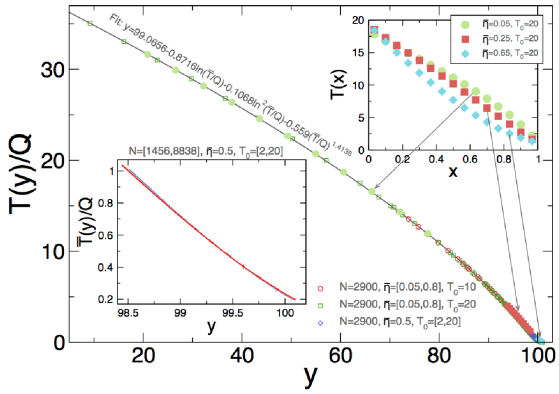

Figure 4.4: Collapse of bulk temperature profiles for the same conditions that the top panel. Note that the shifts ζ are obtained from the density scaling, yielding a perfect scaling for temperature profiles.

intentionally plot the scaled data for each size in different curves to show the strength of the scaling property and its small dependence on the system size. Each curve contains 220 data points. We see there that the data for each size scale very well but there is a small tilt of the scaled curve depending on the system size (we have translated the scaled curves to almost coincide at the beginning point to see clearly the size effect). That is, it seems that, for a given size, the system has the boundary decoupling property and it follows Fourier's law with *a size dependent thermal conductivity*. Maybe this behavior is singular to the hard disks systems alone. We know that strictly speaking, thermal conductivity for hard disks should be infinite on the thermodynamic limit due to the existence of the long time tail behavior of the current-current time correlation functions. Therefore maybe we are detecting the effects of such limiting behavior. We will come back to such effect when analyzing the system thermal conductivity.

Once we managed to scale the areal density profiles, we may check if the temperature profiles divided by their pressure scales as well. In Figure 4.4 we show the scaling of T/Q where we used the same shifts (y_o) as in the case for the packing fraction. Again we see, at the bottom inset, some systematic dependence on the system size. However, this time we translated the curves to coincide in the middle point to stress that this dependence is very subtle. In the top inset we represented the original profiles for different configurations and where they scale to. We managed to interpolate a curve for all data points that we have for $N = 2900$:

$$y = 99.0656 - 0.871563 \ln\left(\frac{\bar{T}}{\bar{Q}}\right) - 0.106756 \left(\ln\left(\frac{\bar{T}}{\bar{Q}}\right)\right)^2 - 0.558971 \left(\frac{\bar{T}}{\bar{Q}}\right)^{1.41381} \tag{4.30}$$

At this point we should say something about profiles where there is co-existing liquid-solid phase. We already shown that on the solid phase lo-

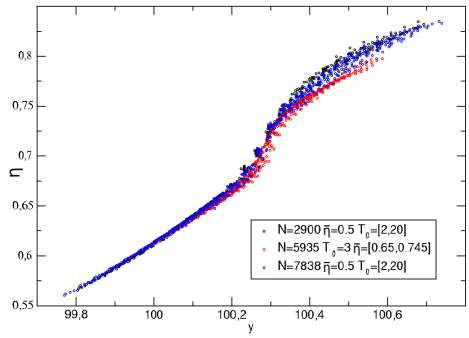

Figure 4.5: Rescaled profiles with coexisting liquid-solid phase for three different sizes and various gradients and densities.

cal equilibrium doesn't hold. Therefore we cannot expect that neither the boundary decoupling, or the scaling behavior of the profiles should apply. In Figure 4.5 we see our best trial of scaling data. We manager to scale the data of the liquid phase for each size separately However we are unable to scale the solid-like part. We see that even for a equal size, the solid part of the profiles do not show scaling that it is consistent with our premises.

Once we have the scaled profiles and its interpolated, to close the strategy, we should be able to recover from them the behavior of the system for any set of external parameters we would like to study. We will assume that $T_1 = 1$ because from the theory above we see that if $T_0 \to \alpha T_0$ and $T_1 \to \alpha T_1$ for any positive *alpha*, the density profile solution of the equations are equal and the temperature profiles, heat current and pressure are multiplied by α, $\alpha^{3/2}$ and α respectively. Let us explicit the path to get any desired result:

- (0) Give T_0 and $\bar{\eta}$ ($T_1 = 1$, $L = 1$).
- (1) Solve the equations to get y_0 and y_1:

$$\frac{\tilde{T}(y_0)}{\tilde{T}(y_1)} = T_0 \quad , \quad \bar{\eta} = \frac{1}{y_1 - y_0} \int_{y_0}^{y_1} dy\, \bar{\eta}(y) \tag{4.31}$$

  where $\tilde{T}(y) \equiv \bar{T}(y)/Q$ and we can use the interpolations that define implicitly $\bar{T}(y)$ and $\bar{\eta}(y)$.

- (2) Obtain the system pressure

$$Q = \frac{1}{\bar{T}(y_1)} \tag{4.32}$$

- (3) Obtain the heat current:

$$J = Q^{3/2}(y_1 - y_0) \tag{4.33}$$

For example, if $T_0 = 10$ and $\bar{\eta} = 0.25$ then $Q = 2.03649$, $J = 21.2774$, $y_0 = -9.10878$ and $y_1 = -1.78731$. The profiles are trivially obtained once

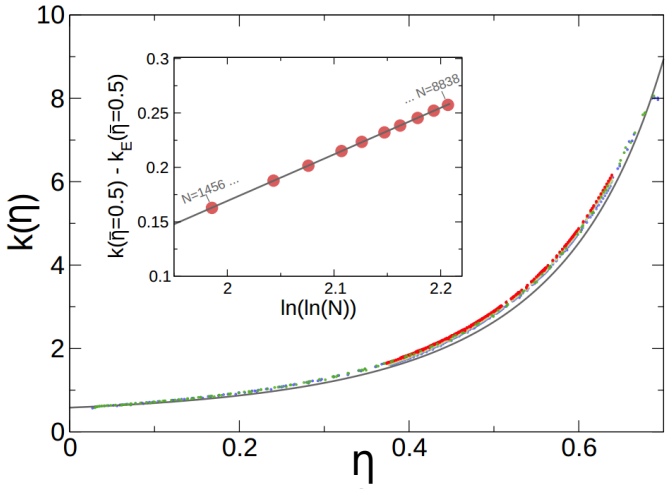

Figure 4.6: Density dependence of the heat conductivity as obtained from the rescaled temperature profiles $\tilde{T}(y) \equiv \bar{T}(y)/Q$ for different $\eta \in [0.05, 0.8]$, $T_0 \in [2, 20]$ and $N \in [1456, 8838]$. A well-defined deviation from Gass result based on Enskog kinetic theory (full line) is found [68]. Moreover, a systematic dependence with system size is also observed, see inset for $\bar{\eta} = 0.5$, which scales as $\ln(\ln(N))$, as expected from the marginally anomalous behavior of heat conductivity in two dimensions.

we know Q, J, y_0 and y_1. Let us obtain some more physical information from our system. The first thing that we see in Figure 4.4 is that there is a convexity change in the scaled temperature curve. By using the above interpolation we can compute the point at which it occurs:

$$\tilde{T}^* = 1.86866 \quad , \quad \left.\frac{d\tilde{T}}{dy}\right|_{\tilde{T}=\tilde{T}^*} = -0.64042 \quad , \quad \eta^* = 0.276182 \tag{4.34}$$

where $\tilde{T} = \bar{T}/Q$. One can compute the set of parameters that one needs in order to see such change of curvature of the temperature profile in an numerical experiment. For instance, assuming $T_1 = 1$, for $\bar{\eta} = 0.5$, $T_0 > 100$, for $\bar{\eta} = 0.4$, $T_0 > 7.05$ and for $\bar{\eta} = 0.3$, $T_0 > 1.37$.

Our detailed data for the universal master curves in Fig. 4.4 allows to do a precise measurement of the hard-disks heat conductivity over a broad range of densities. In fact, by multiplying Fourier's law (4.1) by $Q^{-3/2}$ and recalling the separable form of the conductivity, $\kappa(T, \eta) = \sqrt{T}k(\eta)$, it is easy to show that $k(\eta) = [\tilde{T}(y)^{1/2}\tilde{T}'(y)]^{-1}$, with $\eta = \eta(y)$. We hence performed discrete derivatives of the measured master curve $\tilde{T}(y)$ for each of the different sets of parameters ΔT, $\bar{\eta}$ and N, identifying each value of $[\tilde{T}(y)^{1/2}\tilde{T}'(y)]^{-1}$ with the associated $\eta(y)$. Fig. 4.6 shows the resulting $k(\eta)$, which exhibits deviations from the Gass prediction based on Enskog kinetic theory [68], as already reported [57, 69]. For each size we have interpolated

the data around $\eta = 0.5$ to a line and we have obtained an estimation of the conductivity value at such point (subtracting the Enskog counterpart). We have plotted such values as a function of N and we see a very regular behavior with N. The best fit we have found is

$$g(0.5) - g_{\text{Enskog}}(0.5) = -0.686221 + 0.427707 \ln(\ln(N)) \tag{4.35}$$

This very weak but systematic double-logarithmic N-dependence of $k(\eta)$ is a reminiscent of the marginally anomalous heat conductivity of hard disks resulting from the long time tails in two dimensions [27, 70, 71]. This shows that our scaling method, together with the bulk-boundary decoupling mechanism, allows one to get rid of *spurious* finite-size effects related with the presence of boundaries, keeping physically relevant finite-size information.

Chapter 5

Symmetries in Fluctuations far from Equilibrium

As we argued in the Introduction, most non-equilibrium systems are characterized by currents of locally conserved observables. Therefore understanding current statistics in terms of microscopic dynamics has become one of the main objectives of non-equilibrium statistical physics [14, 13, 54, 72, 20, 73, 15, 17, 19, 74, 75, 76, 77, 31, 34, 78]. Pursuing this line of research is both of fundamental as well as practical importance. At the theoretical level, the function controlling current fluctuations can be identified as the non-equilibrium analog of the free energy functional in equilibrium systems [20, 15, 17, 19], from which macroscopic properties of a non-equilibrium system can be obtained (including its most prominent features, as for instance the ubiquitous long range correlations [79, 80]). On the other hand, the physics of most modern mesoscopic devices is characterized by large fluctuations which determine their behavior and function. In this way understanding current statistics in these systems is of great practical significance.

Despite the considerable interest and efforts on these issues, exact and general results valid arbitrarily far from equilibrium are still very scarce. The reason is that, while in equilibrium phenomena dynamics is irrelevant and the Gibbs distribution provides all the necessary information, in non-equilibrium physics dynamics plays a dominant role, even in the simplest situation of a non-equilibrium steady state [20, 15, 17, 19]. However, there is a remarkable exception to this absence of general results which has triggered an important surge in activity since its formulation in the mid nineties. The Fluctuation Theorem [13, 14], which implies a relation between the probabilities of a given current fluctuation and the inverse event, is a deep statement on the subtle consequences of time-reversal symmetry of microscopic dynamics at the macroscopic level. Particularly important here is the observation that symmetries are reflected at the fluctuating macroscopic level arbitrarily far from equilibrium. Inspired by this illuminating result, we explore in this chapter the behavior of the current distribution under symmetry transfor-

mations [81]. Key to our analysis is the observation that, in order to facilitate a given current fluctuation, the system traverses a well-defined optimal path in phase space [20, 15, 17, 19, 75, 76, 82]. This path is, under very general conditions, invariant under certain symmetry transformations on the current. We confirm here the validity of the new symmetry in extensive numerical simulations of a Hard-Disk fluid in a temperature gradient.

5.1 The Isometric Fluctuation Relation

Our starting point is the continuity equation given by Eq.(5.1), which describes the macroscopic evolution of a wide class of systems characterized by a locally-conserved magnitude (e.g. energy, particle density, momentum, etc.)

$$\partial_t \rho(\mathbf{r},t) = -\boldsymbol{\nabla}\cdot\Big(\mathbf{Q}_{\mathbf{E}}[\rho(\mathbf{r},t)] + \boldsymbol{\xi}(\mathbf{r},t)\Big)\,. \tag{5.1}$$

Here $\rho(\mathbf{r},t)$ is the density field, $\mathbf{j}(\mathbf{r},t) \equiv \mathbf{Q}_{\mathbf{E}}[\rho(\mathbf{r},t)] + \boldsymbol{\xi}(\mathbf{r},t)$ is the fluctuating current, with local average $\mathbf{Q}_{\mathbf{E}}[\rho(\mathbf{r},t)]$, and $\boldsymbol{\xi}(\mathbf{r},t)$ is a Gaussian white noise characterized by a variance (or *mobility*) $\sigma[\rho(\mathbf{r},t)]$. This (conserved) noise term accounts for microscopic random fluctuations at the macroscopic level. Notice that the current functional includes in general the effect of a conservative external field, $\mathbf{Q}_{\mathbf{E}}[\rho(\mathbf{r},t)] = \mathbf{Q}[\rho(\mathbf{r},t)] + \sigma[\rho(\mathbf{r},t)]\mathbf{E}$. Examples of systems described by Eq.(5.1) range from diffusive systems [19, 20, 15, 17, 74, 75, 76, 77], where $\mathbf{Q}[\rho(\mathbf{r},t)]$ is given by Fourier's (or equivalently Fick's) law, $\mathbf{Q}[\rho(\mathbf{r},t)] = -D[\rho]\boldsymbol{\nabla}\rho(\mathbf{r},t)$, to most interacting-particle fluids [83], characterized by a Ginzburg-Landau-type theory for the locally-conserved particle density. To completely define the problem, the above evolution equation must be supplemented with appropriate boundary conditions, which may include an external gradient. We are interested in the probability $\mathrm{P}_\tau(\mathbf{J})$ of observing a space- and time-averaged empirical current $\mathbf{J}$, defined as

$$\mathbf{J} = \frac{1}{\tau}\int_0^\tau dt \int_\Lambda d\mathbf{r}\; \mathbf{j}(\mathbf{r},t)\,. \tag{5.2}$$

where $\Lambda \in [0,1]^d$ is the space domain, being d the dimensionality of the system. This probability obeys a large deviation principle for long times [84, 85, 86], $\mathrm{P}_\tau(\mathbf{J}) \sim \exp[+\tau L^d G(\mathbf{J})]$, where L is the system linear size and $G(\mathbf{J}) \leq 0$ is the current large-deviation function (LDF), meaning that current fluctuations away from the average are exponentially unlikely in time. According to macroscopic fluctuation theory we have [19, 15, 17, 74],

$$G(\mathbf{J}) = -\min_{\rho(\mathbf{r})} \int_\Lambda \frac{\left(\mathbf{J} - \mathbf{Q}_{\mathbf{E}}[\rho(\mathbf{r})]\right)^2}{2\sigma[\rho(\mathbf{r})]} d\mathbf{r}\,, \tag{5.3}$$

which expresses the *locally*-Gaussian nature of fluctuations [74, 75, 76]. The optimal profile $\rho_0(\mathbf{r};\mathbf{J})$ solution of the above variational problem can be interpreted as the density profile the system adopts to facilitate a current fluctuation $\mathbf{J}$ [75, 76, 82]. To derive Eq. (5.3) we assumed the additivity conjecture, namely that (i) the optimal profiles associated to a given current fluctuation are time-independent [19, 20, 15, 17, 74, 75, 76, 77, 82] , and (ii) the optimal current field has no spatial structure. This last hypothesis,

which greatly simplifies the calculation of current statistics, can be however relaxed for our purposes (as shown in appendix C). The probability $\mathrm{P}_\tau(\mathbf{J})$ is thus simply the *Gaussian* weight associated to the optimal profile. Note however that the minimization procedure gives rise to a nonlinear problem which results in general in a current distribution with non-Gaussian tails [20, 15, 17, 19, 74, 75, 76].

The optimal profile is solution of the following equation

$$\frac{\delta\omega_2[\rho(\mathbf{r})]}{\delta\rho(\mathbf{r}')} - 2\mathbf{J}\cdot\frac{\delta\boldsymbol{\omega}_1[\rho(\mathbf{r})]}{\delta\rho(\mathbf{r}')} + \mathbf{J}^2\frac{\delta\omega_0[\rho(\mathbf{r})]}{\delta\rho(\mathbf{r}')} = 0\,, \tag{5.4}$$

where $\frac{\delta}{\delta\rho(\mathbf{r}')}$ stands for functional derivative, and

$$\boldsymbol{\omega}_n[\rho(\mathbf{r})] \equiv \int_\Lambda d\mathbf{r}\,\mathbf{W}_n[\rho(\mathbf{r})] \qquad \text{with} \qquad \mathbf{W}_n[\rho(\mathbf{r})] \equiv \frac{\mathbf{Q}^n_{\mathbf{E}}[\rho(\mathbf{r})]}{\sigma[\rho(\mathbf{r})]}\,. \tag{5.5}$$

Remarkably, the optimal profile $\rho_0(\mathbf{r};\mathbf{J})$ solution of Eq. (5.4) depends exclusively on $\mathbf{J}$ and $\mathbf{J}^2$. Such a simple quadratic dependence, inherited from the locally-Gaussian nature of fluctuations, has important consequences at the level of symmetries of the current distribution. In fact, it is clear from Eq. (5.4) that the condition

$$\frac{\delta\boldsymbol{\omega}_1[\rho(\mathbf{r})]}{\delta\rho(\mathbf{r}')} = 0\,, \tag{5.6}$$

implies that $\rho_0(\mathbf{r};\mathbf{J})$ will depend exclusively on the *magnitude* of the current vector, via $\mathbf{J}^2$, not on its *orientation*. In this way, all isometric current fluctuations characterized by a constant $|\mathbf{J}|$ will have the same associated optimal profile, $\rho_0(\mathbf{r};\mathbf{J}) = \rho_0(\mathbf{r};|\mathbf{J}|)$, independently of whether the current vector $\mathbf{J}$ points along the gradient direction, against it, or along any arbitrary direction. In other words, the optimal profile is invariant under current rotations if Eq. (5.6) holds.

It turns out that condition (5.6) follows from the time-reversibility of the dynamics, in the sense that the evolution operator in the Fokker-Planck formulation of Eq. (5.1) obeys a local detailed balance condition [73, 72]. In this case

$$\mathbf{W}_1[\rho(\mathbf{r})] = \frac{\mathbf{Q}_{\mathbf{E}}[\rho(\mathbf{r})]}{\sigma[\rho(\mathbf{r})]} = -\boldsymbol{\nabla}\frac{\delta\mathcal{H}[\rho]}{\delta\rho}\,, \tag{5.7}$$

where $\mathcal{H}[\rho(\mathbf{r})]$ is the system Hamiltonian. In this case, by using vector integration by parts, it is easy to show that

$$\frac{\delta}{\delta\rho(\mathbf{r}')}\int_\Lambda d\mathbf{r}\mathbf{W}_1[\rho(\mathbf{r})]\cdot\boldsymbol{\mathcal{A}}(\mathbf{r}) = -\frac{\delta}{\delta\rho(\mathbf{r}')}\int_{\partial\Lambda} d\Gamma\frac{\delta\mathcal{H}[\rho]}{\delta\rho}\boldsymbol{\mathcal{A}}(\mathbf{r})\cdot\hat{n} = 0\,, \tag{5.8}$$

for any divergence-free vector field $\boldsymbol{\mathcal{A}}(\mathbf{r})$. The second integral is taken over the boundary $\partial\Lambda$ of the domain Λ where the system is defined, and $\hat{n}$ is the unit vector normal to the boundary at each point. In particular, by taking $\boldsymbol{\mathcal{A}}(\mathbf{r}) = \mathbf{J}$ constant, Eq. (5.8) implies that $\delta\boldsymbol{\omega}_1[\rho(\mathbf{r})]/\delta\rho(\mathbf{r}') = 0$. Hence for time-reversible systems the optimal profile $\rho_0(\mathbf{r};\mathbf{J})$ remains invariant under

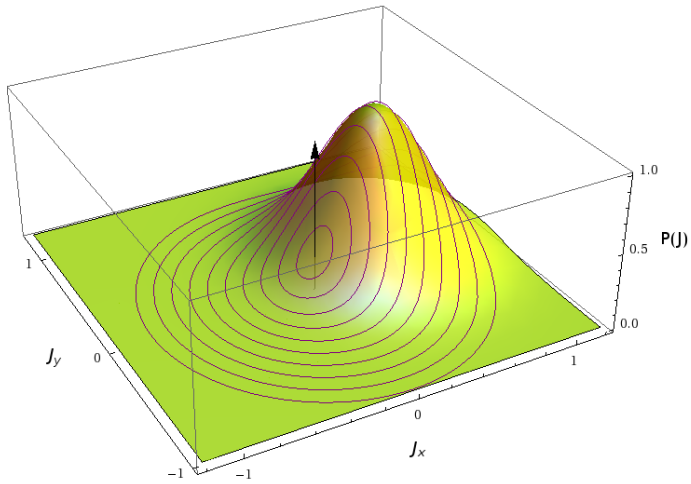

Figure 5.1: The isometric fluctuation relation at a glance. Sketch of the current distribution in two dimensions, peaked around its average $\langle \mathbf{J} \rangle_\epsilon$, and isometric contour lines for different $|\mathbf{J}|$'s. The isometric fluctuation relation, Eq. (5.9) , establishes a simple relation for the probability of current fluctuations along each of these contour lines.

rotations of the current $\mathbf{J}$, see Eq. (5.4). Using this invariance in Eq. (5.3) we can relate in a simple way the current LDF of any pair of isometric current fluctuations $\mathbf{J}$ and $\mathbf{J}'$, with $|\mathbf{J}| = |\mathbf{J}'|$

$$\lim_{\tau\to\infty} \frac{1}{\tau} \ln\left[\frac{\mathrm{P}_\tau(\mathbf{J})}{\mathrm{P}_\tau(\mathbf{J}')}\right] = \boldsymbol{\epsilon}\cdot(\mathbf{J}-\mathbf{J}')\,, \tag{5.9}$$

Here $\boldsymbol{\epsilon} = \boldsymbol{\varepsilon} + \mathbf{E}$ is a constant vector directly related to the rate of entropy production in the system, which depends on the boundary baths via $\boldsymbol{\varepsilon}$.

This *isometric* fluctuation relation (IFR), which includes as a particular case the Gallavotti-Cohen (GC) result for $\mathbf{J}' = -\mathbf{J}$, relates in a strikingly simple manner the probability of a given fluctuation $\mathbf{J}$ with the likelihood of any other current fluctuation on the d-dimensional hypersphere of radius $|\mathbf{J}|$, see figure 5.1 , projecting a complex d-dimensional problem onto a much simpler one-dimensional theory. Unlike the GC relation which is a non-differentiable symmetry involving the inversion of the current sign, $\mathbf{J} \to -\mathbf{J}$, Eq. (5.9) is valid for arbitrary changes in orientation of the current vector.In fact relation (5.9) can be expressed as:

$$G(\mathbf{J}) - G(\mathbf{J}') = |\boldsymbol{\epsilon}||\mathbf{J}|(\cos\theta - \cos\theta')\,, \tag{5.10}$$

where θ and θ' are the angles formed by vectors $\mathbf{J}$ and $\mathbf{J}'$, respectively. By letting $\mathbf{J}$ and $\mathbf{J}'$ differ by an infinitesimal angle, the IFR can be cast in a simple differential form, $\partial_\theta G(\mathbf{J}) = |\boldsymbol{\epsilon}||\mathbf{J}|\sin\theta$. This makes the experimental test of the above relation a feasible problem, as data for current fluctuations

involving different orientations around the average can be gathered with enough statistics to ensure experimental accuracy.

The condition $\delta\boldsymbol{\omega}_1[\rho(\mathbf{r})]/\delta\rho(\mathbf{r}') = 0$ can be seen as a conservation law. It implies that the observable $\boldsymbol{\omega}_1[\rho(\mathbf{r})]$ is in fact a *constant of motion*, $\boldsymbol{\epsilon} \equiv \boldsymbol{\omega}_1[\rho(\mathbf{r})]$, independent of the profile $\rho(\mathbf{r})$, which can be related with the rate of entropy production via the Gallavotti-Cohen theorem [14, 73, 72]. In a way similar to Noether's theorem, the conservation law for $\boldsymbol{\epsilon}$ implies a symmetry for the optimal profiles under rotations of the current and a fluctuation relation for the current LDF. This constant can be easily computed under very general assumptions (see appendix C). Finally, it is also important to notice that the isometric fluctuation relation is valid for arbitrarily large fluctuations, i.e. even for the non-Gaussian far tails of current distribution.

5.2 Checking the Isometric Fluctuation Relation

We have tested the validity of the IFR in extensive numerical simulations of a Hamiltonian hard-disk fluid subject to a temperature gradient. This model is a paradigm in liquid state theory, condensed matter and statistical physics, and has been widely studied during last decades. The model consists in N hard disks of unit diameter interacting via instantaneous collisions and confined to a box of linear size L such that the particle density is fixed to $\Phi = N/L^2 = 0.58$. Here we choose $N = 320$. The box is divided in three parts: a central, bulk region of width $L - 2\alpha$ with periodic boundary conditions in the vertical direction, and two lateral stripes of width $\alpha = L/4$ which act as deterministic heat baths, see bottom inset to figure 5.2. This is achieved by keeping constant the total kinetic energy within each lateral band via a global, instantaneous rescaling of the velocity of bath particles after bath-bulk particle collisions. This heat bath mechanism has been shown to efficiently thermostat the fluid [36]. We performed a large number of steady state simulations of long duration ($\tau > 10^4 N$ collisions per particle) for $T_0 = 4$ and $T_1 = 1$, accumulating statistics for the space- and time-averaged current $\mathbf{J}$ and measuring the average temperature profile associated to each $\mathbf{J}$. figure 5.2 shows the linear collapse of $|\mathbf{J}|^{-1}[G(\mathbf{J}) - G(\mathbf{J}')]$ as a function of $\cos\theta - \cos\theta'$ for different values of $|\mathbf{J}|$, confirming the validity of the IFR for this hard-disk fluid in the moderate range of current fluctuations that we could access. Moreover, the measured optimal profiles for different isometric current fluctuations all nicely collapse onto single curves, see top inset to figure 5.2, confirming their rotational invariance.

5.3 Conclusions

The IFR is a consequence of time-reversibility for systems in the hydrodynamic scaling limit, and reveals an unexpected high level of symmetry in the statistics of non-equilibrium fluctuations. It generalizes and comprises the Gallavotti-Cohen fluctuation theorem for currents, relating the probabilities

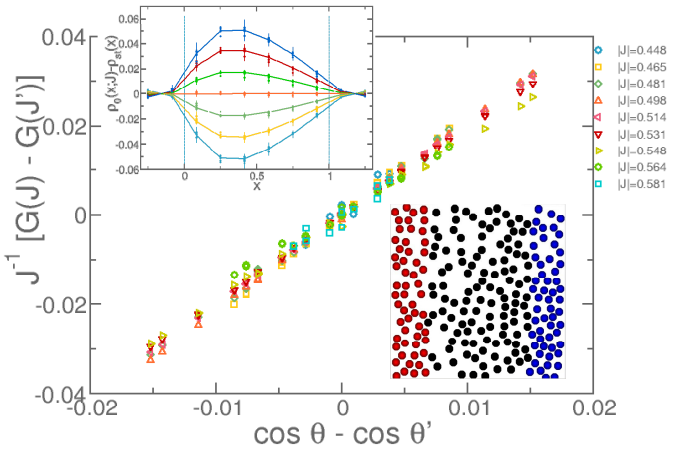

Figure 5.2: IFR in a macroscopic hard-disk fluid. Confirmation of IFR in a two dimensional hard-disk fluid under a temperature gradient after a polar binning of the measured current distribution. As predicted by IFR, the difference of current LDFs for different isometric current fluctuations, once scaled by the current norm, collapses in a line when plotted against $\cos\theta - \cos\theta'$. Top inset: Optimal temperature profiles associated to different current fluctuations. Profiles for a given $|\mathbf{J}|$ and different angles $\theta \in [-7.5°, +7.5°]$ all collapse onto a single curve, thus confirming the invariance of optimal profiles under current rotations. Notice that the profiles smoothly penetrate into the heat baths. Bottom inset: Snapshot of the 2D hard-disk fluid with Gaussian heat baths.

of an event not only with its time-reversal but with any other isometric fluctuation. This has important consequences in the form of hierarchies for the current cumulants and the linear and nonlinear response coefficients, which hold arbitrarily far from equilibrium and can be readily tested in experiments (see appendix C). A natural question thus concerns the level of generality of the isometric fluctuation relation. In this chapter we have demonstrated the IFR for a broad class of systems characterized at the macro-scale by a *single* conserved field, using the tools of macroscopic fluctuation theory (MFT). This theoretical framework has been rigorously proven for a number of interacting particle systems [20, 15, 17, 19], but it is believed to remain valid for a much larger class of systems. The hard-disk fluid is a fully hydrodynamic system, with 4 different locally-conserved coupled fields possibly subject to memory effects, defining a far more complex situation than the one studied here within MFT, see eq. (5.1). Therefore the validity of IFR in this context suggests that this fluctuation relation, based on the invariance of optimal profiles under symmetry transformations, is in fact a rather general result valid for arbitrary fluctuating hydrodynamic systems.

Conclusions and Outlook

In this thesis we have studied the behavior of a system of Hard-Disk under a temperature gradient. Within the out of equilibrium phenomena this is one of the simpler cases. Surprisingly enough, even this simple case, is not fully understood from a theoretical viewpoint. The main drawback is that the theories that describe it use certain assumptions which lack a rigorous demonstration. In our particular case two of these hypotheses stand as pillars on which steady state descriptions are based: Local Thermal Equilibrium and Fourier's law.

Local Thermal Equilibrium is based on the assumption that the times needed to equilibrate the system locally are much shorter than the characteristic time associated with non equilibrium macroscopic phenomena. This allows to define local variables, such as temperature or density, as well as using the thermodynamic relations locally. However when using this concept we have to deal with a very important subtlety. It is known that, from a formal point of view, the *measure* associated with a non-equilibrium system at steady state can not be a local equilibrium measure, i.e. a local Gibbs measure with temperature $T(x)$ and density $\rho(x)$, since, in this case, there would be no long range correlations in the system or a flow associated with the gradient imposed [30]. Thus we can define more precisely a system in Local Thermal Equilibrium as the one in which the configurations associated with the system's steady state are such that any expected local values coincide with the calculated using a equilibrium distribution with temperature $T(x)$ and density $\rho(x)$, but fluctuations calculated with these two methods differ from each other. Thus when study this concept we have to distinguish between the macroscopic level observation and the fluctuating level, being necessary to study both to have a clear confirmation of this hypothesis.

On the other hand the problem associated with the Fourier's law in particular, and constitutive equations in general, is that there is not a rigorous calculation of transport coefficients from the microscopic dynamics of the system, valid arbitrarily far from equilibrium. This has only been possible in very simplified transport models [30, 54]. This has the consequence that it is not known, a priori, whether Fourier's applies to a given system, being necessary to determine it computationally model by model.

Our main motivation for conducting this thesis was to deepen in understanding these theoretical hypotheses that, to date, have not a rigorous mathematical demonstration. This lack of results is due to the complexity associated with the problem. Therefore, a computational characterization

of the limits of validity of these hypothesis has great guidance value in order to find new ways to address these problems. However, this computational approach is not without problems too. Two major drawbacks are boundary and size effects. In particular boundary effects are especially problematic. In equilibrium these effects are, typically, minimized by using periodic boundary conditions. However, this type of boundary conditions are incompatible with the introduction of heat baths at the border [62]. In chapter 1 and 2 of this thesis we study these effects in our system.

In Chapter 1 we found that when the heat sources have the same temperature, i.e. in the equilibrium case, both boundary and size effects disappear when the number of particles tends to infinity. However, as we saw in Chapter 2, when the system is subject to a temperature gradient, these effects get more complicated, in such a way, that the infinite N extrapolation doesnt yield a conclusive result for the profiles of temperature and areal density. Despite these effects, profiles, once discarded those boxes next to the sources, are smooth but not linear, allowing us to obtain experimental fits that reproduce our data very well. Finally we study the energy flow through the system. Although in this case we get a clear limiting behavior, we conclude in this chapter that, of the behavior of the profiles, we can not get a clear picture of the behavior of the thermal conductivity, postponing its analysis to chapter 4 where we introduce a new method to solve these problems.

Keys to make this analysis are the results in chapter 3. In this chapter we study the Local Thermal Equilibrium in detail. To characterize its behavior at the macroscopic level we focus on the study of the Equation of State. We found excellent agreement between the values of the Equation of State calculated in our system and the ones calculated in equilibrium present in the literature, indicating that the assumption of Local Thermal Equilibrium is met in our system at the macroscopic level. Particularly interesting is that we found no dependence of these values with the size, although the magnitudes used to calculate it seem to have it. We therefore conclude that the size effects of the temperature and packing fraction profiles, as well as that of the pressure are only apparent. This property, which we call *Bulk-Boundary Decoupling* allows us to divide our system into two parts: Some effective thermal sources, consisting on the thermal baths itself and neighboring boxes, and the Bulk of the system, compose by the central boxes, which behaves as it was an infinite system. We also note that, for high gradients and high packing fractions, a liquid-solid coexistence occurs already observed in [67]. Studying this coexistence in detail we find that the hypothesis of Local Thermal Equilibrium is not satisfied in the area of the system occupied by the solid phase, i.e. the values calculated for the Equation of State in this part of the system deviate from the equilibrium values, though only slightly, and also have size effects. Finally we study the Local Thermal Equilibrium at the fluctuating level. To do this, we measure the moments of the global distribution of velocities and energies to compare with the prediction given by assuming Local Thermal Equilibrium. Although we found no deviations for the global velocity distribution, the second moment of the energy distribution systematically deviates from the prediction of local equilibrium. We found that the difference between these two quantities depends

linearly on the external gradient squared with a slope of 1/40. This type of behavior, which has been observed in simplified transport models [87], hasn't been observed previously for Hamiltonian systems.

In light of the results of chapter 3 can trust that Local Thermal Equilibrium is satisfied, in such a way, that it didn't present finite size effects. Using this and also assuming that Fourier's law holds for our system, in chapter 4 we theoretically derived scaling law for the profiles of an infinite system of Hard Disks. This scaling Law is characterized by two universal master curves from which we can derive every possible profile. We find that the predictions of this theory are in very good agreement with our data. In particular it is quite remarkable that all the profiles for different system setups, for a given number of particles, collapse into a universal curve, indicating that Fourier's Law holds for our system. This result together with the property of *Bulk-Boundary Decoupling* allows us to get rid of spurious size effects, making it possible, finally, to study the behavior of the thermal conductivity of our system. We note that the thermal conductivity deviates slightly from the prediction given by the Enskog theory for Hard Disks [68] and also depends weakly on the system size. We conclude that this effect is reminiscent of the known long time tails present on Hard Disks systems [27].

As a final comment of this part of the thesis, should be mentioned that this analysis may have many applications in the description of the steady state of more complex fluids. In fact in appendix B we derive a scaling for soft potentials which are, in certain situations, the limiting case of the more realistic Lenard-Jones potentials [45, 46]. In addition, although the scale depends on the athermal character of the system, can be the case that *Bulk-Boundary Decoupling* is satisfied for systems in which the hypothesis of Local Thermal Equilibrium is valid at the macroscopic level.In these cases, although the characteristic scale can not be calculated theoretically could be calculated experimentally by following the strategy described in chapter 4.

In chapter 5 we shown how symmetry principles come forth in fluctuations far from equilibrium. By demanding invariance of the optimal path responsible of a given fluctuation under symmetry transformations, we unveiled a novel and very general isometric fluctuation relation for time-reversible systems which relates in a simple manner the probability of any pair of isometric current fluctuations. We showed that this Isometric Fluctuation Relation holds in our simulations of Hard Disks. However the Hard Disk fluid is a fully hydrodynamic system, with 4 different locally-conserved coupled fields possibly subject to memory effects, defining a far more complex situation than the one studied here within macroscopic fluctuation theory framework. This suggest that the Isometric Fluctuation Relation could be further generalized. Invariance principles of this kind can be applied with great generality in diverse fields where fluctuations play a fundamental role, opening the door to further exact and general results valid arbitrarily far from equilibrium. This is particularly relevant in mesoscopic biophysical systems, where relations similar to the isometric fluctuation relation might be used to efficiently measure free-energy differences in terms of work distributions [88, 89].

Conclusiones

En esta tesis hemos estudiado el comportamiento de un sistema de Discos Rígidos sometido a un gradiente de temperatura. Dentro de los fenómenos de no-equilibrio el estado estacionario de un sistema sometido a un gradiente de temperatura es uno de los más simples. Sorprendentemente, incluso este caso tan sencillo, no se comprende enteramente desde un punto de vista teórico. El principal inconveniente es que las teorías que lo describen se basan en hipótesis que carecen de una demostración rigurosa. En nuestro caso particular dos de estas hipótesis resaltan por ser los pilares en los que se fundamentan las descripciones del estado estacionario: el Equilibrio Local Térmico y la ley de Fourier.

El Equilibrio Local Térmico se basa en la suposición de que los tiempos necesarios para equilibrar el sistema localmente son mucho más cortos que los tiempos característicos asociados con los fenómenos macroscópicos de no equilibrio. Esto permite definir magnitudes locales, como la temperatura o la densidad, así como usar las relaciones termodinámicas localmente. Sin embargo a la hora de usar este concepto hay que lidiar con una sutileza muy importante. Se sabe que desde un punto de vista formal la medida asociada a un sistema fuera del equilibrio en el estado estacionario, en analogía con la medida de Boltzman-Gibs para el caso de equilibrio, de existir, no puede ser exactamente la misma que la de equilibrio, ya que en este caso no existirían ni correlaciones de largo alcance en el sistema ni un flujo asociado al gradiente impuesto [30]. De esta forma una manera más precisa de definir el Equilibrio Local Térmico sería que la medida asociada a las configuraciones de un sistema en el estado estacionario son tales que los valores esperados macroscópicos coinciden con los calculados con una distribución de equilibrio pero que las fluctuaciones calculadas con estos dos métodos no son iguales entre si. Por lo tanto a la hora de estudiar este concepto tenemos que distinguir entre el nivel macroscópico de observación y el nivel fluctuante, siendo necesario estudiar ambos para tener una confirmación clara de esta hipótesis.

Por otro lado el problema asociado a la Ley de Fourier en particular, y a las ecuaciones constitutivas en general, es que no existe un cálculo riguroso de los coeficientes de transporte a partir de la dinámica microscópica del sistema, válido arbitrariamente lejos del equilibrio. Esto sólo ha sido posible hacerlo en modelos muy simplificados de transporte [30, 54]. Esto tiene como consecuencia que no se sepa si a priori la Ley de Fourier es válida para un sistema determinado, siendo necesario determinarlo computacionalmente modelo a modelo.

Nuestra motivación principal para la realización de esta tesis era ahondar en la comprensión de estas hiptesis teóricas que no tienen, a día de hoy, una demostración matemática rigurosa. Esta falta de resultados se debe a la gran complejidad asociada al problema. Por lo tanto una caracterización computacional de los límites de validez de estas hipótesis tiene gran valor orientativo a la hora de encontrar nuevas formas de abordar dichos problemas. Sin embargo este enfoque computacional no está exento de problemas. Dos de los problemas principales son los efectos de tamaño y de frontera. En particular los efectos de frontera son especialmente problemáticos. En equilibrio estos efectos, típicamente, se minimizan mediante el uso de condiciones de contorno periódicas. Sin embargo este tipo de condiciones de contorno son incompatibles con la introducción de fuentes térmicas en la frontera [62]. En los capítulos 1 y 2 de esta tesis estudiamos estos efectos en nuestro sistema.

En el capítulo 1 vimos que cuando la fuentes térmicas tienen la misma temperatura, es decir en el caso de equilibrio, tanto los efectos de borde como los de tamaño desaparecen cuando el número de partículas tiende a infinito. Sin embargo, como vimos en el capítulo 2, cuando el sistema se somete a un gradiente de temperatura, estos efectos se complican de tal manera que la extrapolación a N infinito no arroja un resultado concluyente para los perfiles de temperatura y fracción de volumen. A pesar de estos efectos, los perfiles, una vez descartadas las cajas próximas a las fuentes, son suaves aunque no lineales, permitindonos obtener unos ajustes experimentales que reproducen bien nuestros datos. Finalmente estudiamos el flujo de energía que atraviesa el sistema. Aunque en este caso si obtenemos un límite claro concluimos en este capítulo que, a la luz del comportamiento de los perfiles, no es posible obtener una imagen clara del comportamiento de la conductividad térmica, posponiendo su análisis al capítulo 4 donde introducimos un nuevo método de análisis para solventar estos problemas.

Claves para formular dicho análisis son los resultados obtenidos en el capítulo 3. En este capítulo estudiamos el Equilibrio Local Térmico en detalle. Para caracterizar su comportamiento a nivel macroscópico nos centramos en el estudio de la Ecuación de Estado. Encontramos una excelente concordancia entre los valores de la Ecuación de Estado calculados en nuestro sistema y los calculados para sistemas de equilibrio presentes en la literatura, indicando que se cumple la hipótesis de Equilibrio Local Térmico a nivel macroscópico en nuestro sistema. Particularmente interesante es que no encontramos dependencia de estos valores con el tamaño, a pesar de que las magnitudes usadas para calcularlo si parecen tenerla. Por lo tanto concluimos que los efectos de tamaño de los perfiles de temperatura y fracción de volumen, así como los de la presión son sólo aparentes. Esta propiedad que llamamos *Bulk-Boundary Decoupling* nos permite dividir nuestro sistema en dos partes: Unas fuentes térmicas efectivas, compuesta por las propias fuentes y las cajas vecinas a éstas, y el "bulk" del sistema, compuesto por las cajas centrales del sistema, que se comporta como un sistema infinito. Por otra parte notamos que para gradientes altos y fracciones de volumen altas se produce una coexistencia líquido-sólido ya observada en [67]. Estudiando esta coexistencia en detalle encontramos que la hipótesis de Equilibrio Local Térmico no se cumple en la zona del sistema ocupada por la fase sólida, es

decir que los valores calculados para la Ecuación de Estado en esta parte del sistema se desvían de los valores de equilibrio, aunque sólo ligeramente, y además presentan efectos de tamaño. Finalmente estudiamos el Equilibrio Local Térmico a nivel fluctuante. Para ello medimos los momentos de la distribución global de velocidades y energías para compararlas con la predicción dada suponiendo Equilibrio Local Térmico. Aunque no encontramos desviaciones para la distribución global de la velocidad, salvo efectos de tamaño, los segundos momentos de la distribución de energía se desvían sistemáticamente de la predicción de equilibrio local. Encontramos que la diferencia entre estas dos magnitudes depende linealmente del gradiente externo al cuadrado con una pendiente de 1/40. Este tipo de comportamiento, que ha sido observado en modelos simplificados de transporte [87], no se había observado anteriormente para sistemas Hamiltonianos.

A la luz de los resultados del capítulo 3 podemos confiar que el Equilibrio Local Térmico se cumple de forma que no presenta efectos de tamaño finito. Usando esto y suponiendo, además que la ley de Fourier se cumple para nuestro sistema, en el capítulo 4 derivamos teóricamente una ley de escala para los perfiles de un sistema infinito de Discos Rígidos. Esta ley de escala se caracteriza por dos curvas universales de las que podemos derivar cualquier perfil posible. Encontramos que las predicciones de esta teoría concuerdan muy bien con nuestros datos. En particular es extraordinario que todos los perfiles obtenidos para las distintas condiciones externas, y para un numero de partículas dado, colapsen en una curva universal, indicando que la ley de Fourier se cumple en nuestro sistema. Este resultado junto con la propiedad de *Bulk-Boundary Decoupling* nos permite deshacernos de los efectos de tamaño espurios, haciendo posible, finalmente, estudiar el comportamiento de la conductividad térmica para nuestro sistema. Observamos que esta conductividad térmica se desva ligeramente de la predicción dada por la teoría de Enskog para Discos Rígidos [68] y que además depende débilmente del tamaño del sistema. Concluimos que este efecto es una reminiscencia de las conocidas colas para tiempos largos presentes en sistemas de Discos Rígidos [27].

Como comentario final de esta parte de la tesis debemos mencionar que este análisis puede tener muchas aplicaciones en la descripción del estado estacionario de fluidos más complejos. De hecho en el apndice B derivamos la escala para potenciales de ncleo suave que son, en ciertos casos, el comportamiento límite del más realista potencial de Lenard-Jones [45, 46]. Además, aunque la escala depende del carcter atérmico del sistema, puede darse el caso de que la propiedad de *Bulk-Boundary Decoupling* se cumpla para sistemas en los que la hipótesis de Equilibrio Local Térmico sea válida a nivel macroscópico. En estos casos, aunque la escala característica no se pueda calcular teóricamente, se podrá calcular experimentalmente siguiendo la estrategia descrita en el capítulo 4.

En el capítulo 5 hemos visto como principios de simetría aparecen en fluctuaciones lejos del equilibrio. Exigiendo la invariancia de la trayectoria óptima, responsable de una fluctuación dada, bajo transformaciones de simetría, descubrimos una nueva, y muy general, relación de fluctuación isométrica para sistemas reversibles temporalmente, que relaciona de una

manera sencilla la probabilidad de que cualquier par de fluctuaciones isométricas de la corriente. Hemos demostrado que esta relación de fluctuación isométrica se cumple en nuestras simulaciones de Discos Rígidos. El fluido de Discos Rígidos es un sistema totalmente hidrodinámico, con 4 campos localmente-conservados diferentes, y posiblemente sujeto a efectos de memoria, es decir una situación mucho más compleja que la estudiada en la parte teórica del capítulo 5, en el contexto de la teoría de fluctuaciones macroscópicas. Esto sugiere que la Relación Isomtrica Fluctuante podría admitir futuras generalizaciones. Principios de invariancia de este tipo pueden ser aplicados con gran generalidad en diversos campos donde las fluctuaciones desempeñan un papel fundamental, abriendo la puerta a resultados más generales, válidos arbitrariamente lejos del equilibrio. Esto es particularmente relevante en sistemas biofísicos mesoscópicos, donde relaciones similares a la relación de fluctuación isométrica pueden ser utilizados para medir de manera eficiente las diferencias de energía libre en términos de las distribuciones de trabajo [88, 89].

Appendix A

Source Code

```
!2d hard disk program 18 of July 2010.
 program hardisk2d
 implicit real*8(a-h,o-z)
 parameter (npmax=10000,nklon=1,Nvmax=100,Nal=200)
 common /c/ pi,tabs(nklon),tabstot(nklon),r,De,aN,tini,tpaso
&,iold,jold,Ncm,nl,N,Ncv,klon,Nvflag
 common /pos/ x(0:npmax,nklon),y(0:npmax,nklon)
 common /vel/ vx(0:npmax,nklon),vy(0:npmax,nklon)
 common /cajaV/ nv(Nvmax,Nvmax,0:npmax,nklon)
&,nx(npmax,nklon),ny(npmax,nklon)
 common /Cborde/ lx(9),ly(9),lx2(3),ly2(3)
 common /z/ Ey,Ex,Ex1,Ex2,tv,T1,T2
 common /lma/ al(1:Npmax,0:Nal,nklon),even(1:Npmax,0:Nal,nklon)
&,eveni(1:Npmax,0:Nal,nklon),evenj(1:Npmax,0:Nal,nklon)
&,nchoke(-10:Npmax,nklon)
 common /dsa/ ncbt(1:2*Npmax,nklon),tcol,jcol,icol
 common /medida/ etot(npmax,2),distri(15000,Nvmax)
&,tcolu(Nvmax,npmax),denc(Nvmax,npmax),densi2(Nvmax,npmax)
&,vcmx(Nvmax,npmax),vcmy(Nvmax,npmax),v(npmax,8),distrimax
&,ajgtot(npmax,6),tabs4(npmax,nklon),ecin_b(Nvmax,npmax)
 common /medida2/ tmedias(Nvmax,8),dmedias(Nvmax,8)
&,anmedias(Nvmax,8),emedias(Nvmax,8),pmedias(Nvmax,8)
&,vcymd(Nvmax,8),vmedias(8),ajmedias(6,8),vcxmd(Nvmax,8)
&,xmedtot
 common /medida3/ cpre(Nvmax),ajabs(2),ncol(Nvmax)
&,presion(Nvmax,npmax),ajcurrent(2,npmax),coli(Nvmax,npmax)
&,colmedias(Nvmax,8),ajmb(2,8)

!Maximun number of iterations
 nbumax=1000000000
!Optinal parameter to introduce an external field
!(Ex y Ey), number of clones (klon), and control variable (z)
 Ex=0.d0
 Ey=0.d0
 klon=1
 z=0.d0
! inicialization routine
 tabstot(klon)=0.d0
 tabs(klon)=0.d0
 do klon=1,nklon
  call ini()
  Ncicle=10*N
  write(6,*) N,Ncv
!Thermalization of the sistem
  do lmn=1,100
  call evol(Ncicle,z)
! call check(1.45d0,175) !particle overlap checking
! resetting of tabs to avoid rounding errors
  do is=1,N
   jjs=dint(al(is,0,klon))
   do js=1,jjs
    bal=al(is,js,klon)-tabs(klon)
    al(is,js,klon)=bal
   enddo
  enddo
  tabstot(klon)=tabstot(klon)+tabs(klon)
  tabs(klon)=0.d0
  enddo
!Mesurement of the time between mesurements
!time in wich we get an average of 10 colisions per particle
 stx=tabstot(klon)+tabs(klon)
 sumtx=0.d0
 ntx=0
 tpaso=1.d7
 do lmn=1,1000
 call evol(Ncicle,z)
! call check(1.45d0,175) !particle overlap checking
! resetting of tabs to avoid rounding errors
  do is=1,N
   jjs=dint(al(is,0,klon))
   do js=1,jjs
    bal=al(is,js,klon)-tabs(klon)
    al(is,js,klon)=bal
   enddo
  enddo
  tabstot(klon)=tabstot(klon)+tabs(klon)
  tabs(klon)=0.d0
 enddo
 sumtx=sumtx+tabstot(klon)+tabs(klon)-stx
 stx=tabstot(klon)+tabs(klon)
 ntx=ntx+1
 enddo
 tini=tabs(klon)+tabstot(klon)
 tpaso=sumtx/dble(ntx)
 write(6,*) tini,tpaso,N,r
 enddo
!initialization of colision variables
 do is=1,Ncm+3
  cpre(is)=0.d0
  ncol(is)=0.d0
 enddo
 ajabs(1)=0.d0
 ajabs(2)=0.d0
!principal loop
 z=2.d0
 do nbucle=1,nbumax
 do klon=1,nklon
 do lmn=1,1000
 call evol(Ncicle,z)
! call check(1.45d0,175) !particle overlap checking
! resetting of tabs to avoid rounding errors
  do is=1,N
   jjs=dint(al(is,0,klon))
   do js=1,jjs
    bal=al(is,js,klon)-tabs(klon)
    al(is,js,klon)=bal
   enddo
  enddo
  tabstot(klon)=tabstot(klon)+tabs(klon)
  tabs(klon)=0.d0
  enddo
  enddo
 enddo
 enddo
 end

 subroutine ini()
 implicit real*8(a-h,o-z)
 parameter (npmax=10000,nklon=1,Nvmax=100,Nal=200)
 common /c/ pi,tabs(nklon),tabstot(nklon),r,De,aN,tini,tpaso
&,iold,jold,Ncm,nl,N,Ncv,klon,Nvflag
 common /pos/ x(0:npmax,nklon),y(0:npmax,nklon)
 common /vel/ vx(0:npmax,nklon),vy(0:npmax,nklon)
 common /cajaV/ nv(Nvmax,Nvmax,0:npmax,nklon)
&,nx(npmax,nklon),ny(npmax,nklon)
 common /Cborde/ lx(9),ly(9),lx2(3),ly2(3)
 common /z/ Ey,Ex,Ex1,Ex2,tv,T1,T2
 common /lma/ al(1:Npmax,0:Nal,nklon),even(1:Npmax,0:Nal,nklon)
&,eveni(1:Npmax,0:Nal,nklon),evenj(1:Npmax,0:Nal,nklon)
&,nchoke(-10:Npmax,nklon)
```

```
 common /dsa/ ncbt(1:2*Npmax,nklon),tcol,jcol,icol
 common /medida/ etot(npmax,2),distri(15000,Nvmax)
&,tcolu(Nvmax,npmax),denc(Nvmax,npmax),densi2(Nvmax,npmax)
&,vcmx(Nvmax,npmax),vcmy(Nvmax,npmax),v(npmax,8)
&,ajgtot(npmax,6),tabs4(npmax,nklon),ecin_b(Nvmax,npmax)
&,distrimax
 common /medida2/ tmedias(Nvmax,8),dmedias(Nvmax,8)
&,anmedias(Nvmax,8),emedias(Nvmax,8),pmedias(Nvmax,8)
&,vcymd(Nvmax,8),vmedias(8),ajmedias(6,8),vcxmd(Nvmax,8)
&,xmedtot
 common /medida3/ cpre(Nvmax),ajabs(2),ncol(Nvmax)
&,presion(Nvmax,npmax),ajcurrent(2,npmax),coli(Nvmax,npmax)
&,colmedias(Nvmax,8),ajmb(2,8)
!External input file
 open(unit=1,file="input2.dat",status="unknown")
!number of particles, aspect-ratio,random number seed
 read(1,*) npar,aspect,iseed
!Thermal bath's Temperatures and density of the system
 read(1,*) T1,T2,den
!External field components; nflag if a control variable
!to use a previus configuration (read from an archive)
! or to generate one
 read(1,*) Ex1,Ey1,nflag
 close(1)
!initialization of the matrices
 nl=0
 xmedtot=0.d0
 Nvflag=0
 Ncm=15!number of mesurement boxes
 iold=-10
 jold=-10
 distrimax=dsqrt(T1+T2)
 do ii=1,15000
  do jj=1,Nvmax
   distri(ii,jj)=0.d0
  enddo
 enddo
 if(klon.eq.1 )call dran_ini(iseed)
 ajabs(1)=0.d0
 ajabs(2)=0.d0
 do i=1,Nvmax
  cpre(i)=0.d0
  ncol(i)=0.d0
 enddo
 do i=1,npmax
  do j=1,nklon
   x(i,klon)=0.d0
   y(i,klon)=0.d0
   vx(i,klon)=0.d0
   vy(i,klon)=0.d0
  enddo
 enddo
 do k=1,8
  do i=1,Nvmax
   tmedias(i,k)=0.d0
   dmedias(i,k)=0.d0
   anmedias(i,k)=0.d0
   emedias(i,k)=0.d0
   pmedias(i,k)=0.d0
   vcxmd(i,k)=0.d0
   vcymd(i,k)=0.d0
  enddo
  vmedias(k)=0.d0
  do i=1,6
   ajmedias(i,k)=0.d0
  enddo
 enddo

 pi=4.d0*datan(1.d0)
 dencp=pi/(2.d0*dsqrt(3.d0))!densidad close packing
 if(den.gt.dencp)then
  write(6,*)'densidad superior a close packing'
  stop
 endif
 aly=aspect
 r=dsqrt(dencp/(dble(npar)*pi))
!generation of the initial configuration
 if(nflag.eq.0) then
!Introdution of as many particle as possible in close packing
  x(1,klon)=r
  y(1,klon)=r
  ncont=1
  ncont2=0
  k=0
  do while(ncont2.ne.ncont.or.k.lt.ncont)
   ncont2=ncont
   k=k+1
   do i=0,5
    x2=x(k,klon)+2.d0*r*dcos(dble(i)*pi/3.d0)
    y2=y(k,klon)+2.d0*r*dsin(dble(i)*pi/3.d0)
    control=1.d0
    do j=1,ncont
     x3=x(j,klon)
     y3=y(j,klon)
     if(dsqrt((x3-x2)**2.d0+(y3-y2)**2.d0).lt.2.d0*r-1.d-7)
&control=2.d0
     if(x2.gt.(1.d0-r+1.d-7).or.x2.lt.r-1.d-7) control=2.d0
     if(y2.gt.(1.d0-r+1.d-7).or.y2.lt.r-1.d-7) control=2.d0
    enddo
    if(control.lt.1.5d0) then
     ncont=ncont+1
     x(ncont,klon)=x2
     y(ncont,klon)=y2
    endif
   enddo
  enddo
  N=ncont
!Determination of the velocities of the particles from a
!Maxwellian distrubution at temperature (T1+T2)/2,
!we impose a center of mass velocity equal to 0
  vmax2=(T1+T2)/2.d0
  vmax=dsqrt(vmax2)
 4 do i=3,N
    u1=dran_u()
    u2=dran_u()
    vy(i,klon)=dsqrt(-2.d0*dlog(u1))*dcos(2.d0*pi*u2)*dsqrt(vmax2)
    vx(i,klon)=dsqrt(-2.d0*dlog(u1))*dsin(2.d0*pi*u2)*dsqrt(vmax2)
  enddo
  a=0.d0
  b=0.d0
  do i=3,N
   a=a-vx(i,klon)
   b=b-vy(i,klon)
  enddo
  delta2=4.d0*vmax2-a**2.d0-b**2.d0
  if(delta2.lt.0.d0)goto 4
  vx(1,klon)=(a+b*dsqrt(delta2/(a**2.d0+b**2.d0)))/2.d0
  vy(1,klon)=(b-a*dsqrt(delta2/(a**2.d0+b**2.d0)))/2.d0
  vx(2,klon)=a-vx(1,klon)
  vy(2,klon)=b-vy(1,klon)
 else
!reading of a previus configuration
  open(unit=999,file="configuracion.dat",status="unknown")
  read(999,*) tabstot(klon),tabs(klon),iold,jold
  ncont=1
  do while(ncont.lt.npmax)
   read(999,*,end=998)x(ncont,klon),y(ncont,klon)
&,vx(ncont,klon),vy(ncont,klon)
   ncont=ncont+1
  enddo
998 continue
  close(999)
  ncont=ncont-1
 endif


 N=ncont
 aN=dble(N)
!reseting of the radius to mach the system density
 r=dsqrt(den/(aN*pi))
 Ncv=dint(dsqrt(aN))!number of virtual boxes

 if(Ncv.gt.Nvmax) then
  write(6,*) "numero de cajas virtuales mayor que Nvmax"
  stop
 endif
 De=1.d0/dble(Ncv)
!Asigning to a virtual box the particles within the box
 do i=1,Ncv
  do j=1,Ncv
   nv(i,j,0,klon)=0
  enddo
 enddo
 do i=1,N
  nx(i,klon)=1+dint(x(i,klon)*dble(Ncv))
  ny(i,klon)=min(1+int(y(i,klon)*dble(Ncv)),Ncv)
  ni=nv(nx(i,klon),ny(i,klon),0,klon)+1
  nv(nx(i,klon),ny(i,klon),0,klon)=ni
  nv(nx(i,klon),ny(i,klon),ni,klon)=i
 enddo
!Parametrization of next next neighbors
 lx(1)=-1
 ly(1)=-1
 lx(2)=-1
 ly(2)=0
 lx(3)=-1
 ly(3)=1
 lx(4)=0
 ly(4)=1
 lx(5)=0
 ly(5)=0
 lx(6)=0
 ly(6)=-1
 lx(7)=1
 ly(7)=-1
 lx(8)=1
 ly(8)=0
 lx(9)=1
 ly(9)=1
!Parametrization of next neighbors
 lx2(1)=-1
```

```
 lx2(2)=0
 lx2(3)=1
 ly2(1)=-1
 ly2(2)=0
 ly2(3)=1
 call colinit()
 return
 end

 subroutine colinit()
 implicit real*8(a-h,o-z)
 parameter (npmax=10000,nklon=1,Nvmax=100,Nal=200)
 common /c/ pi,tabs(nklon),tabstot(nklon),r,De,aN,tini,tpaso
&,iold,jold,Ncm,nl,N,Ncv,klon,Nvflag
 common /pos/ x(0:npmax,nklon),y(0:npmax,nklon)
 common /vel/ vx(0:npmax,nklon),vy(0:npmax,nklon)
 common /cajaV/ nv(Nvmax,Nvmax,0:npmax,nklon)
&,nx(npmax,nklon),ny(npmax,nklon)
 common /Cborde/ lx(9),ly(9),lx2(3),ly2(3)
 common /z/ Ey,Ex,Ex1,Ex2,tv,T1,T2
 common /lma/ al(1:Npmax,0:Nal,nklon),even(1:Npmax,0:Nal,nklon)
&,eveni(1:Npmax,0:Nal,nklon),evenj(1:Npmax,0:Nal,nklon)
&,nchoke(-10:Npmax,nklon)
 common /dsa/ ncbt(1:2*Npmax,nklon),tcol,jcol,icol

!inicialization of the local minima list
!al->time list
!even-> particle or wall to colide with particle i
!eveni->control parameter for i
!evenj->control parameter for it's partner
!ncol->number of colision sufered by the particle

 do i=1,N
  al(i,0,klon)=0.d0
  even(i,0,klon)=0.d0
  eveni(i,0,klon)=0.d0
  evenj(i,0,klon)=0.d0
  do j=1,Nal
   al(i,j,klon)=1.d10
   even(i,j,klon)=0
   eveni(i,j,klon)=0
   evenj(i,j,klon)=0
  enddo
  nchoke(i,klon)=0
 enddo
 do i=-10,0
  nchoke(i,klon)=0
 enddo

!Intruduction of the future events on the lists
!particle-particle events
 do i=1,N
  do j=1,9
   nxv=nx(i,klon)+lx(j)
   nyv=mod(ny(i,klon)+ly(j)+Ncv-1,Ncv)+1
   if(nxv.gt.Ncv.or.nxv.lt.1)cycle
   if(nv(nxv,nyv,0,klon).gt.0)then
    do k=1,nv(nxv,nyv,0,klon)
     if(nv(nxv,nyv,k,klon).gt.i)then
      jj=nv(nxv,nyv,k,klon)
      if(i.eq.iold.and.jj.eq.jold)cycle
      xij=x(i,klon)-x(jj,klon)
      yij=y(i,klon)-y(jj,klon)
      vxij=vx(i,klon)-vx(jj,klon)
      vyij=vy(i,klon)-vy(jj,klon)
      aa=xij*vxij+yij*vyij
      if(aa.lt.0.d0)then
       v2ij=vxij**2.d0+vyij**2.d0
       dis=4.d0*r*r*v2ij-(xij*vyij-yij*vxij)**2.d0
       if(dis.ge.0.d0) then
        t7=tabs(klon)+(-aa-dsqrt(dis))/v2ij
        i1=jj
        call almin(t7,i1,i)
       endif
      endif
      yij=-sign(1.d0,yij)*(1.d0-dabs(yij))
      aa=xij*vxij+yij*vyij
      if(aa.lt.0.d0)then
       v2ij=vxij**2.d0+vyij**2.d0
       dis=4.d0*r*r*v2ij-(xij*vyij-yij*vxij)**2.d0
       if(dis.ge.0.d0) then
        t7=tabs(klon)+(-aa-dsqrt(dis))/v2ij
        i1=jj
        call almin(t7,i1,i)
       endif
      endif
     endif
    enddo
   endif
  enddo

!particle-wall events
  if(iold.eq.i.and.jold.eq.-1) goto 4
  if(nx(i,klon).le.2)then
   t7=tabs(klon)+(r-x(i,klon))/vx(i,klon)
   i1=-1
   call almin(t7,i1,i)
  endif
4 if(iold.eq.i.and.jold.eq.0) goto 6
  if(nx(i,klon).ge.(Ncv-1))then
   t7=tabs(klon)+(1.d0-x(i,klon)-r)/vx(i,klon)
   i1=0
   call almin(t7,i1,i)
  endif
!particle-virtual wall events
6 t7=1.d10
  aa=dble(nx(i,klon))/dble(Ncv)
  t72=tabs(klon)+(aa-x(i,klon))/vx(i,klon)
  if(t72.gt.tabs(klon)) then
   i1=-4
   t7=t72
  endif
  aa=dble(nx(i,klon)-1)/dble(Ncv)
  t72=tabs(klon)+(aa-x(i,klon))/vx(i,klon)
  if(t72.gt.tabs(klon).and.t72.lt.t7) then
   i1=-2
   t7=t72
  endif
  aa=dble(ny(i,klon)-1)/dble(Ncv)
  t72=tabs(klon)+(aa-y(i,klon))/vy(i,klon)
  if(t72.gt.tabs(klon).and.t72.lt.t7) then
   i1=-5
   t7=t72
  endif
  aa=dble(ny(i,klon))/dble(Ncv)
  t72=tabs(klon)+(aa-y(i,klon))/vy(i,klon)
  if(t72.gt.tabs(klon).and.t72.lt.t7) then
   i1=-3
   t7=t72
  endif
  call almin(t7,i1,i)
 enddo
!inicialization of the complete binary tree
 do i=N,2*N-1
  ncbt(i,klon)=i-N+1
 enddo
 do i=2*N-1,3,-2
  if(al(ncbt(i,klon),1,klon).le.al(ncbt(i-1,klon),1,klon)) then
   ncbt(i/2,klon)=ncbt(i,klon)
  else
   ncbt(i/2,klon)=ncbt(i-1,klon)
  endif
 enddo
 return
 end

 subroutine almin(t1,mtev,i)
 implicit real*8 (a-h,o-z)
 parameter (npmax=10000,nklon=1,Nvmax=100,Nal=200)
 common /c/ pi,tabs(nklon),tabstot(nklon),r,De,aN,tini,tpaso
&,iold,jold,Ncm,nl,N,Ncv,klon,Nvflag
 common /pos/ x(0:npmax,nklon),y(0:npmax,nklon)
 common /vel/ vx(0:npmax,nklon),vy(0:npmax,nklon)
 common /cajaV/ nv(Nvmax,Nvmax,0:npmax,nklon)
&,nx(npmax,nklon),ny(npmax,nklon)
 common /Cborde/ lx(9),ly(9),lx2(3),ly2(3)
 common /lma/ al(1:Npmax,0:Nal,nklon),even(1:Npmax,0:Nal,nklon)
&,eveni(1:Npmax,0:Nal,nklon),evenj(1:Npmax,0:Nal,nklon)
&,nchoke(-10:Npmax,nklon)
 common /dsa/ ncbt(1:2*Npmax,nklon),tcol,jcol,icol

 if(t1.gt.tabs(klon)) then
  nk=1
  do while(t1.gt.al(i,nk,klon))
   nk=nk+1
  enddo
  if(nk.le.al(i,0,klon)) then
   nmax=al(i,0,klon)+1
   do k=nmax,nk+1,-1
    al(i,k,klon)=al(i,k-1,klon)
    even(i,k,klon)=even(i,k-1,klon)
    eveni(i,k,klon)=eveni(i,k-1,klon)
    evenj(i,k,klon)=evenj(i,k-1,klon)
   enddo
  endif
  nm=al(i,0,klon)+1
  al(i,0,klon)=nm
  even(i,0,klon)=nm
  eveni(i,0,klon)=nm
  evenj(i,0,klon)=nm
  al(i,nk,klon)=t1
  even(i,nk,klon)=mtev
  eveni(i,nk,klon)=nchoke(i,klon)
  evenj(i,nk,klon)=nchoke(mtev,klon)
 endif
 return
 end

 subroutine evol(ns,z)
 implicit real*8(a-h,o-z)
 parameter (npmax=10000,nklon=1,Nvmax=100,Nal=200)
 common /c/ pi,tabs(nklon),tabstot(nklon),r,De,aN,tini,tpaso
```

```
&,iold,jold,Ncm,nl,N,Ncv,klon,Nvflag
 common /pos/ x(0:npmax,nklon),y(0:npmax,nklon)
 common /vel/ vx(0:npmax,nklon),vy(0:npmax,nklon)
 common /cajaV/ nv(Nvmax,Nvmax,0:npmax,nklon)
&,nx(npmax,nklon),ny(npmax,nklon)
 common /Cborde/ lx(9),ly(9),lx2(3),ly2(3)
 common /z/ Ey,Ex,Ex1,Ex2,tv,T1,T2
 common /lma/ al(1:Npmax,0:Nal,nklon),even(1:Npmax,0:Nal,nklon)
&,eveni(1:Npmax,0:Nal,nklon),evenj(1:Npmax,0:Nal,nklon)
&,nchoke(-10:Npmax,nklon)
 common /dsa/ ncbt(1:2*Npmax,nklon),tcol,jcol,icol

 do j=1,ns
  tcol=al(ncbt(1,klon),1,klon)
  icol=ncbt(1,klon)
  jcol=even(icol,1,klon)
!executing the virtual colitions
  do while(jcol.le.-2)
   tv=tcol
   call virtuacol(icol,jcol)
   call rencbt(icol,jcol)
   tcol=al(ncbt(1,klon),1,klon)
   icol=ncbt(1,klon)
   jcol=even(icol,1,klon)
  enddo
!Calls to the mesurement and save data routines
!activated for z greater than 1
  if (z.gt.1.d0) then
   ab=tabstot(klon)+tcol
   ac=tini+tpaso
   if(ab.ge.ac) then
    tini=tini+tpaso
    nl=nl+1
    call measure(nl)
    if(nl.eq.1000)then
     call salvar()
     nl=0
    endif
    call mov(tcol,jcol)
   else
    call mov(tcol,jcol)
   endif
  else
   call mov(tcol,jcol)
  endif

  if(jcol.gt.-2) then
   iold=icol
   jold=jcol
   call choq(icol,jcol)
   nchoke(icol,klon)=nchoke(icol,klon)+1
   if(nchoke(icol,klon).gt.100000) nchoke(icol,klon)=0
   call colision(icol)
   if (jcol.gt.0.) then
    nchoke(jcol,klon)=nchoke(jcol,klon)+1
    if(nchoke(jcol,klon).gt.100000) nchoke(jcol,klon)=0
    call colision(jcol)
   endif
  endif
  if(Nvflag.gt.0) then
   nchoke(Nvflag,klon)=nchoke(Nvflag,klon)+1
   if(nchoke(Nvflag,klon).gt.100000) nchoke(Nvflag,klon)=0
   call colision(Nvflag)
   Nvflag=0
  endif
  call rencbt(icol,jcol)
 enddo
 return
 end

 subroutine virtuacol(i,jcol2)
 implicit real*8(a-h,o-z)
 parameter (npmax=10000,nklon=1,Nvmax=100,Nal=200)
 common /c/ pi,tabs(nklon),tabstot(nklon),r,De,aN,tini,tpaso
&,iold,jold,Ncm,nl,N,Ncv,klon,Nvflag
 common /pos/ x(0:npmax,nklon),y(0:npmax,nklon)
 common /vel/ vx(0:npmax,nklon),vy(0:npmax,nklon)
 common /cajaV/ nv(Nvmax,Nvmax,0:npmax,nklon)
&,nx(npmax,nklon),ny(npmax,nklon)
 common /Cborde/ lx(9),ly(9),lx2(3),ly2(3)
 common /z/ Ey,Ex,Ex1,Ex2,tv,T1,T2
 common /lma/ al(1:Npmax,0:Nal,nklon),even(1:Npmax,0:Nal,nklon)
&,eveni(1:Npmax,0:Nal,nklon),evenj(1:Npmax,0:Nal,nklon)
&,nchoke(-10:Npmax,nklon)
 common /dsa/ ncbt(1:2*Npmax,nklon),tcol,jcol,icol


!actualization of the virtual box
 ncan=i
 nmk=dint(al(ncan,0,klon))
 do nor=1,nmk
  al(ncan,nor,klon)=al(ncan,nor+1,klon)
  even(ncan,nor,klon)=even(ncan,nor+1,klon)
  eveni(ncan,nor,klon)=eveni(ncan,nor+1,klon)
  evenj(ncan,nor,klon)=evenj(ncan,nor+1,klon)
 enddo
 al(ncan,0,klon)=al(ncan,0,klon)-1
 even(ncan,0,klon)=even(ncan,0,klon)-1
 eveni(ncan,0,klon)=eveni(ncan,0,klon)-1
 evenj(ncan,0,klon)=evenj(ncan,0,klon)-1

 if(jcol2.eq.-2) then
  if(nx(i,klon).eq.1) then
   nx2=nx(i,klon)
   ny2=ny(i,klon)
   lxflag=0
   lyflag=1
  else
   nx2=nx(i,klon)-2
   ny2=ny(i,klon)
   lxflag=0
   lyflag=1
   nor1=nv(nx(i,klon),ny(i,klon),0,klon)
   do lnk=1,nor1
    if(i.eq.nv(nx(i,klon),ny(i,klon),lnk,klon)) nr=lnk
   enddo
   nx3=nx(i,klon)
   ny3=ny(i,klon)
   do lnk=nr,nor1-1
    nv(nx3,ny3,lnk,klon)=nv(nx3,ny3,lnk+1,klon)
   enddo
   nv(nx3,ny3,0,klon)=nv(nx3,ny3,0,klon)-1
   nx(i,klon)=nx(i,klon)-1
   nv(nx(i,klon),ny(i,klon),0,klon)
&=nv(nx(i,klon),ny(i,klon),0,klon)+1
   nor=nv(nx(i,klon),ny(i,klon),0,klon)
   nv(nx(i,klon),ny(i,klon),nor,klon)=i
  endif
 endif
 if(jcol2.eq.-3) then
  nx2=nx(i,klon)
  ny2=mod(ny(i,klon)+2+Ncv-1,Ncv)+1
  lxflag=1
  lyflag=0
  nor1=nv(nx(i,klon),ny(i,klon),0,klon)
  do lnk=1,nor1
   if(i.eq.nv(nx(i,klon),ny(i,klon),lnk,klon)) nr=lnk
  enddo
  do lnk=nr,nor1-1
   nbc=nv(nx(i,klon),ny(i,klon),lnk+1,klon)
   nv(nx(i,klon),ny(i,klon),lnk,klon)=nbc
  enddo
  nv(nx(i,klon),ny(i,klon),0,klon)
&=nv(nx(i,klon),ny(i,klon),0,klon)-1
  ny(i,klon)=ny(i,klon)+1
  if(ny(i,klon).gt.Ncv)ny(i,klon)=1
  nv(nx(i,klon),ny(i,klon),0,klon)
&=nv(nx(i,klon),ny(i,klon),0,klon)+1
  nor=nv(nx(i,klon),ny(i,klon),0,klon)
  nv(nx(i,klon),ny(i,klon),nor,klon)=i
 endif
 if(jcol2.eq.-4) then
  if(nx(i,klon).eq.Ncv) then
   nx2=nx(i,klon)
   ny2=ny(i,klon)
   lxflag=0
   lyflag=1
  else
   nx2=nx(i,klon)+2
   ny2=ny(i,klon)
   lxflag=0
   lyflag=1
   nor1=nv(nx(i,klon),ny(i,klon),0,klon)
   do lnk=1,nor1
    if(i.eq.nv(nx(i,klon),ny(i,klon),lnk,klon)) nr=lnk
   enddo
   do lnk=nr,nor1-1
    nbc=nv(nx(i,klon),ny(i,klon),lnk+1,klon)
    nv(nx(i,klon),ny(i,klon),lnk,klon)=nbc
   enddo
   nv(nx(i,klon),ny(i,klon),0,klon)
&=nv(nx(i,klon),ny(i,klon),0,klon)-1
   nx(i,klon)=nx(i,klon)+1
   nv(nx(i,klon),ny(i,klon),0,klon)
&=nv(nx(i,klon),ny(i,klon),0,klon)+1
   nor=nv(nx(i,klon),ny(i,klon),0,klon)
   nv(nx(i,klon),ny(i,klon),nor,klon)=i
  endif
 endif
 if(jcol2.eq.-5) then
  nx2=nx(i,klon)
  ny2=mod(ny(i,klon)-2+Ncv-1,Ncv)+1
  lxflag=1
  lyflag=0
  nor1=nv(nx(i,klon),ny(i,klon),0,klon)
  do lnk=1,nor1
   if(i.eq.nv(nx(i,klon),ny(i,klon),lnk,klon)) nr=lnk
  enddo
  do lnk=nr,nor1-1
   nbc=nv(nx(i,klon),ny(i,klon),lnk+1,klon)
   nv(nx(i,klon),ny(i,klon),lnk,klon)=nbc
  enddo
```

```
  nv(nx(i,klon),ny(i,klon),0,klon)
&=nv(nx(i,klon),ny(i,klon),0,klon)-1
  ny(i,klon)=ny(i,klon)-1
  if(ny(i,klon).lt.1)ny(i,klon)=Ncv
  nv(nx(i,klon),ny(i,klon),0,klon)
&=nv(nx(i,klon),ny(i,klon),0,klon)+1
  nor=nv(nx(i,klon),ny(i,klon),0,klon)
  nv(nx(i,klon),ny(i,klon),nor,klon)=i
 endif

! scheduling of the new particle-particle events
 do j=1,3
  nxv=nx2+lx2(j)*lxflag
  lk=ny2+ly2(j)*lyflag+Ncv-1
  nyv=mod(lk,Ncv)+1
  if(nxv.gt.Ncv.or.nxv.lt.1)cycle
  if(nv(nxv,nyv,0,klon).gt.0)then
   do k=1,nv(nxv,nyv,0,klon)
    jj=nv(nxv,nyv,k,klon)
    if(i.eq.iold.and.jj.eq.jold)cycle
    xij=x(i,klon)-x(jj,klon)
    yij=y(i,klon)-y(jj,klon)
    vxij=vx(i,klon)-vx(jj,klon)
    vyij=vy(i,klon)-vy(jj,klon)
    aa=xij*vxij+yij*vyij
    if(aa.lt.0.d0)then
     v2ij=vxij**2.d0+vyij**2.d0
     dis=4.d0*r*r*v2ij-(xij*vyij-yij*vxij)**2.d0
     if(dis.ge.0.d0) then
      t7=tabs(klon)+(-aa-dsqrt(dis))/v2ij
      i1=jj
      call almin(t7,i1,i)
     endif
    endif
    yij=-sign(1.d0,yij)*(1.d0-dabs(yij))
    aa=xij*vxij+yij*vyij
    if(aa.lt.0.d0)then
     v2ij=vxij**2.d0+vyij**2.d0
     dis=4.d0*r*r*v2ij-(xij*vyij-yij*vxij)**2.d0
     if(dis.ge.0.d0) then
      t7=tabs(klon)+(-aa-dsqrt(dis))/v2ij
      i1=jj
      call almin(t7,i1,i)
     endif
    endif
   enddo
  endif
 enddo

! scheduling of the new particle-wall events
 if(iold.eq.i.and.jold.eq.-1) goto 4
  if(nx(i,klon).le.2)then
   t7=tabs(klon)+(r-x(i,klon))/vx(i,klon)
   i1=-1
   call almin(t7,i1,i)
  endif
4 if(iold.eq.i.and.jold.eq.0) goto 6
 if(nx(i,klon).ge.(Ncv-1))then
  t7=tabs(klon)+(1.d0-x(i,klon)-r)/vx(i,klon)
  i1=0
  call almin(t7,i1,i)
 endif
6 continue
! scheduling of the new particle-virtual wall events
 t7=1.d10
 tv2=tv+1.d-13
 tabs2=tv2-tabs(klon)
 if(vx(i,klon).gt.0.d0) then
  aa=dble(nx(i,klon))/dble(Ncv)
  xvir=x(i,klon)+vx(i,klon)*tabs2
  t72=tv2+(aa-xvir)/vx(i,klon)
  if(t72.gt.tv2.and.t72.lt.t7) then
   i1=-4
   t7=t72
  endif
 endif

 if(vx(i,klon).lt.0.d0) then
  aa=dble(nx(i,klon)-1)/dble(Ncv)
  xvir=x(i,klon)+vx(i,klon)*tabs2
  t72=tv2+(aa-xvir)/vx(i,klon)
  if(t72.gt.tv2.and.t72.lt.t7) then
   i1=-2
   t7=t72
  endif
 endif

 if(vy(i,klon).lt.0.d0) then
  aa=dble(ny(i,klon)-1)/dble(Ncv)
  yvir=y(i,klon)+vy(i,klon)*tabs2
  yvir=yvir+1.d0-dint(yvir+1.d0)
  t72=tv2+(aa-yvir)/vy(i,klon)
  if(t72.gt.tv2.and.t72.lt.t7) then
   i1=-5
   t7=t72
  endif
 endif
 if(vy(i,klon).gt.0.d0) then
  aa=dble(ny(i,klon))/dble(Ncv)
  yvir=y(i,klon)+vy(i,klon)*tabs2
  yvir=yvir+1.d0-dint(yvir+1.d0)
  t72=tv2+(aa-yvir)/vy(i,klon)
  if(t72.gt.tv2.and.t72.lt.t7) then
   i1=-3
   t7=t72
  endif
 endif
 call almin(t7,i1,i)
 return
 end

 subroutine rencbt(i,j)
 implicit real*8(a-h,o-z)
 parameter (npmax=10000,nklon=1,Nvmax=100,Nal=200)
 common /c/ pi,tabs(nklon),tabstot(nklon),r,De,aN,tini,tpaso
&,iold,jold,Ncm,nl,N,Ncv,klon,Nvflag
 common /pos/ x(0:npmax,nklon),y(0:npmax,nklon)
 common /vel/ vx(0:npmax,nklon),vy(0:npmax,nklon)
 common /cajaV/ nv(Nvmax,Nvmax,0:npmax,nklon)
&,nx(npmax,nklon),ny(npmax,nklon)
 common /Cborde/ lx(9),ly(9),lx2(3),ly2(3)
 common /z/ Ey,Ex,Ex1,Ex2,tv,T1,T2
 common /lma/ al(1:Npmax,0:Nal,nklon),even(1:Npmax,0:Nal,nklon)
&,eveni(1:Npmax,0:Nal,nklon),evenj(1:Npmax,0:Nal,nklon)
&,nchoke(-10:Npmax,nklon)
 common /dsa/ ncbt(1:2*Npmax,nklon),tcol,jcol,icol

 control=0.d0
 nor=1
 do while(control.lt.1)
  if (j.gt.0) then
!trace back in the tree for the two particles
   np1=i
   np2=j
!the one with grater local colision time first
   if (al(np1,1,klon).lt.al(np2,1,klon)) then
    np1=j
    np2=i
   endif

   npadre=(N-1+np1)/2
   do while (npadre.ge.1)
    if(al(ncbt(2*npadre,klon),1,klon).le.
&al(ncbt(2*npadre+1,klon),1,klon)) then
     ncbt(npadre,klon)=ncbt(2*npadre,klon)
     npadre=npadre/2.d0
    else
     ncbt(npadre,klon)=ncbt(2*npadre+1,klon)
     npadre=npadre/2.d0
    endif
   enddo

   npadre=(N-1+np2)/2
   do while (npadre.ge.1)
    if(al(ncbt(2*npadre,klon),1,klon).le.
&al(ncbt(2*npadre+1,klon),1,klon)) then
     ncbt(npadre,klon)=ncbt(2*npadre,klon)
     npadre=npadre/2
    else
     ncbt(npadre,klon)=ncbt(2*npadre+1,klon)
     npadre=npadre/2
    endif
   enddo
  else
!trace back in the tree for one particle
   npadre=(N-1+i)/2
   do while (npadre.ge.1)
    if(al(ncbt(2*npadre,klon),1,klon).le.
&al(ncbt(2*npadre+1,klon),1,klon)) then
     ncbt(npadre,klon)=ncbt(2*npadre,klon)
     npadre=npadre/2
    else
     ncbt(npadre,klon)=ncbt(2*npadre+1,klon)
     npadre=npadre/2
    endif
   enddo
  endif
!new candidates to colision event
  ncan=ncbt(1,klon)
  njcan=even(ncan,1,klon)
!check of valid event
  if (eveni(ncan,1,klon).eq.nchoke(ncan,klon).and.
&evenj(ncan,1,klon).eq.nchoke(njcan,klon)) then
!valid event
   control=1.d0
  else
!invalid event is erased from the list
!and another candidate event it's selected
   nmk=dint(al(ncan,0,klon))
   do nor=1,nmk
    al(ncan,nor,klon)=al(ncan,nor+1,klon)
    even(ncan,nor,klon)=even(ncan,nor+1,klon)
```

```
    eveni(ncan,nor,klon)=eveni(ncan,nor+1,klon)
    evenj(ncan,nor,klon)=evenj(ncan,nor+1,klon)
   enddo
   al(ncan,0,klon)=al(ncan,0,klon)-1
   even(ncan,0,klon)=even(ncan,0,klon)-1
   eveni(ncan,0,klon)=eveni(ncan,0,klon)-1
   evenj(ncan,0,klon)=evenj(ncan,0,klon)-1
   i=ncan
   j=njcan
  endif
 enddo
 return
 end

 subroutine mov(tt2,iflag)
 implicit real*8(a-h,o-z)
 parameter (npmax=10000,nklon=1,Nvmax=100,Nal=200)
 common /c/ pi,tabs(nklon),tabstot(nklon),r,De,aN,tini,tpaso
&,iold,jold,Ncm,nl,N,Ncv,klon,Nvflag
 common /pos/ x(0:npmax,nklon),y(0:npmax,nklon)
 common /vel/ vx(0:npmax,nklon),vy(0:npmax,nklon)
 common /cajaV/ nv(Nvmax,Nvmax,0:npmax,nklon)
&,nx(npmax,nklon),ny(npmax,nklon)
 common /Cborde/ lx(9),ly(9),lx2(3),ly2(3)
 common /z/ Ey,Ex,Ex1,Ex2,tv,T1,T2
 common /lma/ al(1:Npmax,0:Nal,nklon),even(1:Npmax,0:Nal,nklon)
&,eveni(1:Npmax,0:Nal,nklon),evenj(1:Npmax,0:Nal,nklon)
&,nchoke(-10:Npmax,nklon)
 common /dsa/ ncbt(1:2*Npmax,nklon),tcol,jcol,icol

 tt=tt2-tabs(klon)
!check of a valid time
 if(tt.lt.0.d0) then
  write(6,*) icol,jcol,tabstot(klon),tabs(klon),tt2
 stop
 endif

 tabs(klon)=tt2
 do i=1,N
  nxv=1+dint(x(i,klon)*dble(Ncv))
  nyv=1+dint(y(i,klon)*dble(Ncv))
  tv=tabs(klon)
  yy=y(i,klon)+vy(i,klon)*tt+0.5d0*Ey*tt**2.d0
  vy(i,klon)=vy(i,klon)+Ey*tt
  x(i,klon)=x(i,klon)+vx(i,klon)*tt+0.5d0*Ex*tt**2.d0
  vx(i,klon)=vx(i,klon)+Ex*tt
  y(i,klon)=yy+1.d0-dint(yy+1.d0)
  nxv=1+dint(x(i,klon)*dble(Ncv))
  nyv=1+dint(y(i,klon)*dble(Ncv))

!check that particle i is in the right virtual box
  if(nyv.ne.ny(i,klon).or.nxv.ne.nx(i,klon)) then
   ncontrol=0
   jcol2=even(i,1,klon)
   nvxd=(nxv-nx(i,klon))
   nvyd=(nyv-ny(i,klon))

   if(nvxd.eq.1.and.jcol2.eq.-4) ncontrol=1
   if(nvxd.eq.-1.and.jcol2.eq.-2) ncontrol=1
   if(nvyd.eq.1.and.jcol2.eq.-3) ncontrol=1
   if(nvyd.eq.-(Ncv-1).and.jcol2.eq.-3) ncontrol=1
   if(nvyd.eq.-1.and.jcol2.eq.-5) ncontrol=1
   if(nvyd.eq.(Ncv-1).and.jcol2.eq.-5) ncontrol=1
!  write(6,*)"nvmal",nxv,nx(i,klon),nyv,ny(i,klon),tabstot(klon)

   if(ncontrol.eq.0) then
!in this case we just move the particle to the correct box
    nor1=nv(nx(i,klon),ny(i,klon),0,klon)
    do lnk=1,nor1
     if(i.eq.nv(nx(i,klon),ny(i,klon),lnk,klon)) nr=lnk
    enddo
!     write(6,*) nr
    nx3=nx(i,klon)
    ny3=ny(i,klon)
    do lnk=nr,nor1-1
     nv(nx3,ny3,lnk,klon)=nv(nx3,ny3,lnk+1,klon)
    enddo
    nv(nx3,ny3,0,klon)=nv(nx3,ny3,0,klon)-1
    nx(i,klon)=nxv
    ny(i,klon)=nyv
    nv(nx(i,klon),ny(i,klon),0,klon)
&=nv(nx(i,klon),ny(i,klon),0,klon)+1
    nor=nv(nx(i,klon),ny(i,klon),0,klon)
    nv(nx(i,klon),ny(i,klon),nor,klon)=i
!   write(6,*)"nvmal0",nxv,nx(i,klon),nyv,ny(i,klon),i,jcol2,tt2
   else
! in this case we recalculate the particle-virtual wall events
    tv=tt2
    call virtuacol(i,jcol2)
    do m=N,2*N-1
     ncbt(m,klon)=m-N+1
    enddo
    do m=2*N-1,3,-2
     if(al(ncbt(m,klon),1,klon).le.
&al(ncbt(m-1,klon),1,klon)) then
      ncbt(m/2,klon)=ncbt(m,klon)
     else
      ncbt(m/2,klon)=ncbt(m-1,klon)
     endif
    enddo
   endif
  endif
 enddo
 return
 end

 subroutine choq(i1,i2)
 implicit real*8(a-h,o-z)
 parameter (npmax=10000,nklon=1,Nvmax=100,Nal=200)
 common /c/ pi,tabs(nklon),tabstot(nklon),r,De,aN,tini,tpaso
&,iold,jold,Ncm,nl,N,Ncv,klon,Nvflag
 common /pos/ x(0:npmax,nklon),y(0:npmax,nklon)
 common /vel/ vx(0:npmax,nklon),vy(0:npmax,nklon)
 common /cajaV/ nv(Nvmax,Nvmax,0:npmax,nklon)
&,nx(npmax,nklon),ny(npmax,nklon)
 common /Cborde/ lx(9),ly(9),lx2(3),ly2(3)
 common /z/ Ey,Ex,Ex1,Ex2,tv,T1,T2
 common /lma/ al(1:Npmax,0:Nal,nklon),even(1:Npmax,0:Nal,nklon)
&,eveni(1:Npmax,0:Nal,nklon),evenj(1:Npmax,0:Nal,nklon)
&,nchoke(-10:Npmax,nklon)
 common /dsa/ ncbt(1:2*Npmax,nklon),tcol,jcol,icol
 common /medida3/ cpre(Nvmax),ajabs(2),ncol(Nvmax)
&,presion(Nvmax,npmax),ajcurrent(2,npmax),coli(Nvmax,npmax)
&,colmedias(Nvmax,8),ajmb(2,8)

 if(i2.gt.0)then
!particle-particle colision
  xx=x(i2,klon)-x(i1,klon)
  yy=y(i2,klon)-y(i1,klon)
  if(dabs(yy).gt.2.d0*De)yy=-sign(1.d0,yy)*(1.d0-dabs(yy))
  AD=xx*(vx(i2,klon)-vx(i1,klon))+yy*(vy(i2,klon)-vy(i1,klon))
  x1=x(i1,klon)
  nx1=1+dint(x1*dble(Ncm))
  cpre(nx1)=cpre(nx1)-AD
  cpre(Ncm+1)=cpre(Ncm+1)-AD
  vx(i1,klon)=vx(i1,klon)+xx*AD/(4.d0*r**2.d0)
  vy(i1,klon)=vy(i1,klon)+yy*AD/(4.d0*r**2.d0)
  vx(i2,klon)=vx(i2,klon)-xx*AD/(4.d0*r**2.d0)
  vy(i2,klon)=vy(i2,klon)-yy*AD/(4.d0*r**2.d0)
  ncol(nx1)=ncol(nx1)+1
  ncol(Ncm+1)=ncol(Ncm+1)+1
 else
  if(i2.eq.-1) then
!particle-wall colision. Hot thermal bath
   ecivo=(vx(i1,klon)**2.d0+vy(i1,klon)**2.d0)/2.d0
   u1=dran_u()
   u2=dran_u()
   vy(i1,klon)=dsqrt(-2.d0*dlog(u1))*dcos(2.d0*pi*u2)*dsqrt(T1)
   ac=dran_u()
   vx2=dsqrt(-2.d0*T1*dlog(1.d0-ac))
   cpre(Ncm+2)=cpre(Ncm+2)+vx(i1,klon)-vx2
   vx(i1,klon)=vx2
   cc=ecivo-(vx(i1,klon)**2.d0+vy(i1,klon)**2.d0)/2.d0
   ajabs(1)=ajabs(1)-cc
   ncol(Ncm+2)=ncol(Ncm+2)+1
  endif
  if(i2.eq.0) then
!particle-wall colision. Cold thermal bath
   ecivo=(vx(i1,klon)**2.d0+vy(i1,klon)**2.d0)/2.d0
   u1=dran_u()
   u2=dran_u()
   vy(i1,klon)=dsqrt(-2.d0*dlog(u1))*dcos(2.d0*pi*u2)*dsqrt(T2)
   ac=dran_u()
   vx2=-dsqrt(-2.d0*T2*dlog(1.d0-ac))
   cpre(Ncm+3)=cpre(Ncm+3)+vx(i1,klon)-vx2
   vx(i1,klon)=vx2
   cc=ecivo-(vx(i1,klon)**2.d0+vy(i1,klon)**2.d0)/2.d0
   ajabs(2)=ajabs(2)-cc
   ncol(Ncm+3)=ncol(Ncm+3)+1
  endif
 endif
 return
 end

 subroutine colision(i)
 implicit real*8(a-h,o-z)
 parameter (npmax=10000,nklon=1,Nvmax=100,Nal=200)
 common /c/ pi,tabs(nklon),tabstot(nklon),r,De,aN,tini,tpaso
&,iold,jold,Ncm,nl,N,Ncv,klon,Nvflag
 common /pos/ x(0:npmax,nklon),y(0:npmax,nklon)
 common /vel/ vx(0:npmax,nklon),vy(0:npmax,nklon)
 common /cajaV/ nv(Nvmax,Nvmax,0:npmax,nklon)
&,nx(npmax,nklon),ny(npmax,nklon)
 common /Cborde/ lx(9),ly(9),lx2(3),ly2(3)
 common /z/ Ey,Ex,Ex1,Ex2,tv,T1,T2
 common /lma/ al(1:Npmax,0:Nal,nklon),even(1:Npmax,0:Nal,nklon)
&,eveni(1:Npmax,0:Nal,nklon),evenj(1:Npmax,0:Nal,nklon)
&,nchoke(-10:Npmax,nklon)
 common /dsa/ ncbt(1:2*Npmax,nklon),tcol,jcol,icol
!Same routine that colinit but for only one particle
 al(i,0,klon)=0.d0
 even(i,0,klon)=0.d0
```

```
 eveni(i,0,klon)=0.d0
 evenj(i,0,klon)=0.d0

 do j=1,Nal
  al(i,j,klon)=1.d10
  even(i,j,klon)=0
  eveni(i,j,klon)=0
  evenj(i,j,klon)=0
 enddo
 do j=1,9
  nxv=nx(i,klon)+lx(j)
  nyv=mod(ny(i,klon)+ly(j)+Ncv-1,Ncv)+1
  if(nxv.gt.Ncv.or.nxv.lt.1)cycle
  if(nv(nxv,nyv,0,klon).gt.0)then
   do k=1,nv(nxv,nyv,0,klon)
    jj=nv(nxv,nyv,k,klon)
    if(i.eq.iold.and.jj.eq.jold)cycle
    xij=x(i,klon)-x(jj,klon)
    yij=y(i,klon)-y(jj,klon)
    vxij=vx(i,klon)-vx(jj,klon)
    vyij=vy(i,klon)-vy(jj,klon)
    aa=xij*vxij+yij*vyij
    if(aa.lt.0.d0)then
     v2ij=vxij**2.d0+vyij**2.d0
     dis=4.d0*r*r*v2ij-(xij*vyij-yij*vxij)**2.d0
     if(dis.ge.0.d0) then
      t7=tabs(klon)+(-aa-dsqrt(dis))/v2ij
      i1=jj
      call almin(t7,i1,i)
     endif
    endif
    yij=-sign(1.d0,yij)*(1.d0-dabs(yij))
    aa=xij*vxij+yij*vyij
    if(aa.lt.0.d0)then
     v2ij=vxij**2.d0+vyij**2.d0
     dis=4.d0*r*r*v2ij-(xij*vyij-yij*vxij)**2.d0
     if(dis.ge.0.d0) then
      t7=tabs(klon)+(-aa-dsqrt(dis))/v2ij
      i1=jj
      call almin(t7,i1,i)
     endif
    endif
   enddo
  endif
 enddo

 if(iold.eq.i.and.jold.eq.-1) goto 4
 if(nx(i,klon).le.2)then
  t7=tabs(klon)+(r-x(i,klon))/vx(i,klon)
  i1=-1
  call almin(t7,i1,i)
 endif
4 if(iold.eq.i.and.jold.eq.0) goto 6
 if(nx(i,klon).ge.(Ncv-1))then
  t7=tabs(klon)+(1.d0-x(i,klon)-r)/vx(i,klon)
  i1=0
  call almin(t7,i1,i)
 endif


6 t7=1.d10
 aa=dble(nx(i,klon))/dble(Ncv)
 t72=tabs(klon)+(aa-x(i,klon))/vx(i,klon)+1.d-13
 if(t72.gt.tabs(klon).and.t72.lt.t7)then
  i1=-4
  t7=t72
 endif
 aa=dble(nx(i,klon)-1)/dble(Ncv)
 t72=tabs(klon)+(aa-x(i,klon))/vx(i,klon)+1.d-13
 if(t72.gt.tabs(klon).and.t72.lt.t7) then
  i1=-2
  t7=t72
 endif
 aa=dble(ny(i,klon)-1)/dble(Ncv)
 t72=tabs(klon)+(aa-y(i,klon))/vy(i,klon)+1.d-13
 if(t72.gt.tabs(klon).and.t72.lt.t7) then
  i1=-5
  t7=t72
 endif
 aa=dble(ny(i,klon))/dble(Ncv)
 t72=tabs(klon)+(aa-y(i,klon))/vy(i,klon)+1.d-13
 if(t72.gt.tabs(klon).and.t72.lt.t7) then
  i1=-3
  t7=t72
 endif

 call almin(t7,i1,i)

 return
 end

 subroutine check(tlim,nbadpar)
 implicit real*8(a-h,o-z)
 parameter (npmax=10000,nklon=1,Nvmax=100,Nal=200)
 common /c/ pi,tabs(nklon),tabstot(nklon),r,De,aN,tini,tpaso
&,iold,jold,Ncm,nl,N,Ncv,klon,Nvflag
 common /pos/ x(0:npmax,nklon),y(0:npmax,nklon)
 common /vel/ vx(0:npmax,nklon),vy(0:npmax,nklon)
 common /cajaV/ nv(Nvmax,Nvmax,0:npmax,nklon)
&,nx(npmax,nklon),ny(npmax,nklon)
 common /Cborde/ lx(9),ly(9),lx2(3),ly2(3)
 common /z/ Ey,Ex,Ex1,Ex2,tv,T1,T2
 common /lma/ al(1:Npmax,0:Nal,nklon),even(1:Npmax,0:Nal,nklon)
&,eveni(1:Npmax,0:Nal,nklon),evenj(1:Npmax,0:Nal,nklon)
&,nchoke(-10:Npmax,nklon)

 if(tabstot(klon).gt.tlim) then
 jjs=dint(al(10,0,klon))
 do js=1,jjs
  write(6,*)al(i,js,klon),even(i,js,klon),10,tabstot(klon)
 enddo
 jjs=dint(al(nbadpar,0,klon))
 do js=1,jjs
   write(6,*)al(i,js,klon),even(i,js,klon),nbadpar,tabs(klon)
 enddo
 endif
!overlapping and scaping particles check
 do kkl=1,N
  x3=x(kkl,klon)
  y3=y(kkl,klon)
  do kkl2=kkl,N
   if(kkl.ne.kkl2) then
    x2=x(kkl2,klon)
    y2=y(kkl2,klon)
    dist=dsqrt((x3-x2)**2.d0+(y3-y2)**2.d0)+1.d-7
    if(dist.lt.2.d0*r) then
     write(6,*)"s",x3,y3,x2,y2,klon,kkl,kkl2
     jjs=dint(al(kkl,0,klon))
     do js=1,jjs
      write(6,*)al(kkl,js,klon),even(kkl,js,klon)
     &,icol,jcol,tt,tt2,tabstot(klon)
     enddo
     stop
    endif
   endif
  enddo
  if(x3.gt.(1.d0-r+1.d-7).or.x3.lt.r-1.d-7) then
   write(6,*) "particle out",kkl,x3,r
  endif
 enddo
 return
 end

 subroutine measure(ns)
 implicit real*8(a-h,o-z)
 parameter (npmax=10000,nklon=1,Nvmax=100,Nal=200)
 dimension vcmden(Nvmax)
 dimension densi(Nvmax),auxt(Nvmax)
 common /c/ pi,tabs(nklon),tabstot(nklon),r,De,aN,tini,tpaso
&,iold,jold,Ncm,nl,N,Ncv,klon,Nvflag
 common /pos/ x(0:npmax,nklon),y(0:npmax,nklon)
 common /vel/ vx(0:npmax,nklon),vy(0:npmax,nklon)
 common /cajaV/ nv(Nvmax,Nvmax,0:npmax,nklon)
&,nx(npmax,nklon),ny(npmax,nklon)
 common /Cborde/ lx(9),ly(9),lx2(3),ly2(3)
 common /z/ Ey,Ex,Ex1,Ex2,tv,T1,T2
 common /lma/ al(1:Npmax,0:Nal,nklon),even(1:Npmax,0:Nal,nklon)
&,eveni(1:Npmax,0:Nal,nklon),evenj(1:Npmax,0:Nal,nklon)
&,nchoke(-10:Npmax,nklon)
 common /dsa/ ncbt(1:2*Npmax,nklon),tcol,jcol,icol
 common /medida/ etot(npmax,2),distri(15000,Nvmax)
&,tcolu(Nvmax,npmax),denc(Nvmax,npmax),densi2(Nvmax,npmax)
&,vcmx(Nvmax,npmax),vcmy(Nvmax,npmax),v(npmax,8)
&,ajgtot(npmax,6),tabs4(npmax,nklon),ecin_b(Nvmax,npmax)
$,distrimax
 common /medida2/ tmedias(Nvmax,8),dmedias(Nvmax,8)
&,anmedias(Nvmax,8),emedias(Nvmax,8),pmedias(Nvmax,8)
&,vcymd(Nvmax,8),vmedias(8),ajmedias(6,8),vcxmd(Nvmax,8)
&,xmedtot
 common /medida3/ cpre(Nvmax),ajabs(2),ncol(Nvmax)
&,presion(Nvmax,npmax),ajcurrent(2,npmax),coli(Nvmax,npmax)
&,colmedias(Nvmax,8),ajmb(2,8)
 Ncmt=Ncm+1
 aN=dble(N)
 aNc=dble(Ncm)
 tabs4(ns,klon)=tabstot(klon)+tabs(klon)
 do i=1,Ncmt
  vcmx(i,ns)=0.d0
  vcmy(i,ns)=0.d0
  vcmden(i)=0.d0
  densi(i)=0.d0
  auxt(i)=0.d0
  densi2(i,ns)=0.d0
 enddo
!Mesurement of presures and currents at the border
 tf=tpaso
 ajcurrent(1,ns)=ajabs(1)/tf
 ajcurrent(2,ns)=ajabs(2)/tf
 ajabs(1)=0.d0
 ajabs(2)=0.d0
 do i=1,Ncm+3
  coli(i,ns)=ncol(i)
```

```
  presion(i,ns)=cpre(i)
  cpre(i)=0.d0
  ncol(i)=0
 enddo

!mesurement of velocity of the center of mass,
! per boxes and global
 do i=1,N
  ii=1+dint(x(i,klon)*dble(Ncm))
  vcmy(ii,ns)=vcmy(ii,ns)+vy(i,klon)
  vcmx(ii,ns)=vcmx(ii,ns)+vx(i,klon)
  vcmx(Ncmt,ns)=vcmx(Ncmt,ns)+vx(i,klon)
  vcmy(Ncmt,ns)=vcmy(Ncmt,ns)+vy(i,klon)
  vcmden(ii)=vcmden(ii)+1.d0
  vcmden(Ncmt)=vcmden(Ncmt)+1.d0
 enddo

 do i=1,Ncmt
  vcmy(i,ns)=vcmy(i,ns)/vcmden(i)
  vcmx(i,ns)=vcmx(i,ns)/vcmden(i)
 enddo

!mesurement of the mean velocity
 do i=1,8
  v(ns,i)=0.d0
 enddo
 do i=1,N
  vmodulo=dsqrt(vx(i,klon)**2.d0+vy(i,klon)**2.d0)
c      write(6,*) vmodulo
  do kk=1,8
   akk=dble(kk)
   v(ns,kk)=v(ns,kk)+vmodulo**akk
  enddo
 enddo
!mesurement of the global current by componets and modulus
!with and without sustracting the mean center of mass velocity
 ajglox1=0.d0
 ajglox2=0.d0
 ajgloy1=0.d0
 ajgloy2=0.d0
 ajgloz1=0.d0
 ajgloz2=0.d0
 ecin1=0.d0
 ecin2=0.d0
 vcx=vcmx(Ncmt,ns)
 vcy=vcmy(Ncmt,ns)
 do i=1,N
  ev1=(vx(i,klon))**2.d0+(vy(i,klon))**2.d0
  ev2=(vx(i,klon)-vcx)**2.d0+(vy(i,klon)-vcy)**2.d0
  ecin1=ecin1+ev1
  ecin2=ecin2+ev2
  ajglox1=ajglox1+ev1*(vx(i,klon))
  ajgloy1=ajgloy1+ev1*(vy(i,klon))
  zz1=dsqrt((ev1*vx(i,klon))**2.d0+(ev1*vy(i,klon))**2.d0)
  ajgloz1=ajgloz1+zz1
  ajglox2=ajglox2+ev2*(vx(i,klon)-vcx)
  ajgloy2=ajgloy2+ev2*(vy(i,klon)-vcy)
  zz2=(ev2*(vx(i,klon)-vcx))**2.d0
  zz1=dsqrt(zz2+(ev2*(vy(i,klon)-vcy))**2.d0)
  ajgloz2=ajgloz2+zz1
 enddo

 ajgtot(ns,1)=ajglox1/(2.d0*aN)
 ajgtot(ns,2)=ajgloy1/(2.d0*aN)
 ajgtot(ns,3)=ajgloz1/(2.d0*aN)

 ajgtot(ns,4)=ajglox2/(2.d0*aN)
 ajgtot(ns,5)=ajgloy2/(2.d0*aN)
 ajgtot(ns,6)=ajgloz2/(2.d0*aN)
 etot(ns,1)=ecin1/(2.d0*aN)
 etot(ns,2)=ecin2/(2.d0*aN)

!mesurement of the temperature number of particles and density
!and velocity distribution for each box.
 do i=1,N
  ii=1+dint(x(i,klon)*dble(Ncm))
  ecin=dsqrt((vx(i,klon))**2.d0+(vy(i,klon))**2.d0)
  densi2(ii,ns)=densi2(ii,ns)+1.d0
  densi2(Ncmt,ns)=densi2(Ncmt,ns)+1.d0
  auxt(Ncmt)=auxt(Ncmt)+0.5d0*ecin*ecin
  densi(Ncmt)=densi(Ncmt)+pi*r*r
  jik=1+dint(3500.d0*ecin/distrimax)
  if (jik.le.15000) then
   distri(jik,ii)=distri(jik,ii)+1
   distri(jik,Ncmt)=distri(jik,Ncmt)+1
  endif
  xmu=abs(dble(ii)/aNc-x(i,klon))
  cont=0
  if(xmu.lt.r.and.ii.ne.Ncm) then
   fi=pi/2.d0-dasin(xmu/r)
   atri=fi*r*r-xmu*dsqrt(r*r-xmu*xmu)
   densi(ii)=densi(ii)+pi*r*r-atri
   densi(ii+1)=densi(ii+1)+atri
   auxt(ii)=auxt(ii)+(pi*r*r-atri)*ecin*ecin/(pi*r*r*2.d0)
   auxt(ii+1)=auxt(ii+1)+(atri)*ecin*ecin/(pi*r*r*2.d0)
   cont=2
  endif
  xmu=abs(dble(ii-1)/aNc-x(i,klon))
  if(xmu.lt.r.and.ii.ne.1) then
   fi=pi/2.d0-dasin(xmu/r)
   atri=fi*r*r-xmu*dsqrt(r*r-xmu*xmu)
   densi(ii)=densi(ii)+pi*r*r-atri
   densi(ii-1)=densi(ii-1)+atri
   auxt(ii)=auxt(ii)+(pi*r*r-atri)*ecin*ecin/(pi*r*r*2.d0)
   auxt(ii-1)=auxt(ii-1)+(atri)*ecin*ecin/(pi*r*r*2.d0)
   cont=2
  endif
  if(cont.lt.1) then
   densi(ii)=densi(ii)+pi*r*r
   auxt(ii)=auxt(ii)+ecin*ecin/2.d0
  endif
 enddo
 do i=1,Ncmt
  denc(i,ns)=densi(i)*aNc
  ecin_b(i,ns)=auxt(i)
  tcolu(i,ns)=auxt(i)*pi*r*r/densi(i)
 enddo
 end




 subroutine salvar()
 implicit real*8(a-h,o-z)
 parameter (npmax=10000,nklon=1,Nvmax=100,Nal=200)
 common /c/ pi,tabs(nklon),tabstot(nklon),r,De,aN,tini,tpaso
&,iold,jold,Ncm,nl,N,Ncv,klon,Nvflag
 common /pos/ x(0:npmax,nklon),y(0:npmax,nklon)
 common /vel/ vx(0:npmax,nklon),vy(0:npmax,nklon)
 common /cajaV/ nv(Nvmax,Nvmax,0:npmax,nklon)
&,nx(npmax,nklon),ny(npmax,nklon)
 common /Cborde/ lx(9),ly(9),lx2(3),ly2(3)
 common /z/ Ey,Ex,Ex1,Ex2,tv,T1,T2
 common /lma/ al(1:Npmax,0:Nal,nklon),even(1:Npmax,0:Nal,nklon)
&,eveni(1:Npmax,0:Nal,nklon),evenj(1:Npmax,0:Nal,nklon)
&,nchoke(-10:Npmax,nklon)
 common /dsa/ ncbt(1:2*Npmax,nklon),tcol,jcol,icol
 common /medida/ etot(npmax,2),distri(15000,Nvmax)
&,tcolu(Nvmax,npmax),denc(Nvmax,npmax),densi2(Nvmax,npmax)
&,vcmx(Nvmax,npmax),vcmy(Nvmax,npmax),v(npmax,8)
&,ajgtot(npmax,6),tabs4(npmax,nklon),ecin_b(Nvmax,npmax)
,distrimax
 common /medida2/ tmedias(Nvmax,8),dmedias(Nvmax,8)
&,anmedias(Nvmax,8),emedias(Nvmax,8),pmedias(Nvmax,8)
&,vcymd(Nvmax,8),vmedias(8),ajmedias(6,8),vcxmd(Nvmax,8)
&,xmedtot
 common /medida3/ cpre(Nvmax),ajabs(2),ncol(Nvmax)
&,presion(Nvmax,npmax),ajcurrent(2,npmax),coli(Nvmax,npmax)
&,colmedias(Nvmax,8),ajmb(2,8)
 character*1 iklon

 open(unit=21,file="tmedia.dat",status="unknown"
&,position="append")
 open(unit=22,file="dmedia.dat",status="unknown"
&,position="append")
 open(unit=23,file="anmedia.dat",status="unknown"
&,position="append")
 open(unit=24,file="emedia.dat",status="unknown"
&,position="append")
 open(unit=25,file="vmedia.dat",status="unknown"
&,position="append")
 open(unit=26,file="ajgmedia.dat",status="unknown"
&,position="append")
 open(unit=27,file="ajbmedia.dat",status="unknown"
&,position="append")
 open(unit=28,file="evol.dat",status="unknown"
&,position="append")
 open(unit=29,file="distribucion.dat",status="unknown")
 open(unit=30,file="pmedia.dat",status="unknown"
&,position="append")
 open(unit=31,file="colisiones.dat",status="unknown"
&,position="append")
 open(unit=33,file="vxcmmedia.dat",status="unknown"
&,position="append")
 open(unit=34,file="vycmmedia.dat",status="unknown"
&,position="append")
 open(unit=667,file="configuracion.dat",status="unknown")
 write(667,*) tabstot(klon),tabs(klon),iold,jold
 do is=1,N
  write(667,*) x(is,klon),y(is,klon),vx(is,klon),vy(is,klon)
 enddo
 close(667)
 con=0
 Ncmt=Ncm+1
 do k=1,8
  do i=1,Ncmt+2
   tmedias(i,k)=0.d0
   dmedias(i,k)=0.d0
   anmedias(i,k)=0.d0
   emedias(i,k)=0.d0
   pmedias(i,k)=0.d0
   colmedias(i,k)=0.d0
   vcxmd(i,k)=0.d0
```

```
   vcymd(i,k)=0.d0
  enddo
  vmedias(k)=0.d0
  do i=1,6
   ajmedias(i,k)=0.d0
  enddo
  do i=1,2
   ajmb(i,k)=0.d0
  enddo
 enddo

 do kj=1,Ncmt
  do i=1,15000
   write(29,*) i,distri(i,kj),kj
  enddo
 enddo

 do j=1,1000
  do kk=1,8
   akk=dble(kk)
   do i=1,Ncmt
    tmedias(i,kk)=tmedias(i,kk)+tcolu(i,j)**akk
    pmedias(i,kk)=pmedias(i,kk)+presion(i,j)**akk
    colmedias(i,kk)=colmedias(i,kk)+coli(i,j)**akk
    dmedias(i,kk)=dmedias(i,kk)+denc(i,j)**akk
    anmedias(i,kk)=anmedias(i,kk)+densi2(i,j)**akk
    emedias(i,kk)=emedias(i,kk)+ecin_b(i,j)**akk
    vcxmd(i,kk)=vcxmd(i,kk)+vcmx(i,j)**akk
    vcymd(i,kk)=vcymd(i,kk)+vcmy(i,j)**akk
   enddo
   pmedias(Ncm+2,kk)=pmedias(Ncm+2,kk)+presion(Ncm+2,j)**akk
   pmedias(Ncm+3,kk)=pmedias(Ncm+3,kk)+presion(Ncm+3,j)**akk
   colmedias(Ncm+2,kk)=colmedias(Ncm+2,kk)+coli(Ncm+2,j)**akk
   colmedias(Ncm+3,kk)=colmedias(Ncm+3,kk)+coli(Ncm+3,j)**akk
   vmedias(kk)=vmedias(kk)+v(j,kk)
   do i=1,6
    akk=dble(kk)
    ajmedias(i,kk)=ajmedias(i,kk)+ajgtot(j,i)**akk
   enddo
   do i=1,2
    ajmb(i,kk)=ajmb(i,kk)+ajcurrent(i,j)**akk
   enddo
  enddo
 enddo
 xmedtot=xmedtot+1000.d0

 do i=1,Ncmt+2
  write(30,*) pmedias(i,1),pmedias(i,2),
&pmedias(i,3),pmedias(i,4),pmedias(i,5),
&pmedias(i,6),pmedias(i,7),pmedias(i,8)!,xmedtot

  write(31,*) colmedias(i,1),colmedias(i,2),
&colmedias(i,3),colmedias(i,4),colmedias(i,5),
&colmedias(i,6),colmedias(i,7),colmedias(i,8)!,xmedtot
 enddo

 do i=1,Ncmt
  write(21,*) tmedias(i,1),tmedias(i,2),
&tmedias(i,3),tmedias(i,4),tmedias(i,5),
&tmedias(i,6),tmedias(i,7),tmedias(i,8)!,xmedtot

  write(22,*) dmedias(i,1),dmedias(i,2),
&dmedias(i,3),dmedias(i,4),dmedias(i,5),
&dmedias(i,6),dmedias(i,7),dmedias(i,8)!,xmedtot

  write(23,*) anmedias(i,1),anmedias(i,2),
&anmedias(i,3),anmedias(i,4),anmedias(i,5)
&,anmedias(i,6),anmedias(i,7),anmedias(i,8)!,xmedtot

  write(24,*) emedias(i,1),emedias(i,2),
&emedias(i,3),emedias(i,4),emedias(i,5),
&emedias(i,6),emedias(i,7),emedias(i,8)!,xmedtot

 write(33,*) vcxmd(i,1),vcxmd(i,2),
 &vcxmd(i,3),vcxmd(i,4),vcxmd(i,5),
 &vcxmd(i,6),vcxmd(i,7),vcxmd(i,8)!,xmedtot

write(34,*) vcymd(i,1),vcymd(i,2),
&vcymd(i,3),vcymd(i,4),vcymd(i,5),
&vcymd(i,6),vcymd(i,7),vcymd(i,8)!,xmedtot
 enddo

 write(25,*) vmedias(1),vmedias(2),
&vmedias(3),vmedias(4),vmedias(5),
&vmedias(6),vmedias(7),vmedias(8),xmedtot,N,tpaso,r
 do i=1,6
  write(26,*) ajmedias(i,1),ajmedias(i,2),
&ajmedias(i,3),ajmedias(i,4),
&ajmedias(i,5),ajmedias(i,6),
&ajmedias(i,7),ajmedias(i,8)!,xmedtot
 enddo
 do i=1,2
  write(27,*) ajmb(i,1),ajmb(i,2),
&ajmb(i,3),ajmb(i,4),
&ajmb(i,5),ajmb(i,6),
&ajmb(i,7),ajmb(i,8)!,xmedtot
 enddo
 call flush(21)
 call flush(25)
 call flush(22)
 call flush(23)
 call flush(24)
 call flush(26)
 call flush(27)
 call flush(28)
 call flush(29)
 call flush(30)
 call flush(31)
 call flush(33)
 call flush(34)
 close(21)
 close(22)
 close(25)
 close(23)
 close(24)
 close(26)
 close(27)
 close(29)
 close(30)
 close(31)
 close(33)
 close(34)

 end



cxxxxxxxxxxxxxxxxxxxxxxxxxxxxxxxxxxxxxxxxxxxxxxxxxxxxxxxxxxx
!random number
 subroutine dran_ini(iseed0)
 integer*8::ip,np,nbit,m,np1,nn,nn1,ic,i,j
 real*8::dseed,rand_xx,p,t,x
 parameter(ip=1279)
 parameter(np=14)
 parameter(nbit=31)
 integer*8,dimension(1:ip)::ix
 common /ixx/ ix
 common /icc/ ic

 dseed=iseed0

 do i=1,ip
  ix(i)=0
  do j=0,nbit-1
   if(rand_xx(dseed).lt.0.5d0) ix(i)=ibset(ix(i),j)
  enddo
 enddo
 ic=0
 end subroutine dran_ini

 subroutine dran_read(iunit)
 parameter(ip=1279)
 parameter(np=14)
 integer*8::ic,i
 integer*8,dimension(1:ip)::ix
 common /ixx/ ix
 common /icc/ ic
 read(iunit,*)ic
 read(iunit,*)(ix(i),i=1,ip)
 end subroutine dran_read

 subroutine dran_write(iunit)
 parameter(ip=1279)
 parameter(np=14)
 integer*8,dimension(1:ip)::ix
 integer*8::i,ic
 common /ixx/ ix
 common /icc/ ic
 write(iunit,*) ic
 write(iunit,*) (ix(i),i=1,ip)
 end subroutine dran_write

 integer*8 function i_dran(n)
 integer*8::ip,iq,is,ic,i_ran
 parameter(ip=1279)
 parameter(iq=418)
 parameter(is=ip-iq)
 integer*8,dimension(1:ip)::ix
 common /ixx/ ix
 common /icc/ ic
 ic=ic+1
 if(ic.gt.ip) ic=1
 if(ic.gt.iq)then
  ix(ic)=ieor(ix(ic),ix(ic-iq))
 else
  ix(ic)=ieor(ix(ic),ix(ic+is))
 endif
 i_ran=ix(ic)
 if(n.gt.0)i_dran=mod(i_ran,n)+1
 end function i_dran

 real*8 function dran_u()
```

```
integer*8::ip,iq,is,ic
real*8::rmax
parameter(ip=1279)
parameter(iq=418)
parameter(is=ip-iq)
parameter (rmax=2147483647.0)
integer*8,dimension(1:ip)::ix
common /ixx/ ix
common /icc/ ic
ic=ic+1
if(ic.gt.ip) ic=1
if(ic.gt.iq)then
 ix(ic)=ieor(ix(ic),ix(ic-iq))
else
 ix(ic)=ieor(ix(ic),ix(ic+is))
endif
dran_u=dble(ix(ic))/rmax
end function dran_u

real*8 function rand_xx(dseed)
real*8:: a,c,xm,rm,dseed
parameter (xm=2.d0**32,rm=1.d0/xm,a=69069.d0,c=1.d0)
dseed=mod(dseed*a+c,xm)
rand_xx=dseed*rm
end function rand_xx
```

Appendix B

General Scaling for Soft Potentials in d-Dimensions

The scaling properties for the density and temperature profiles saw in chapter 4 can be further generalized to d-dimension soft potentials of the form:

$$V(x) = \epsilon \left(\frac{\sigma}{x}\right)^n \tag{B.1}$$

where x is the d-dimensional euclidean distance between two particles. Hard d-dimensional spheres can be obtained in the limit $n \to \infty$:

$$\begin{aligned} V(x) &= 0 \qquad \text{if} \quad x > \sigma \\ &= \infty \qquad \text{if} \quad x < \sigma \end{aligned} \tag{B.2}$$

where $\sigma = 2r$ where r is the radius of the d-dimensional sphere.

General forms for the equation of state and conductivity can be derived for this class of soft potentials:

$$\begin{aligned} \text{EOS: } P &= \tilde{\beta}^{-1} g(\tilde{\rho}) \\ \text{Thermal conductivity: } \kappa &= \frac{k_B}{2m} \sigma^a \epsilon^b \tilde{\beta}^c y(\tilde{\rho}) \end{aligned} \tag{B.3}$$

where

$$\begin{aligned} \tilde{\beta} &= \beta(\beta\epsilon)^{d/n} \sigma^d \\ \tilde{\rho} &= \rho(\beta\epsilon)^{d/n} \sigma^d \end{aligned} \tag{B.4}$$

and

$$a = \frac{n(2-d)}{2(n+d)} \quad ; \quad b = \frac{2-d}{2(n+d)} \quad ; \quad c = \frac{2-2d-n}{2(n+d)} \tag{B.5}$$

$g(x)$ and $y(x)$ have no dimensions and $g(x) \simeq x$ when $x \simeq 0$. In order to obtain such general scaled forms one should prove the following properties.
(1) Scaling form of the canonical partition function:

$$Z(N,V,T) = \left[\sigma(\beta\epsilon)^{1/n} \left(\frac{\beta}{2m}\right)^{1/2}\right]^{Nd} \bar{Z}\left(N, \frac{V}{(\beta\epsilon)^{d/n}\sigma^d}\right) \tag{B.6}$$

Proof: The canonical partition function is:

$$Z(N,V,T) = \frac{1}{N!h^{dN}} \int_V d\vec{r}_N \int_{R^d} d\vec{p}_N \exp\left[-\beta H(\vec{r}_N, \vec{p}_N)\right] \tag{B.7}$$

where the Hamiltonian is given in our case by:

$$H(\vec{r}_N, \vec{p}_N) = \sum_{i=1}^{N} \frac{\vec{p}_i^2}{2m} + \epsilon\sigma^n \sum_{i<j} \frac{1}{|\vec{r}_i - \vec{r}_j|^n} \tag{B.8}$$

We change the variables of the integrals to extract the system parameters out of the exponential:

$$\vec{k}_i = \left(\frac{\beta}{2m}\right)^{1/2} \vec{p}_i \quad , \quad \vec{q}_i = (\beta\epsilon)^{-1/n}\sigma^{-1}\vec{r}_i \tag{B.9}$$

And we get B.6 with

$$\bar{Z}\,(N,V) = \frac{1}{N!h^{dN}} \int_V d\vec{q}_N \int_{R^d} d\vec{k}_N \exp\left[-\bar{H}(\vec{q}_N, \vec{k}_N)\right] \tag{B.10}$$

where

$$\bar{H}(\vec{q}_N, \vec{k}_N) = \sum_{i=1}^{N} \vec{k}_i^2 + \sum_{i<j} \frac{1}{|\vec{q}_i - \vec{q}_j|^n} \tag{B.11}$$

(2) Scaling form of the equation of state:

$$P = \tilde{\beta}^{-1} g(\tilde{\rho}) \tag{B.12}$$

Proof:
The equation of state is obtain from the canonical partition function:

$$P = \frac{1}{\beta}\frac{\partial}{\partial V} \ln Z(N,V,T)\Big|_{N,T} \tag{B.13}$$

When substituting the scaling form of Z we get

$$P = \beta^{-1}(\beta\epsilon)^{-d/n}\sigma^{-d}\frac{\partial}{\partial \bar{V}} \ln \bar{Z}(N,\bar{V})\Big|_N \tag{B.14}$$

where $\bar{V} = V(\beta\epsilon)^{-d/n}\sigma^{-d}$. One should note that if the system has a well defined thermodynamic limit, then

$$\frac{\partial}{\partial \bar{V}} \ln \bar{Z}(N,\bar{V})\Big|_N = P(\beta = 1, m = 1/2, \epsilon^{1/n}\sigma = 1; N, \bar{V}) = g(\frac{N}{\bar{V}}) \tag{B.15}$$

and we get the above form of the eos.

(3) Thermal conductivity: We know the Green-Kubo expression for the thermal conductivity:

$$\kappa = k_B V \beta^2 \int_0^\infty dt \langle J(0)J(t)\rangle_{eq} \tag{B.16}$$

where:

$$J = \frac{1}{mV}\sum_{i=1}^{N}\left[e_i p_{x,i} - \frac{1}{2}\sum_{j\neq i}(\vec{r}_{ij}\cdot\vec{p}_i)\frac{r_{x,ij}}{r_{ij}}V'(r_{ij})\right] \tag{B.17}$$

where $r_{ij} = |\vec{r}_i - \vec{r}_j|$ and $e_i = \vec{p}_i^2/2m + 1/2\sum_{j\neq i}V(r_{ij})$. And

$$J(t) = e^{tL}J(0) \quad , \quad Lb = \{b, H\} = \sum_{i,\alpha}\left[\frac{\partial H}{\partial p_{i\alpha}}\frac{\partial b}{\partial r_{i\alpha}} - \frac{\partial H}{\partial r_{i\alpha}}\frac{\partial b}{\partial p_{i\alpha}}\right] \tag{B.18}$$

We can express all these equations in function of $\vec{k}$ and $\vec{q}$ variables defined above. We find that:

$$L = \sigma^{-1}(\beta\epsilon)^{-1/n}(2m\beta)^{-1/2}\bar{L} \tag{B.19}$$

with

$$\bar{L} = \sum_{i,\alpha}\left[2k_{i\alpha}\frac{\partial}{\partial q_{i\alpha}} + n\sum_{j\neq i}\frac{q_{i\alpha}-q_{j\alpha}}{|\vec{q}_i-\vec{q}_j|^{n+2}}\frac{\partial}{\partial k_{i\alpha}}\right] \tag{B.20}$$

$$e_i = \beta^{-1}\bar{e}_i \quad , \quad \bar{e}_i = \vec{k}_i^2 + \frac{1}{2}\sum_{j\neq i}\frac{1}{|\vec{q}_i-\vec{q}_j|^n} \tag{B.21}$$

$$J = (V\beta)^{-1}(2m\beta)^{-1/2}\bar{J} \quad , \quad \bar{J} = \sum_{i=1}^{N}\left[2\bar{e}_i k_{i,x} + n\sum_{j\neq i}(\vec{q}_{ij}\cdot\vec{k}_{ij})\frac{q_{ij,x}}{q_{ij}^{n+2}}\right] \tag{B.22}$$

Substituting all these expressions on the κ definition, we get the above expression for the thermal conductivity.

Let us note that, in particular, for d-dimensional spheres ($n \to \infty$) we get:

$$\begin{aligned} P &= \beta^{-1}\sigma^{-d}g(\eta) \quad , \quad \eta = \rho\sigma^d \\ \kappa &= \frac{k_B}{(2m)^{1/2}}\sigma^{1-d}\beta^{-1/2}y(\eta) \end{aligned} \tag{B.23}$$

We can use the scaled forms for the eos and κ to get a closed expression of the Fourier law in density variables as we did in the hard disk case:

$$(2m)^{1/2}\left(1+\frac{d}{n}\right)J\sigma^{\bar{a}}\epsilon^{\bar{b}}P^{\bar{c}} = \bar{F}(\tilde{\rho})\frac{d\tilde{\rho}}{dx} \tag{B.24}$$

where $\bar{F}(\tilde{\rho}) = y(\tilde{\rho})g(\tilde{\rho})^{\bar{c}-1}g'(\tilde{\rho})$, and

$$\begin{aligned} \bar{a} &= -\frac{n(d+2)}{2(n+d)} \\ \bar{b} &= -\frac{d+2}{2(n+d)} \\ \bar{c} &= \frac{2-2d-3n}{2(n+d)} \end{aligned} \tag{B.25}$$

We recover the expression found in the hard disk case when $n \to \infty$ and $d = 2$. From eq. B.24 we can redo the computations for hard disks and we get similar four properties by changing $\rho \to \tilde{\rho}$ and $\beta \to \tilde{\beta}$.

Appendix C

Implications and Generalizations of the IFR

The isometric fluctuation relation, Eq. (5.9), has far-reaching and nontrivial consequences. As we shall see, the IFR implies remarkable hierarchies of equations for the current cumulants, see Eq. (C.4), and the nonlinear response coefficients, see eqs. (C.6)-(C.9), going far beyond Onsager's reciprocity relations and Green-Kubo formulas.

C.1 Hierarchies for the cumulants and response coefficients

The moment-generating function associated to $\mathrm{P}_\tau(\mathbf{J})$, defined as

$$\Pi_\tau(\boldsymbol{\lambda}) = \int \mathrm{P}_\tau(\mathbf{J}) \exp(\tau L^d \boldsymbol{\lambda}\cdot\mathbf{J}) d\mathbf{J}, \tag{C.1}$$

scales for long times as $\Pi_\tau(\boldsymbol{\lambda}) \sim \exp[+\tau L^d \mu(\boldsymbol{\lambda})]$, where $\mu(\boldsymbol{\lambda}) = \max_{\mathbf{J}}[G(\mathbf{J}) + \boldsymbol{\lambda}\cdot\mathbf{J}]$ is the cumulant generating function and corresponds to the Legendre transform of the current LDF. The cumulants of the current distribution can be obtained from the derivatives of $\mu(\boldsymbol{\lambda})$ evaluated at $\boldsymbol{\lambda} = 0$, i.e.

$$\mu^{(n)}_{(n_1\ldots n_d)} \equiv \left[\frac{\partial^n \mu(\boldsymbol{\lambda})}{\partial\lambda_1^{n_1}\ldots\lambda_d^{n_d}}\right]_{\lambda=0} = (\tau L^d)^{n-1}\langle \Delta J_1^{n_1}\ldots\Delta J_d^{n_d}\rangle_\epsilon \quad \text{for } n \geq 1, \tag{C.2}$$

where $\Delta J_\alpha \equiv J_\alpha - (1-\delta_{n,1})\langle J_\alpha\rangle_\epsilon$ and $\delta_{n,m}$ is the Kronecker symbol. In virtue of the IFR, which states that $G(\mathbf{J}) - G(\mathcal{R}\mathbf{J}) = \boldsymbol{\epsilon}\cdot(\mathbf{J} - \mathcal{R}\mathbf{J})$, the Legendre transform of the current LDF fulfills

$$\mu(\boldsymbol{\lambda}) = \max_{\mathbf{J}}[G(\mathbf{J}) + \boldsymbol{\lambda}\cdot\mathbf{J}] = \max_{\mathbf{J}'}[G(\mathbf{J}') + (\mathcal{R}(\boldsymbol{\lambda}+\boldsymbol{\epsilon}) - \boldsymbol{\epsilon})\cdot\mathbf{J}'] = \mu[\mathcal{R}(\boldsymbol{\lambda}+\boldsymbol{\epsilon}) - \boldsymbol{\epsilon})],$$

where we have used the change of variables $\mathbf{J}' = \mathcal{R}\mathbf{J}$. Hence, the IFR can be stated for $\mu(\boldsymbol{\lambda})$ as

$$\mu(\boldsymbol{\lambda}) = \mu[\mathcal{R}(\boldsymbol{\lambda} + \boldsymbol{\epsilon}) - \boldsymbol{\epsilon}], \tag{C.3}$$

where $\mathcal{R}$ is any d-dimensional rotation. Using this relation in the definition of the n-th order cumulant in the limit of infinitesimal rotations, $\mathcal{R} = \mathbb{I} + \Delta\theta\mathcal{L}$, it is easy to show that

$$n_\alpha \mathcal{L}_{\beta\alpha} \mu^{(n)}_{(n_1 \ldots n_\alpha - 1 \ldots n_\beta + 1 \ldots n_d)} + \epsilon_\nu \mathcal{L}_{\gamma\nu} \mu^{(n+1)}_{(n_1 \ldots n_\gamma + 1 \ldots n_d)} = 0\,, \tag{C.4}$$

where $\mathcal{L}$ is any generator of d-dimensional rotations, and summation over repeated Greek index ($\in [1, d]$) is assumed. The above hierarchy relates in a simple way cumulants of orders n and $n+1$ $\forall n \geq 1$, and is valid arbitrarily far from equilibrium. As an example, eqs. (C.10) and (C.11) below show the first two sets of relations ($n = 1, 2$) of the above hierarchy in two dimensions.

In a similar way, we can explore the consequences of the IFR on the linear and nonlinear response coefficients. For that, we now expand the cumulants of the current in powers of $\boldsymbol{\epsilon}$

$$\mu^{(n)}_{(n_1 \ldots n_d)}(\boldsymbol{\epsilon}) = \sum_{k=0}^{\infty} \frac{1}{k!} \sum_{\substack{k_1 \ldots k_d = 0 \\ \sum_i k_i = k}}^{k} {}^{(k)}_{(n)}\chi^{(k_1 \ldots k_d)}_{(n_1 \ldots n_d)}\, \epsilon_1^{k_1} \ldots \epsilon_d^{k_d} \tag{C.5}$$

Inserting expansion (C.5) into the cumulant hierarchy, Eq. (C.4), and matching order by order in k, we derive another interesting hierarchy for the response coefficients of the different cumulants. For $k = 0$ this reads

$$n_\alpha \mathcal{L}_{\beta\alpha}\, {}^{(0)}_{(n)}\chi^{(0 \ldots 0)}_{(n_1 \ldots n_\alpha - 1 \ldots n_\beta + 1 \ldots n_d)} = 0\,, \tag{C.6}$$

which is a symmetry relation for the equilibrium ($\boldsymbol{\epsilon} = 0$) current cumulants. For $k \geq 1$ we obtain

$$\sum_{\substack{k_1 \ldots k_d = 0 \\ \sum_i k_i = k \geq 1}}^{k} \left[\frac{n_\alpha}{k} \mathcal{L}_{\beta\alpha}\, {}^{(k)}_{(n)}\chi^{(k_1 \ldots k_d)}_{(n_1 \ldots n_\alpha - 1 \ldots n_\beta + 1 \ldots n_d)} + \mathcal{L}_{\gamma\nu}\, {}^{(k-1)}_{(n+1)}\chi^{(k_1 \ldots k_\nu - 1 \ldots k_d)}_{(n_1 \ldots n_\gamma + 1 \ldots n_d)} \right] = 0\,, \tag{C.7}$$

which relates k-order response coefficients of n-order cumulants with $(k-1)$-order coefficients of $(n+1)$-order cumulants. Relations (C.6)-(C.7) for the response coefficients result from the IFR in the limit of infinitesimal rotations. For a finite rotation $\mathcal{R} = -\mathbb{I}$, which is equivalent to a current inversion, we have $\mu(\boldsymbol{\lambda}) = \mu(-\boldsymbol{\lambda} - 2\boldsymbol{\epsilon})$ and we may use this in the definition of response coefficients,

$${}^{(k)}_{(n)}\chi^{(k_1 \ldots k_d)}_{(n_1 \ldots n_d)} \equiv k! \left[\frac{\partial^{n+k} \mu(\boldsymbol{\lambda})}{\partial \lambda_1^{n_1} \ldots \lambda_d^{n_d} \partial \epsilon_1^{k_1} \ldots \epsilon_d^{k_d}} \right]_{\lambda = 0 = \epsilon}\,, \tag{C.8}$$

see Eq. (C.5), to obtain a complementary relation for the response coefficients

$${}^{(k)}_{(n)}\chi^{(k_1 \ldots k_d)}_{(n_1 \ldots n_d)} = k! \sum_{p_1 = 0}^{k_1} \ldots \sum_{p_d = 0}^{k_d} \frac{(-1)^{n+p} 2^p}{(k-p)!}\, {}^{(k-p)}_{(n+p)}\chi^{(k_1 - p_1 \ldots k_d - p_d)}_{(n_1 + p_1 \ldots n_d + p_d)}\,, \tag{C.9}$$

where $p = \sum_i p_i$. A similar equation was derived in [90] from the standard fluctuation theorem, although the IFR adds further relations. All together, eqs. (C.6)-(C.9) imply deep relations between the response coefficients at arbitrary orders which go far beyond Onsager's reciprocity relations and Green-Kubo formalism. As an example, the cumulant hierarchy in two dimensions implies the following relations

$$\begin{aligned} \langle J_x\rangle_\epsilon &= \tau L^2\left[\epsilon_x\langle\Delta J_y^2\rangle_\epsilon - \epsilon_y\langle\Delta J_x\Delta J_y\rangle_\epsilon\right] \\ \langle J_y\rangle_\epsilon &= \tau L^2\left[\epsilon_y\langle\Delta J_x^2\rangle_\epsilon - \epsilon_x\langle\Delta J_x\Delta J_y\rangle_\epsilon\right] \end{aligned} \tag{C.10}$$

$$\begin{aligned} 2\langle\Delta J_x\Delta J_y\rangle_\epsilon &= \tau L^2\left[\epsilon_y\langle\Delta J_x^3\rangle_\epsilon - \epsilon_x\langle\Delta J_x^2\Delta J_y\rangle_\epsilon\right] \\ &= \tau L^2\left[\epsilon_x\langle\Delta J_y^3\rangle_\epsilon - \epsilon_y\langle\Delta J_x\Delta J_y^2\rangle_\epsilon\right] \\ \langle\Delta J_x^2\rangle_\epsilon - \langle\Delta J_y^2\rangle_\epsilon &= \tau L^2\left[\epsilon_x\langle\Delta J_x\Delta J_y^2\rangle_\epsilon - \epsilon_y\langle\Delta J_x^2\Delta J_y\rangle_\epsilon\right], \end{aligned} \tag{C.11}$$

for the first cumulants, with $\Delta J_\alpha \equiv J_\alpha - \langle J_\alpha\rangle_\epsilon$. It is worth stressing that the cumulant hierarchy is valid arbitrarily far from equilibrium.

In a similar way, the IFR implies a set of hierarchies for the nonlinear response coefficients, see eqs. (C.6)-(C.9) above. In our two-dimensional example, let ${}^{(k)}_{(n)}\chi^{(k_x,k_y)}_{(n_x,n_y)}$ be the response coefficient of the $n = n_x + n_y$ order cumulant $\langle\Delta J_x^{n_x}\Delta J_y^{n_y}\rangle_\epsilon$ to order $\epsilon_x^{k_x}\epsilon_y^{k_y}$, with $n = n_x + n_y$ and $k = k_x + k_y$. To the lowest order these hierarchies imply Onsager's reciprocity symmetries and Green-Kubo relations for the linear response coefficients of the current.

They further predict that in fact the linear response matrix is proportional to the identity, so in our two-dimensional example

$${}^{(1)}_{(1)}\chi^{(1,0)}_{(1,0)} = {}^{(1)}_{(1)}\chi^{(0,1)}_{(0,1)} = {}^{(0)}_{(2)}\chi^{(0,0)}_{(2,0)} = {}^{(0)}_{(2)}\chi^{(0,0)}_{(0,2)},$$

while

$${}^{(1)}_{(1)}\chi^{(0,1)}_{(1,0)} = 0 = {}^{(1)}_{(1)}\chi^{(1,0)}_{(0,1)}.$$

The first nonlinear coefficients of the current can be simply written in terms of the linear coefficients of the second cumulants as

$${}^{(2)}_{(1)}\chi^{(2,0)}_{(1,0)} = 2{}^{(1)}_{(2)}\chi^{(1,0)}_{(2,0)} \quad \text{and} \quad {}^{(2)}_{(1)}\chi^{(0,2)}_{(1,0)} = -2{}^{(1)}_{(2)}\chi^{(1,0)}_{(1,1)},$$

while the cross-coefficient reads

$${}^{(2)}_{(1)}\chi^{(1,1)}_{(1,0)} = 2\left[{}^{(1)}_{(2)}\chi^{(0,1)}_{(2,0)} + {}^{(1)}_{(2)}\chi^{(0,1)}_{(1,1)}\right]$$

(symmetric results hold for $n_x = 0$, $n_y = 1$). Linear response coefficients for the second-order cumulants also obey simple relations, e.g.

$${}^{(1)}_{(2)}\chi^{(1,0)}_{(1,1)} = -{}^{(1)}_{(2)}\chi^{(0,1)}_{(1,1)} \quad \text{and} \quad {}^{(1)}_{(2)}\chi^{(1,0)}_{(2,0)} + {}^{(1)}_{(2)}\chi^{(0,1)}_{(2,0)} = {}^{(1)}_{(2)}\chi^{(1,0)}_{(0,2)} + {}^{(1)}_{(2)}\chi^{(0,1)}_{(0,2)},$$

and the set of relations continues to arbitrary high orders. In this way hierarchies (C.6)-(C.9), which derive from micro-reversibility as reflected in the IFR, provide deep insights into nonlinear response theory for non-equilibrium systems [90].

C.2 Generalized IFR

The IFR and the above hierarchies all follow from the invariance of optimal profiles under certain transformations. This idea can be further exploited in more general settings. In fact, by writing explicitly the dependence on the external field $\mathbf{E}$ in Eq. (5.4) for the optimal profile, one realizes that if

$$\frac{\delta}{\delta\rho(\mathbf{r}')}\int_\Lambda \mathbf{Q}[\rho(\mathbf{r})]d\mathbf{r} = 0, \tag{C.12}$$

together with the time-reversibility condition, Eq. (5.6), the resulting optimal profiles are invariant under *independent* rotations of the current and the external field. It thus follows that the current LDFs for pairs $(\mathbf{J},\mathbf{E})$ and $(\mathbf{J}'=\mathcal{R}\mathbf{J},\mathbf{E}^*=\mathcal{S}\mathbf{E})$, with $\mathcal{R}$, $\mathcal{S}$ independent rotations, obey a generalized isometric fluctuation relation

$$G_{\mathbf{E}}(\mathbf{J}) - G_{\mathbf{E}^*}(\mathbf{J}') = \boldsymbol{\varepsilon}\cdot(\mathbf{J}-\mathbf{J}') - \boldsymbol{\nu}\cdot(\mathbf{E}-\mathbf{E}^*) + \mathbf{J}\cdot\mathbf{E} - \mathbf{J}'\cdot\mathbf{E}^*\,, \tag{C.13}$$

where we write explicitly the dependence of the current LDF on the external field. The vector $\boldsymbol{\nu} \equiv \int_\Lambda \mathbf{Q}[\rho(\mathbf{r})]d\mathbf{r}$ is now another constant of motion, independent of $\rho(\mathbf{r})$, which can be easily computed (see Sec. C.3). For a fixed boundary gradient, the above equation relates any current fluctuation $\mathbf{J}$ in the presence of an external field $\mathbf{E}$ with any other isometric current fluctuation $\mathbf{J}'$ in the presence of an arbitrarily-rotated external field $\mathbf{E}^*$, and reduces to the standard IFR for $\mathbf{E}=\mathbf{E}^*$. Condition $\frac{\delta}{\delta\rho(\mathbf{r}')}\int_\Lambda \mathbf{Q}[\rho(\mathbf{r})]d\mathbf{r}=0$ is rather general, as most time-reversible systems with a local mobility $\sigma[\rho]$ do fulfill this condition (e.g., diffusive systems).

The IFR can be further generalized. Let us remember the hypothesis used in the derivation of the IFR:

- (i) The optimal profiles associated to a given current fluctuation are time-independent
- (ii) The optimal current field has no spatial structure.

Relaxing hypothesis (ii) we can generalize the IFR to cases where the current profile is not constant. Let $\mathrm{P}_\tau[\boldsymbol{\mathcal{J}}(\mathbf{r})]$ be the probability of observing a time-averaged current field $\boldsymbol{\mathcal{J}}(\mathbf{r}) = \tau^{-1}\int_0^\tau dt\,\mathbf{j}(\mathbf{r},t)$. Notice that this vector field must be divergence-free because it is coupled via the continuity equation to an optimal density profile which is assumed to be time-independent, see hypothesis (i). This probability also obeys a large deviation principle,

$$\mathrm{P}_\tau[\boldsymbol{\mathcal{J}}(\mathbf{r})] \sim \exp\left(+\tau L^d G[\boldsymbol{\mathcal{J}}(\mathbf{r})]\right), \tag{C.14}$$

with a current LDF equivalent to that in Eq. (5.3) but with a space-dependent current field $\boldsymbol{\mathcal{J}}(\mathbf{r})$. The optimal density profile $\rho_0[\mathbf{r};\boldsymbol{\mathcal{J}}(\mathbf{r})]$ is now solution of

$$\frac{\delta}{\delta\rho(\mathbf{r}')}\int_\Lambda d\mathbf{r}\left(W_2[\rho(\mathbf{r})] - 2\boldsymbol{\mathcal{J}}(\mathbf{r})\cdot\mathbf{W}_1[\rho(\mathbf{r})] + \boldsymbol{\mathcal{J}}^2(\mathbf{r})W_0[\rho(\mathbf{r})]\right) = 0\,, \tag{C.15}$$

which is the equivalent to Eq. (5.4) in this case. For time-reversible systems condition (5.8) holds and $\rho_0[\mathbf{r};\boldsymbol{\mathcal{J}}(\mathbf{r})]$ remains invariant under (local or global)

rotations of $\boldsymbol{\mathcal{J}}(\mathbf{r})$. In this way we can simply relate $\mathrm{P}_\tau[\boldsymbol{\mathcal{J}}(\mathbf{r})]$ with the probability of any other divergence-free current field $\boldsymbol{\mathcal{J}}'(\mathbf{r})$ locally-isometric to $\boldsymbol{\mathcal{J}}(\mathbf{r})$, i.e. $\boldsymbol{\mathcal{J}}'(\mathbf{r})^2 = \boldsymbol{\mathcal{J}}(\mathbf{r})^2 \ \forall \mathbf{r}$, via a generalized isometric fluctuation relation,

$$\lim_{\tau\to\infty} \frac{1}{\tau} \ln\left[\frac{\mathrm{P}_\tau[\boldsymbol{\mathcal{J}}(\mathbf{r})]}{\mathrm{P}_\tau[\boldsymbol{\mathcal{J}}'(\mathbf{r})]}\right] = \int_{\partial\Lambda} d\Gamma \, \frac{\delta\mathcal{H}[\rho]}{\delta\rho} \hat{n}\cdot[\boldsymbol{\mathcal{J}}'(\mathbf{r}) - \boldsymbol{\mathcal{J}}(\mathbf{r})]\,, \tag{C.16}$$

where the integral (whose result is independent of $\rho(\mathbf{r})$) is taken over the boundary $\partial\Lambda$ of the domain Λ where the system is defined, and $\hat{n}$ is the unit vector normal to the boundary at each point. Notice that in general an arbitrary local or global rotation of a divergence-free vector field does not conserve the zero-divergence property, so this constraints the current fields and/or local rotations for which this generalized IFR applies. Note that the probability of observing a time averaged integrated current, $\mathrm{P}_\tau(\mathbf{J})$, is given by

$$\mathrm{P}_\tau(\mathbf{J}) = \int \mathcal{D}\boldsymbol{\mathcal{J}} \mathrm{P}_\tau[\boldsymbol{\mathcal{J}}(\mathbf{r})] \delta\left(\mathbf{J} - \int_\Lambda d\mathbf{r}\, \boldsymbol{\mathcal{J}}(\mathbf{r})\right). \tag{C.17}$$

Hence, taking into account the above equation and that for long times Eq. (C.14) holds and $\mathrm{P}_\tau(\mathbf{J}) \sim \exp\left(+\tau L^d G(\mathbf{J})\right)$, we can relate the large deviation function for the space- and time-averaged current, $G(\mathbf{J})$, to $G[\boldsymbol{\mathcal{J}}(\mathbf{r})]$ via a contraction principle

$$G(\mathbf{J}) = \max_{\substack{\boldsymbol{\mathcal{J}}(\mathbf{r}):\boldsymbol{\nabla}\cdot\boldsymbol{\mathcal{J}}(\mathbf{r})=0 \\ \mathbf{J}=\int_\Lambda d\mathbf{r}\,\boldsymbol{\mathcal{J}}(\mathbf{r})}} G[\boldsymbol{\mathcal{J}}(\mathbf{r})]\,. \tag{C.18}$$

The optimal, divergence-free current field $\boldsymbol{\mathcal{J}}_0(\mathbf{r};\mathbf{J})$ solution of this variational problem may have spatial structure in general. Eq. (C.16) generalizes the IFR to situations where hypothesis (*ii*) is violated, opening the door to isometries based on local (in addition to global) rotations. However, numerical results and phenomenological arguments strongly suggest that the constant solution, $\boldsymbol{\mathcal{J}}_0(\mathbf{r};\mathbf{J}) = \mathbf{J}$, is the optimizer at least for a wide interval of current fluctuations, showing that hypothesis (ii) is not only plausible but also well justified on physical grounds. In any case, the range of validity of this hypothesis can be explored by studying the limit of local stability of the constant current solution using tools similar to those in Ref.[77].

C.3 Constants of motion

A sufficient condition for the IFR to hold is that

$$\frac{\delta\boldsymbol{\omega}_1[\rho(\mathbf{r})]}{\delta\rho(\mathbf{r}')} = 0\,, \tag{C.19}$$

with the functional $\boldsymbol{\omega}_1[\rho(\mathbf{r})]$ defined in Eq. (5.5) of chapter 5. We have shown that condition (C.19) follows from the time-reversibility of the dynamics, in the sense that the evolution operator in the Fokker-Planck formulation of Eq. (5.1) obeys a local detailed balance condition, see Eq. (5.8). Condition (C.19) implies that $\boldsymbol{\omega}_1[\rho(\mathbf{r})]$ is in fact a *constant of motion*, $\boldsymbol{\epsilon}$, independent of

the profile $\rho(\mathbf{r})$. Therefore we can use an arbitrary profile $\rho(\mathbf{r})$, compatible with boundary conditions, to compute $\boldsymbol{\epsilon}$. We now choose boundary conditions to be gradient-like in the $\hat{x}$-direction, with densities ρ_L and ρ_R at the left and right reservoirs, respectively, and periodic boundary conditions in all other directions. Given these boundaries, we now select a linear profile

$$\rho(\mathbf{r}) = \rho_L + (\rho_R - \rho_L)x\,, \tag{C.20}$$

to compute $\boldsymbol{\epsilon}$, with $x \in [0,1]$, and assume very general forms for the current and mobility functional

$$\begin{aligned}
\mathbf{Q}[\rho(\mathbf{r})] &\equiv D_{0,0}[\rho]\boldsymbol{\nabla}\rho + \sum_{n,m>0} D_{nm}[\rho](\boldsymbol{\nabla}^m\rho)^{2n}\boldsymbol{\nabla}\rho\,,\\
\sigma[\rho(\mathbf{r})] &\equiv \sigma_{0,0}[\rho] + \sum_{n,m>0} \sigma_{nm}[\rho](\boldsymbol{\nabla}^m\rho)^{2n}\,,
\end{aligned}$$

where as a convention we denote as $F[\rho]$ a generic functional of the profile but not of its derivatives. It is now easy to show that $\boldsymbol{\epsilon} = \varepsilon\hat{x} + \mathbf{E}$, with

$$\varepsilon = \int_{\rho_L}^{\rho_R} d\rho \frac{D_{0,0}(\rho) + \sum_{n>0} D_{n1}(\rho)(\rho_R - \rho_L)^{2n}}{\sigma_{0,0}(\rho) + \sum_{m>0} \sigma_{m1}(\rho)(\rho_R - \rho_L)^{2m}}\,, \tag{C.21}$$

and $\hat{x}$ the unit vector along the gradient direction. In a similar way, if the following condition holds

$$\frac{\delta}{\delta\rho(\mathbf{r}')}\int_\Lambda \mathbf{Q}[\rho(\mathbf{r})]d\mathbf{r} = 0\,, \tag{C.22}$$

together with time-reversibility, Eq. (C.19), the system can be shown to obey an extended isometric fluctuation relation which links any current fluctuation $\mathbf{J}$ in the presence of an external field $\mathbf{E}$ with any other isometric current fluctuation $\mathbf{J}'$ in the presence of an arbitrarily-rotated external field $\mathbf{E}^*$, and reduces to the standard IFR for $\mathbf{E} = \mathbf{E}^*$, see Eq. (11) in the chapter. Condition (C.22) implies that $\boldsymbol{\nu} \equiv \int \mathbf{Q}[\rho(\mathbf{r})]d\mathbf{r}$ is another constant of motion, which can be now written as $\boldsymbol{\nu} = \nu\hat{x}$, with

$$\nu = \int_{\rho_L}^{\rho_R} d\rho \left[D_{0,0}(\rho) + \sum_{n>0} D_{n1}(\rho)(\rho_R - \rho_L)^{2n} \right]\,, \tag{C.23}$$

As an example, for a diffusive system $\mathbf{Q}[\rho(\mathbf{r})] = -D[\rho]\boldsymbol{\nabla}\rho(\mathbf{r})$, with $D[\rho]$ the diffusivity functional, and the above equations yield the familiar results

$$\begin{aligned}
\varepsilon &= \int_{\rho_R}^{\rho_L} \frac{D(\rho)}{\sigma(\rho)}d\rho\,,\\
\nu &= \int_{\rho_R}^{\rho_L} D(\rho)d\rho\,,
\end{aligned}$$

for a standard local mobility $\sigma[\rho]$.

Appendix D

List of Publications

D.1 Publications

D1 Hurtado, Pablo I., Carlos P. Espigares, Jess J. del Pozo, and Pedro L. Garrido. "Thermodynamics of currents in nonequilibrium diffusive systems: theory and simulation." Journal of Statistical Physics (2013): 1-51.

D2 Hurtado, Pablo I., Carlos Prez-Espigares, Jess J. del Pozo, and Pedro L. Garrido. "Symmetries in fluctuations far from equilibrium." Proceedings of the National Academy of Sciences 108, no. 19 (2011): 7704-7709.

D.2 Preprints

- del Pozo, J. J., P. L. Garrido, and P. I. Hurtado. "Universal scaling laws and bulk-boundary decoupling in fluids out of equilibrium." arXiv preprint arXiv:1401.5244 (2014).

D.3 Contribution to Conference Proceedings

- C. Pérez-Espigares, J.J. del Pozo, P.L. Garrido and P.I. Hurtado, *AIP Conf. Proc* **1332**, 204 (2011)

D.4 In Preparation

- del Pozo, J. J., P. L. Garrido, and P. I. Hurtado, "Scaling Laws in Strongly Driven Fluids".
- del Pozo, J. J., P. L. Garrido, and P. I. Hurtado, "Local Thermodynamic Equilibrium in Non-equilibrium Fluids".
- del Pozo, J. J., P. L. Garrido, and P. I. Hurtado, "Non-equilibrium Fluid-Solid Coexistence: Scaling and Local Equilibrium".

- del Pozo, J. J., P. L. Garrido, and P. I. Hurtado, "Current Fluctuations in Hydrodynamic Like Theories".

List of figures

List of tables

Bibliography

[1] Hannes Alfvén. Existence of electromagnetic-hydrodynamic waves. *Nature*, 150(3805):405–406, 1942.

[2] Joseph Fourier. *Theorie analytique de la chaleur, par M. Fourier*. Chez Firmin Didot, père et fils, 1822.

[3] Jean Baptiste Joseph baron Fourier. *The analytical theory of heat*. The University Press, 1878.

[4] Alexander Tenenbaum, Giovanni Ciccotti, and Renato Gallico. Stationary nonequilibrium states by molecular dynamics. Fourier's law. *Physical Review A*, 25(5), 1982.

[5] Lars Onsager. Reciprocal relations in irreversible processes. i. *Physical Review*, 37(4):405, 1931.

[6] Lars Onsager. Reciprocal relations in irreversible processes. ii. *Physical Review*, 38(12):2265, 1931.

[7] Sybren Ruurds De Groot and Peter Mazur. *Non-equilibrium thermodynamics*. Courier Dover Publications, 2013.

[8] Albert Einstein. *Investigations on the Theory of the Brownian Movement*. Courier Dover Publications, 1956.

[9] Harry Nyquist. Thermal agitation of electric charge in conductors. *Physical review*, 32(1):110–113, 1928.

[10] Herbert B Callen and Theodore A Welton. Irreversibility and generalized noise. *Physical Review*, 83(1):34–40, 1951.

[11] Melville S Green. Markoff random processes and the statistical mechanics of time-dependent phenomena. ii. irreversible processes in fluids. *Journal of Chemical Physics*, 22:398–413, 1954.

[12] Ryogo Kubo. Statistical-mechanical theory of irreversible processes. i. general theory and simple applications to magnetic and conduction problems. *Journal of the Physical Society of Japan*, 12(6):570–586, 1957.

[13] Denis J Evans, EGD Cohen, and GP Morriss. Probability of second law violations in shearing steady states. *Physical Review Letters*, 71(15):2401, 1993.

[14] G Gallavotti and EGD Cohen. Dynamical ensembles in nonequilibrium statistical mechanics. *Physical Review Letters*, 74(14):2694, 1995.

[15] Lorenzo Bertini, Alberto De Sole, Davide Gabrielli, Giovanni Jona-Lasinio, and Claudio Landim. Fluctuations in stationary nonequilibrium states of irreversible processes. *Physical Review Letters*, 87(4):040601, 2001.

[16] L Bertini, A De Sole, and D Gabrielli. Macroscopic fluctuation theory for stationary non-equilibrium states. *Journal of statistical ...*, 107(May):635–675, 2002.

[17] L Bertini, A De Sole, and D Gabrielli. Current fluctuations in stochastic lattice gases. *Physical review ...*, 030601(January):1–4, 2005.

[18] L Bertini, AD Sole, and D Gabrielli. Non equilibrium current fluctuations in stochastic lattice gases. *Journal of statistical ...*, 123(2):237–276, 2006.

[19] L Bertini, A De Sole, D Gabrielli, G Jona-Lasinio, and C Landim. Stochastic interacting particle systems out of equilibrium. *Journal of Statistical Mechanics: Theory and Experiment*, 2007(07):P07014, 2007.

[20] Bernard Derrida. Non-equilibrium steady states: fluctuations and large deviations of the density and of the current. *Journal of Statistical Mechanics: Theory and ...*, (1), 2007.

[21] Udo Seifert. Stochastic thermodynamics, fluctuation theorems and molecular machines. *Reports on Progress in Physics*, 75(12):126001, 2012.

[22] Mulero A. (ed.). *Theory and Simulation of Hard-Sphere Fluids and Related Systems*. Springer, Heidelberg, 2008.

[23] Ludovic Berthier, Giulio Biroli, Jean-Philippe Bouchaud, Luca Cipelletti, and Wim van Saarloos. *Dynamical heterogeneities in glasses, colloids, and granular media*. Oxford University Press, 2011.

[24] J Prost. *The physics of liquid crystals*. Number 83. Oxford university press, 1995.

[25] Anita Mehta. *Granular physics*. Cambridge University Press, 2007.

[26] Pablo I Hurtado, Carlos Pérez-Espigares, Jesús J del Pozo, and Pedro L Garrido. Symmetries in fluctuations far from equilibrium. *Proceedings of the National Academy of Sciences of the United States of America*, 108(19):7704–9, 2011.

[27] BJ Alder and TE Wainwright. Velocity autocorrelations for hard spheres. *Physical review letters*, 18(23):988, 1967.

[28] B. J. Alder and T. E. Wainwright. Phase Transition for a Hard Sphere System. *The Journal of Chemical Physics*, 27(5):1208, 1957.

[29] Marshall N Rosenbluth and Arianna W Rosenbluth. Further results on monte carlo equations of state. *The Journal of Chemical Physics*, 22(5):881–884, 2004.

[30] F Bonetto and J L Lebowitz. Fourier law: a challenge to theorists. 0(1):1–23, 2008.

[31] Abhishek Dhar. Heat transport in low-dimensional systems. *Advances in Physics*, 57(5):457–537, 2008.

[32] NI Chernov and Joel L Lebowitz. Stationary nonequilibrium states in boundary-driven hamiltonian systems: shear flow. *Journal of statistical physics*, 86(5-6):953–990, 1997.

[33] F Bonetto, G Gallavotti, and PL Garrido. Chaotic principle: an experimental test. *Physica D: Nonlinear Phenomena*, 105(4):226–252, 1997.

[34] Pedro L Garrido, Pablo I Hurtado, and Bjoern Nadrowski. Simple one-dimensional model of heat conduction which obeys fouriers law. *Physical review letters*, 86(24):5486, 2001.

[35] P L Garrido, S Goldstein, and J L Lebowitz. *Physical review letters*.

[36] PL Garrido and G Gallavotti. Boundary dissipation in a driven hard disk system. *Journal of Statistical Physics*, (1):4–6, 2007.

[37] Etienne P Bernard and Werner Krauth. Two-step melting in two dimensions: First-order liquid-hexatic transition. *Physical review letters*, 107(15):155704, 2011.

[38] Michael Engel, Joshua A Anderson, Sharon C Glotzer, Masaharu Isobe, Etienne P Bernard, and Werner Krauth. Hard-disk equation of state: First-order liquid-hexatic transition in two dimensions with three simulation methods. *Physical Review E*, 87(4):042134, 2013.

[39] Erpenbeck J.J. and Luban M. Equation of state of the classical hard-disk fluid. *Physcal Review A*, 32(5):2920–2922, 1985.

[40] J. Kolafa and M. Rottner. Simulation-based equation of state of the hard disk fluid and prediction of higher-order virial coefficients. *Molecular Physics*, 104(22-24):3435–3441, 2006.

[41] Nicholas Metropolis, Arianna W Rosenbluth, Marshall N Rosenbluth, Augusta H Teller, and Edward Teller. Equation of state calculations by fast computing machines. *The journal of chemical physics*, 21(6):1087–1092, 2004.

[42] T. Einwohner. Molecular Dynamics. VI. Free-Path Distributions and Collision Rates for Hard-Sphere and Square-Well Molecules. *The Journal of Chemical Physics*, 49(4):1458, 1968.

[43] CH Mak. Large-scale simulations of the two-dimensional melting of hard disks. *Physical Review E*, pages 1–4, 2006.

[44] Michael Engel, JA Anderson, and SC Glotzer. Hard-disk equation of state: First-order liquid-hexatic transition in two dimensions with three simulation methods. *Physical Review E*, (1):1–7, 2013.

[45] Ulf R Pedersen, Nicholas P Bailey, Thomas B Schrøder, and Jeppe C Dyre. Strong pressure-energy correlations in van der waals liquids. *Physical review letters*, 100(1):015701, 2008.

[46] Nicoletta Gnan, Thomas B Schrøder, Ulf R Pedersen, Nicholas P Bailey, and Jeppe C Dyre. Pressure-energy correlations in liquids. iv.isomorphs? in liquid phase diagrams. *The Journal of chemical physics*, 131(23):234504, 2009.

[47] B. J. Alder and T. E. Wainwright. Studies in Molecular Dynamics. I. General Method. *The Journal of Chemical Physics*, 31(2):459, 1959.

[48] Mauricio Marı?n, Dino Risso, and Patricio Cordero. Efficient algorithms for many-body hard particle molecular dynamics. *Journal of Computational Physics*, 109(2):306–317, 1993.

[49] DC Rapaport. The event scheduling problem in molecular dynamic simulation. *Journal of Computational Physics*, 34(2):184–201, 1980.

[50] Etienne P Bernard, Werner Krauth, and David B Wilson. Event-chain monte carlo algorithms for hard-sphere systems. *Physical Review E*, 80(5):056704, 2009.

[51] Masaharu Isobe. Simple and efficient algorithm for large scale molecular dynamics simulation in hard disk system. *International Journal of Modern Physics C*, 10(07):1281–1293, 1999.

[52] T.E. Alder B.J. , Wainwright. Phase Transition in Elastic Fluids. *Physical Review*, 127(2):359, 1962.

[53] C. Kipnis, C. Marchioro, and E. Presutti. Heat flow in an exactly solvable model. *Journal of Statistical Physics*, 27(1):65–74, 1982.

[54] Stefano Lepri, Roberto Livi, and Antonio Politi. Thermal conduction in classical low-dimensional lattices. *Physics Reports*, 377(1):1–80, 2003.

[55] C Kipnis, S Olla, and SRS Varadhan. Hydrodynamics and large deviation for simple exclusion processes. *Communications on Pure and Applied Mathematics*, 42(2):115–137, 1989.

[56] M Mareschal and E Kestemont. Nonequilibrium states by molecular dynamics: Transport coefficients in constrained fluids. *Physical ...*, 1987.

[57] Dino Risso and Patricio Cordero. Two-dimensional gas of disks: Thermal conductivity. *Journal of statistical physics*, 82(5-6):1453–1466, 1996.

[58] Alder B.J. Hoover, William G. Studies in Molecular Dynamics. IV. The Pressure, Collision Rate, and Their Number Dependence for Hard Disks. *The Journal of Chemical Physics*, 46(2):686, 1967.

[59] Dino Risso and Patricio Cordero. Dilute gas Couette flow: Theory and molecular dynamics simulation. *Physical Review E*, 56(1):489–498, July 1997.

[60] M Mareschal and E Kestemont. Order and fluctuations in nonequilibrium molecular dynamics simulations of two-dimensional fluids. *Journal of statistical physics*, 48:1187–1201, 1987.

[61] Michel Mareschal, M Malek Mansour, A Puhl, and Edouard Kestemont. Molecular dynamics versus hydrodynamics in a two-dimensional rayleigh-bénard system. *Physical review letters*, 61:2550–2553, 1988.

[62] Mike P Allen and Dominic J Tildesley. *Computer simulation of liquids*. Oxford university press, 1989.

[63] William G Hoover and William T Ashurst. Nonequilibrium molecular dynamics. *Theoretical Chemistry: Advances and Perspectives*, 1:1–51, 1975.

[64] J.-P Eckmann and L.-S Young. Temperature profiles in Hamiltonian heat conduction. *Europhysics Letters (EPL)*, 68(6):790–796, dec 2004.

[65] F Bonetto, JL Lebowitz, and L Rey-bellet. Fourier Law: A Challenge To Theorists. *ukpmc.ac.uk*, 0(1):1–23, 2004.

[66] Roland Roth, Klaus Mecke, and Martin Oettel. Communication: Fundamental measure theory for hard disks: fluid and solid. *The Journal of chemical physics*, 136(8):081101, 2012.

[67] S. Wooszczuk and a. Lipowski. Crystallization of hard disks induced by a temperature gradient. *Physical Review E*, 81(6):061132, 2010.

[68] DM Gass. Enskog theory for a rigid disk fluid. *The Journal of Chemical Physics*, 54(5):1898–1902, 1971.

[69] Ramón García-Rojo, Stefan Luding, and J Javier Brey. Transport coefficients for dense hard-disk systems. *Physical Review E*, 74(6):061305, 2006.

[70] BJ Alder, DM Gass, and TE Wainwright. Studies in Molecular Dynamics. VIII. The Transport Coefficients for a Hard-?Sphere Fluid. *The Journal of Chemical Physics*, 1970.

[71] Pierre MV Résibois and Marcel De Leener. *Classical kinetic theory of fluids*. Wiley New York, 1977.

[72] JL Lebowitz and Herbert Spohn. A GallavottiCohen-type symmetry in the large deviation functional for stochastic dynamics. *Journal of Statistical Physics*, 1999.

[73] Jorge Kurchan. Fluctuation theorem for stochastic dynamics. *Journal of Physics A: Mathematical and General*, 31(16):3719, 1998.

[74] T Bodineau and B Derrida. Current fluctuations in non-equilibrium diffusive systems: an additivity principle, 2004. *Phys. Rev. Lett*, 3(5):1–4, 2004.

[75] Pablo I Hurtado and Pedro L Garrido. Test of the additivity principle for current fluctuations in a model of heat conduction. *Physical review letters*, 102(25):250601, 2009.

[76] Pablo I Hurtado and Pedro L Garrido. Large fluctuations of the macroscopic current in diffusive systems: A numerical test of the additivity principle. *Physical Review E*, 81(4):041102, 2010.

[77] Thierry Bodineau and Bernard Derrida. Distribution of current in nonequilibrium diffusive systems and phase transitions. *Physical Review E*, 72(6):066110, 2005.

[78] Pablo I Hurtado. Breakdown of hydrodynamics in a simple one-dimensional fluid. *Physical review letters*, 96(1):010601, 2006.

[79] Pedro L Garrido, Joel L Lebowitz, Christian Maes, and Herbert Spohn. Long-range correlations for conservative dynamics. *Physical Review A*, 42(4):1954, 1990.

[80] L Bertini, A De Sole, D Gabrielli, G Jona-Lasinio, and C Landim. On the long range correlations of thermodynamic systems out of equilibrium. *arXiv preprint arXiv:0705.2996*, 2007.

[81] David J Gross. The role of symmetry in fundamental physics. *Proceedings of the National Academy of Sciences of the United States of America*, 93(25):14256, 1996.

[82] DG Luchinsky and Peter VE McClintock. Irreversibility of classical fluctuations studied in analogue electrical circuits. *Nature*, 389(6650):463–466, 1997.

[83] Herbert Spohn. *Large scale dynamics of interacting particles*, volume 825. Springer, 1991.

[84] Richard Ellis. *Entropy, large deviations, and statistical mechanics*, volume 1431. Taylor & Francis, 2005.

[85] Hugo Touchette. The large deviation approach to statistical mechanics. *Physics Reports*, pages 1–89, 2009.

[86] Hugo Touchette and Rosemary J Harris. 1 Large deviation approach to nonequilibrium systems. pages 1–25, 2011.

[87] B Derrida, JL Lebowitz, and ER Speer. Large deviation of the density profile in the steady state of the open symmetric simple exclusion process. *Journal of statistical physics*, 107(3-4):599–634, 2002.

[88] D Collin, F Ritort, C Jarzynski, SB Smith, I Tinoco, and C Bustamante. Verification of the crooks fluctuation theorem and recovery of rna folding free energies. *Nature*, 437(7056):231–234, 2005.

[89] Felix Ritort. Nonequilibrium fluctuations in small systems: From physics to biology. *Advances in Chemical Physics*, 137:31, 2008.

[90] David Andrieux and Pierre Gaspard. A fluctuation theorem for currents and non-linear response coefficients. *Journal of Statistical Mechanics: Theory and Experiment*, 2007(02):P02006, 2007.